

Evaluation of basal heave in the Marieholm tunnel project

Comparison of two excavation methods

Master's Thesis in the Master's Programme Infrastructure and Environmental Engineering

STINA BERG
NAOMI LICUDI

MASTER'S THESIS BOMX02-17-24

Evaluation of basal heave in the Marieholm tunnel project

Comparison of two excavation methods

Master's Thesis in the Master's Programme Infrastructure and Environmental Engineering

STINA BERG

NAOMI LICUDI

Department of Civil and Environmental Engineering
Division of GeoEngineering
Research Group Engineering geology and geotechnics
CHALMERS UNIVERSITY OF TECHNOLOGY
Goteborg, Sweden 2017

Evaluation of basal heave in the Marieholm tunnel project
Comparison of two excavation methods

Master's Thesis in the Master's Programme Infrastructure and Environmental Engineering

STINA BERG

NAOMI LICUDI

© Stina Berg, Naomi Licudi, 2017

Examensarbete BOMX02-17-24/ Institutionen för bygg- och miljöteknik,
Chalmers tekniska högskola 2017

Department of Civil and Environmental Engineering
Division of GeoEngineering
Research Group Engineering geology and geotechnics
Chalmers University of Technology
SE-412 96 Göteborg
Sweden
Telephone: + 46 (0)31-772 1000

Cover:

Deformed mesh, true scale. Obtained from the Soft Soil model calculations for the LCC in PLAXIS.

Department of Civil and Environmental Engineering
Göteborg, Sweden, 2017

Evaluation of basal heave in the Marieholm tunnel project project

Comparison of two excavation methods

Master's thesis in the Master's Programme Infrastructure and Environmental Engineering

STINA BERG

NAOMI LICUDI

Department of Civil and Environmental Engineering

Division of GeoEngineering

Research Group Engineering geology and geotechnics

Chalmers University of Technology

ABSTRACT

Marieholm tunnel will serve as an extra connection point between the island of Hisingen and mainland Gothenburg. In this project a deep excavation in soft clay is required which means that basal heave needs to be carefully monitored. The aim of this thesis is to evaluate and compare the current method of minimizing basal heave, concrete slab at the bottom of the excavation, with lime-cement columns placed in the passive side of the excavation.

The problem was modelled in PLAXIS 2D with the constitutive models, Soft Soil and the Hardening Soil with small-strain stiffness models, and analytical calculations for the safety factor were performed. The parameters were obtained from field and lab data of the area and calibrated in PLAXIS to ensure that the correct stress paths were modelled. Parametric studies were also conducted. The basal heave predictions were then compared to real measurements.

The results show that the concrete slab is more favorable for minimizing basal heave in the deep excavation. The basal heave predictions for the concrete slab are approximately one centimeter larger than in reality. However, given that no constitutive model is able to capture the soil behavior perfectly and the evaluated tests were not of the best quality, the results are considered to be acceptable. The safety factor prediction were significantly lower for the analytical calculations since the failure surface is assumed.

It can be concluded that lime-cement columns can be used on the passive side of deep excavations if it is proven to be a cost-effective alternative. The difference in basal heave is only approximately three centimeters when compared to the concrete slab model prediction. Moreover, once the excavation is completed the tunnel segments will be constructed on the excavation bottom and basal heave will be reduced. However, there are numerous uncertainties regarding assumptions and which values should be used. Therefore, it is recommended to investigate this further.

Key words: Soft Soil, Hardening Soil with small-strain stiffness, basal heave, PLAXIS, SoilTest, Marieholm tunnel, soft clay, deep excavation, lime-cement columns.

Utvärdering av bottenuppträckning i projektet Marieholmstunneln
En jämförelse mellan två utgrävningsmetoder

Examensarbete inom masterprogrammet Infrastructure and Environmental
Engineering

STINA BERG

NAOMI LICUDI

Institutionen för bygg- och miljöteknik

Avdelningen för Geoteknik

Forskningsgrupp teknisk geologi och geoteknik

Chalmers tekniska högskola

SAMMANFATTNING

Det pågående projektet Marieholmstunneln skall utgöra en extra förbindelse mellan Hisingen och fastlandet i Göteborg. I och med konstruktionen av tunneln kommer ett djup schakt av lera att grävas, vilket ställer extra krav på kontroll av bottenuppträckningen. Syftet med detta arbete har varit att jämföra den nuvarande konstruktionen, en betongplatta med kalkcementpelare installerade i den passiva zonen för att motverka bottenuppträckning.

Modellen har utvärderas i datorprogrammet PLAXIS 2D med de konstitutiva modellerna "Soft Soil" och "Hardening Soil with small-strain stiffness". Analytiska beräkningar har även utförts för beräkning av säkerhetsfaktorn. Parametrar har utvärderas från fält- och laborierdata som utförts på området, och har sedan kalibreras i PLAXIS. En parametrisk studie har även gjorts och slutligen har de beräknade värdena för bottenuppträckningen jämförts med uppmätt data.

Resultatet från PLAXIS beräkningarna visar på att betongplattan ger mindre bottenuppträckning för en djup utgrävning. Beräkningarna är ungefär en centimeter större än vad som är uppmätt. Dock var det ingen av de två konstruktiva modellerna som kunde representera jordens beteende perfekt och beräkningen baserats på något defekt data, men trots allt anses resultatet vara trovärdigt. Den beräknade säkerhetsfaktorn för analytiska beräkningarna var betydligt lägre i och med att den baserades på en antagen glidyta.

Sammanfattningsvis kan en slutsats dras att kalkcementpelare kan används i den passiva zonen i djupa schakter om de bevisas vara ekonomisk hållbara. Skillnaden i bottenuppträckningen mellan betongplattan och kalkcementpelarna är ca tre centimeter. Dessutom när tunnelsegmentens kommer att börja byggas kommer de att utgöra en extra last och därmed motverka bottenuppträckningen. Däremot finns det en del osäkerheter kring valet av parametrar och antaganden som gjorts. Det är därför rekommenderat att undersöka detta vidare.

Nyckelord: Soft Soil, Hardening Soil with small-strain stiffness, bottenuppträckning, PLAXIS, SoilTest, Marieholmstunneln, lös lera, djup schakt, kalkcementpelare.

Contents

ABSTRACT	I
SAMMANFATTNING	II
CONTENTS	IV
PREFACE	VI
NOTATIONS	VII
1 INTRODUCTION	1
1.1 Aim	1
1.2 Method	1
1.3 Limitations	2
1.4 Assumptions	2
2 LITERATURE STUDY	3
2.1 Ground improvements methods	3
2.1.1 Concrete slab	3
2.1.2 Lime-cement columns	3
2.2 Previous studies- Lime-cement columns in soft soil	5
2.3 Constitutive models	6
2.3.1 Linear Elastic model	6
2.3.2 Mohr-Coulomb model	6
2.3.3 Soft Soil model	8
2.3.4 Hardening Soil model with small-strain stiffness model	9
2.4 Analytical safety calculations	13
2.4.1 Terzaghi's method	13
2.4.2 Bjerrum and Eide's method	14
3 BACKGROUND	17
3.1 Area description	17
3.2 Geology of the area	18
3.3 Dry dock	19
3.4 Description of the planned construction	20
4 PARAMETERS	21
4.1 Structure and fill parameters	21
4.2 Lime-cement columns parameters	21
4.3 Clay parameters	23
4.4 Calibration and validation of parameters	26
4.4.1 Parameters for the Soft Soil model	26

4.4.2	Parameters for the Hardening Soil model with small-strain stiffness	29
4.4.3	Correlation between the Soft Soil and the Hardening Soil small-strain stiffness models parameters	32
5	CALCULATIONS	34
5.1	Analytical safety calculations	34
5.1.1	Terzaghi's method	34
5.1.2	Bjerrum and Eide's method	34
5.2	PLAXIS	34
5.2.1	Model 1-Concrete slab	34
5.2.2	Model 2-Lime-cement columns	35
5.2.3	Influence of load, piles and lime-cement columns	37
5.2.4	Parametric studies- Model 1	38
5.2.5	Parametric studies- Model 2	41
6	RESULT	42
6.1	Analytical safety calculations	42
6.2	PLAXIS	42
6.2.1	Model 1-Concrete slab	43
6.2.2	Model 2-Lime-cement columns	45
6.3	Comparison of model 1 and model 2	47
6.4	Influence of load, piles and lime-cement columns	48
6.5	Parametric studies- Model 1	49
6.5.1	Soft Soil	49
6.5.2	Hardening Soil with small-strain stiffness	50
6.6	Parametric studies- Model 2	51
6.7	Corroboration with measured data	51
7	DISCUSSION	52
7.1	Parameters	52
7.2	Constitutive model	53
7.3	Analytical calculations	54
7.4	Result	54
7.5	LCC-Preventing basal heave?	55
7.6	Further studies	56
8	CONCLUSION	58
9	REFERENCES	59

Preface

In this thesis, basal heave at Marieholms tunnel project has been investigated. This work has been done between January and May 2017 at the Department of Civil and Environmental Engineering, Division of GeoEngineering, Chalmers University of Technology and ÅF AB, Sweden.

This thesis has been carried out under the supervision of Mats Karlsson at division of GeoEngineering and Roger Oscarsson at ÅF AB, who we would like to thank for their guidance.

Göteborg May 2017

Stina Berg & Naomi Licudi

Notations

Roman letters

A_0	Area of overlap between the columns	[m ²]
A_c	Area of lime-cement columns	[m ²]
A_s	Area of soil	[m ²]
a_{s0}	Area replacement ratio of overlap zone	[m ²]
a_{sc}	Area replacement ratio of columns	[m ²]
A_T	Total area	[m ²]
B	Width of the excavation	[m]
c	Chord length of overlap	[m]
$b_{0.2D}$	Effective width of overlap zone	[m]
b_{c2D}	Effective width of the columns	[m]
c_{crit}	Critical undrained shear strength	[kPa]
c_u	Undrained shear strength	[kPa]
c'	Effective cohesion	[kPa]
c'_{incr}	Effective cohesion increase	[kPa/m]
c'_{ref}	Effective reference cohesion	[kPa]
d	Diameter of LCC column	[m]
d_e	Equivalent diameter of LCC columns	[m]
D	Depth to stiff layer	[m]
e	Overlap distance between the columns	[m]
EA	Axial stiffness	[kN/m]
EI	Flexural rigidity	[kNm ² /m]
E	Young's modulus	[kPa]
E_{50}	Undrained secant stiffness in drained triaxial test	[kPa]
E'_{col}	Effective Young's modulus for LCC	[kPa]
E'_{equi}	Effective equivalent Young's Modulus for the LCC-block	[kPa]
E'_{soil}	Effective Young's modulus for soil	[kPa]
E_{oed}	Tangent stiffness for primary oedometer loading	[kPa]
E_{ur}	Undrained unload-reload stiffness from drained triaxial test	[kPa]
E'	Effective Young's Modulus	[kPa]

E_{50}^{ref}	Undrained secant stiffness in standard drained triaxial test	[kPa]
E_{oed}^{ref}	Undrained tangent stiffness for primary oedometer loading	[kPa]
E_{ur}^{ref}	Undrained unload-reload stiffness	[kPa]
f	Yield surface	[kPa]
F_b	Safety factor against basal heave	[-]
F_{max}	Maximum base resistance of the piles	[kN]
$F_{max,comp}$	Maximum resistance of the strut	[kN]
g	Plastic potential function	[kPa]
G	Undrained shear modulus	[kPa]
G_0	Undrained initial shear modulus	[kPa]
G_0^{ref}	Undrained initial shear modulus at ref. pressure (p^{ref})	[kPa]
G_0^{rref}	Effective unload-reload stiffness at ref. pressure (p^{ref})	[kPa]
H_e	Height of the excavation	[m]
k_x	Permeability in the x-direction	[m/day]
k_y	Permeability in the y-direction	[m/day]
K_0	Coefficient of lateral earth pressure (initial stress state)	[-]
K_0^{nc}	Coefficient of lateral earth pressure at rest for normally consolidated clays	[-]
$L_{spacing}$	Piles spacing	[m]
m	Power for stress-level dependency of stiffness	[-]
M	Slope of line in a p'-q plot	[-]
M_0	Compression modulus, elastic part	[kPa]
M_p	Maximum bending moment	[kNm/m]
M_L	Compression modulus, plastic part	[kPa]
N_c	Bearing capacity factor	[-]
N_p	Maximum force in 1-direction (in-plane)	[kN/m]
p_c	Vertical preconsolidation pressure	[kPa]
p_p	Preconsolidation stress	[kPa]
p_{ref}	Reference stress	[kPa]
p'	Mean effective stress	[kPa]

p^0	Initial effective stress	[kPa]
p'_0	Effective earth pressure at rest	[kPa]
q	Deviator stress	[kPa]
q_c	Load at excavation bottom	[kPa]
q_s	Surcharge load	[kPa]
R_f	Scaling factor	[-]
R_{inter}	Interface value	[-]
S_{col}	Distance between column to column center	[m]
S_{row}	CC-distance between LCC panels	[m]
s_{u1}	Shear strength of the soil above the excavation	[kPa]
s_{u2}	Shear strength of the soil below the excavation	[kPa]
s_{u0}	Shear strength of overlap	[kPa]
s_{us}	Shear strength of columns	[kPa]
s_{uc}	Shear strength of soil between columns	[kPa]
$s_{u,02D}$	Composite shear strength of overlap	[kPa]
$s_{u,c2D}$	Composite shear strength of columns	[kPa]
$T_{bot,max}$	Maximum axial skin resistance at the bottom of the piles	[kN/m]
T_{min}	Minimum axial skin resistance	[kN/m]
$T_{top,max}$	Maximum axial skin resistance at the bottom of the piles	[kN/m]
u	Pore pressure	[kPa]
u_y	Vertical displacement	[m]
w_L	Liquid limit	[%]
w_N	Water content	[%]

Greek letters

α	One half of the chord angle	[rad]
γ	Soil weight	[kN/m ³]
γ_{unsat}	Unsaturated soil weight	[kN/m ³]
γ_{sat}	Saturated soil weight	[kN/m ³]
$\gamma_{0.7}$	Shear stain level when $G = 0.722G_0$	[-]

γ_s	Shear strain amplitude	[-]
ε	Total strain	[-]
ε_1	Axial strain	[-]
ε_v	Volumetric strain	[-]
ε_v^e	Elastic volumetric strain	[-]
ε_v^0	Initial volumetric strain	[-]
ε_v^{e0}	Initial elastic volumetric strain	[-]
κ^*	Modified swelling index	[-]
λ^*	Modified compression index	[-]
ν	Poisson's ratio	[-]
ν_{ur}	Poisson's ratio for unloading-reloading	[-]
ν'	Effective Poisson's ratio	[-]
ν'_{ur}	Effective Poisson's ratio for unloading-reloading	[-]
σ'	Effective stress	[kPa]
σ'_1	Effective major principal stress	[kPa]
σ'_3	Effective minor principal stress	[kPa]
σ'_c	Preconsolidation pressure	[kPa]
σ_t	Tensile stresses	[kPa]
τ_f	Mohr-Coulomb failure envelope	[kPa]
τ_{fu}	Undrained shear strength	[kPa]
φ	Friction angle of soil	[°]
φ'	Effective friction angle of soil	[°]
ψ	Dilatancy angle	[°]

Abbreviations

CRS	Constant Rate of Strain
CS	Concrete slab
HS	Hardening Soil
HSs	Hardening Soil with small-strain stiffness
LCC	Lime-Cement Column
LE	Linear Elastic
MC	Mohr-Coulomb

OCR	Over Consolidation Ratio
PI	Plasticity Index
SS	Soft Soil

1 Introduction

Currently in the city of Gothenburg, Sweden, there are four connecting points between the island Hisingen and the mainland (WSP, 2009a). Frequent maintenance is required quite often which further aggravates the congestion problem in Gothenburg. Therefore, an additional connection will be constructed. This will be Marieholm's tunnel which will be constructed underneath Göta älv river and it will connect E45 Marieholm/ Partihallsförbindelsen to E6 Tingstadsmotet/Ringömotet. The construction started in 2014 and is expected to be completed by 2020.

The purpose of the tunnel is to lower the high demand of Tingstad tunnel and add an extra link over the Göta älv river (Trafikverket, 2016). It will also promote traffic safety, environmental and regional development and increase the accessibility to Norra Älvstaden, the port of Gothenburg and the industries located at Hisingen. The tunnel will consist of three lanes in each direction and will be 500 m long, where 300 m consists of an immersed tunnel. The immersed tunnel will be built in segments on land and thereafter will be floated and sunk in to place. Each element will be approximately 100 m long, 30 m wide, 10 m high and weigh about 25 000 tonnes. To be able to construct the tunnel sections on land, a 15 m deep excavation in soft clay is required. One important factor to take into consideration when constructing a deep excavation in soft soil is basal heave (Karlsruud & Andresen, 2008).

Therefore, this MSc thesis will evaluate the basal heave in the deep excavation for the Marieholm tunnel project. The current method to minimize and prevent basal heave failure is underwater excavation and placement of a concrete slab on the bottom of the excavation. Another solution, that is not so well understood or used in Sweden, is the placement of lime-cement columns in the passive side of the retaining wall in order to decrease settlements, wall deformations and basal heave (Ignat, 2015). This method is cost effective and since it is not often used in Sweden it was decided to investigate if this could be a solution for other projects (Larson, 2006).

1.1 Aim

The aim of this thesis is to evaluate if lime-cement columns (LCC) could be used instead of a concrete slab in the Marieholm tunnel project to minimize basal heave. A comparison of the two methods will be performed by using both analytical calculations and the computer program PLAXIS 2D. Given that no constitutive model in PLAXIS captures the real soil behavior, two models will be used, compared and discussed.

1.2 Method

Firstly, a literature study was conducted. The materials reviewed include research articles, master theses and PhDs. Secondly, data from soil investigations in the area were analyzed to determine the required parameters. The values were then inserted in FEM (finite element method) program PLAXIS and calibrated by using the SoilTest option, so that the relevant soil behavior was

captured. Afterwards, basal heave stability was analyzed both in PLAXIS and by analytical calculations. Parametric studies were performed to determine which soil parameters are the most significant for basal heave and analyze how they will influence the behavior of the excavation. To ensure that the problem has been modelled correctly, the obtained values were compared to the real case. Lastly, the two construction methods and two constitutive models were compared and discussed.

1.3 Limitations

Limitations were set to be able to finish the work in a timely manner, these are the following:

- Only basal heave, retaining wall deformations and stability problems in the excavation were considered.
- The installation effects of piles, retaining wall, etc. were not considered.
- The long-term behavior or the cyclic effect of reusing the deep excavation for construction of three tunnel segments were not considered.
- The basal heave stability is only relevant to the behavior that can be found at Marieholm, Gothenburg.
- Only one section was modelled.
- The section was only modelled in 2D.

1.4 Assumptions

The following assumptions were made:

- Isotropic soil layers.
- The section modelled was assumed to be symmetrical and therefore only half of the section was modelled.
- The strut system was simplified and it was assumed that there was no concrete waler for modelling purposes.
- The lime-cement columns were assumed to have the same length and be equally spaced.
- The effect of the excavation on the surrounding infrastructure was not considered since they were deemed to be far enough to not be influenced significantly by the excavation.
- The permeability and the Poisson's ratio for the LCC were assumed to be equal to those of clay layer one.
- The fill layer is 2.4 meters.
- Plane strain model was used in PLAXIS.

2 Literature Study

The following chapters will present two ground improvements methods for deep excavations, concrete slab and lime cement columns. Additionally similar previous studies for the lime-cement columns, a description of the different constitutive models and an explanation of the different methods used for the analytical calculations are presented.

2.1 Ground improvements methods

There is a large array of ground improvements methods that can be used to minimize basal heave. In this thesis only concrete slab and lime cement columns will be considered.

2.1.1 Concrete slab

To prevent basal heave, a concrete plate can be placed in the bottom of the excavation, which acts as a counteracting weight. Given that the excavation is carried out underwater, tremie concrete can be used (Concrete Construction, 1962). The cement is fed by a vertical pipe from a hopper which is spread out to the edges by gravity. The pipe is then raised by the growing cement thickness to achieve a continuously flow of concrete.

2.1.2 Lime-cement columns

Lime-cement columns (LCC) can be used in order to increase the strength and stiffness properties of the soil (SGF, 2000). The main benefits of using LCC are the ability to choose the installation pattern, distance between columns, depth and diameter of the columns. Additionally, it can lead to lower transportation and energy costs and therefore be an economically viable solution (Larsson, 2006).

LCC was initially used for deep stabilization in the 1970s in Sweden. Nowadays there are a range of installation methods and different compositions of lime and cement. Currently, LCC are mostly used beneath road and railway tracks and smaller bridges. This method can be used for soil stabilization, in stability problems and in order not to spread impurities to the ground. However, this report will only focus on the use of LCC to prevent basal heave failure in the deep excavation in Marieholm. The principal difference between this and the other methods is that the columns are installed in the passive part of the soil instead of the active or the shearing side. This is not very common in Sweden and is therefore not so well understood (Ignat, 2015). However, this method has been used successfully for a few case studies, which are presented in Chapter 2.2 Previous studies.

LCC are placed in the ground by mixing the in situ soil and the binder with help of a machine (Larsson, 2006). The machines' mixing head has a nozzle where the binder is fed from. Normally, in Sweden, feeding occurs when the machine is driven into the ground and mixing when the machine is raised. Once the binder is inserted into the ground, a chemical reaction occurs between the binder, water

and the soil. The shear strength of the columns depends on the soil, amount and composition of the binder, temperature of the soil and how well it has been mixed. The hardening process will occur faster with a greater volume of columns.

The above mentioned technique can be carried out with both dry and wet binder. In the wet method, the binder is mixed with water before it is inserted in the soil, whereas in the dry method, the binder is pressed out by air into the soil. The chemical reaction still needs water, and therefore the dry method is more suitable for loose sands and clays with a high water content. However, in the dry method, some water can be used to increase the water content in layers with lower permeability. The composition of the binder is often based on laboratory and field tests and on previous experience of similar soil types since the composite of the binder depends on the actual soil and the requirements that should be fulfilled.

To minimize installation effects, all columns should not be installed at the same time. Instead a gap of one or two rows should be left out and constructed at a later stage. A column which has been damaged during installation will have lower buckling strength, lower capacity against tension and lower bending stresses since there will be layers with weaker zones. Even for a good mixed column, there can be weaker zones due to variations of the soil properties.

To minimize the risk for bending or buckling the columns can be placed in blocks or panels with overlapping zones, see different installation pattern in Figure 1. However, the overlapping zones are weaker which strength decreases with depth.

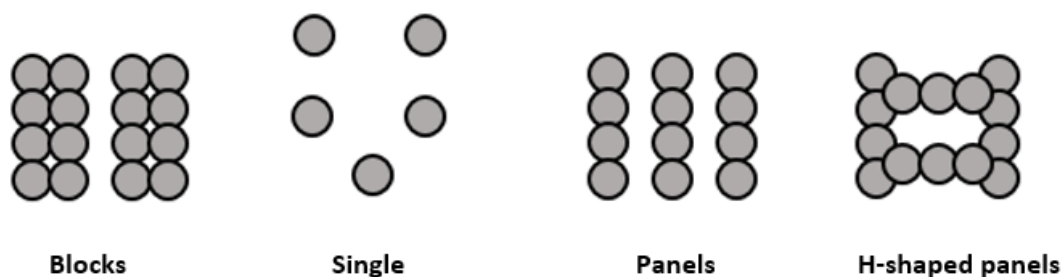


Figure 1: Different installations patterns for Lime-Cement columns.

To produce columns in panels or blocks there should not be any interruptions in order to get a good overlapping zone, even at great depths. The resulting shear stress of the overlap is inversely proportional to installation time, e.g. an installation time of one week will result in zero shear stress.

When strengthening passive zones, as is the case to decrease basal heave and minimize wall movements, it is recommended to use panels, H-shaped panels or blocks.

In Sweden columns are divided into three different categories depending on the hardness and brittleness. The soft columns refers to columns with an undrained

shear strength below 150 kPa, medium hard between 150-300 kPa and hard above 300 kPa. The main difference between the categories is that the strength of the soil between the hard columns is not assumed to have any effect, but in the soft columns the strength of the soil is fully considered, and for the medium hard column, a part of the strength of the soil is considered. In Sweden the maximum length of the column is about 25 m and the diameter of the columns is often 0.5, 0.6 or 0.8 m, where 0.6 m is the most common. However, in Japan larger machines have been used that can produce columns at larger depths, both in land and in water. In the EuroSoilStab, a design guide for soft soil stabilization, the installation methods varies from Swedish standards and maximum column length is about 40 m (EuroSoilStab, 2002).

The columns are placed in the ground by means of a base machine and a drill rod with a mixing tool. This base machine, usually an excavator, has a rotary motor. Before drilling can proceed, the position of each column should be marked on the ground surface, and when the columns are placed in panels, they should be placed very carefully to avoid deviations as it will negatively affect the properties of the columns. The weight of the base machine is about 12-39 ton, diameter of columns 0.5-1.0 m and length 25 m. Additionally the maximum vertical speed is 15 mm/circle and the rotational speed is normally 100-200 circles/min.

When columns are to be used for reinforcement the dry crust needs to be removed. Approximately the uppermost meter of the LCC cannot be considered since it does not have the required strength. Therefore, the weaker part of the columns should be removed and friction material should be placed on the top. Alternatively, geotextile can be placed on the surface and then the columns can be installed underneath the geotextile and be a part of the construction. Additionally, stabilizing work should not be carried out during the coldest months since the equipment cannot penetrate frozen ground and the hardening process of the LCC will be delayed.

2.2 Previous studies- Lime-cement columns in soft soil

Lime-cement columns, LCC, installed on the passive zone of an excavation have been shown to reduce the excavation induced deflections behind retaining structures, reduce structural forces (bending moments in retaining structure, strut and anchor forces) and improve the safety against basal heave failure by several previous studies (Ignat, 2015). However, according to Swedish design guidelines, TK Geo (2013) and Larsson (2006), several assumptions need to be made, where one of them is that the properties of the columns have to be significantly reduced (when they are installed on the passive side). Therefore, the effect of LCC will be reduced in calculations. Due to the uncertainties around the behavior of laterally loaded LCC, Ignat (2015) investigated this phenomenon with both field and laboratory tests.

The main findings of his work were the following: the interaction increases between the soil and the columns with decreasing distance between the LCC rows, and if the distance between the rows is less than three meters, failure will only occur in the clay between the rows. Additionally, the behavior of the LCC

proved to be similar to overconsolidated material in case of extension loading where failure occurs in the weakest zones.

Another similar study was performed by Ignat et al. (2015) where 2D and 3D modelling LCC was compared with PLAXIS. LCC should ideally be analyzed in 3D, however, this study proved that it is possible to model it in 2D. The study looked at failure loss and mechanism, stress-strain relationship and deformation up to failure. The 2D model takes into account the strength reduction in the overlapping zones by defining vertical joints in the soil material. The result of the study showed a good agreement between the 2D and 3D models when considering full overlap strength or overlap strength less than 50%. It also showed good agreement regarding the development of shear stresses in the overlap zones and deformations if the effect of the overlap zone are accounted for (if the yield criteria is not reached). The final conclusions of the study are that the 2D model should include the overlap zone between the columns and the replacement ratio should be higher than 50% in order to get an accurate 2D model.

2.3 Constitutive models

In PLAXIS there are several different constitutive models that can be used to analyze geotechnical problems (PLAXIS, 2016). The two most basic models, the Linear Elastic (LE) and the Mohr-Coulomb (MC) model will be presented in the subchapters below. Additionally, the Soft Soil (SS) and Hardening Soil with small-strain stiffness (HSs) models can be used to model deep excavations and are therefore also presented below.

2.3.1 Linear Elastic model

The Linear Elastic model (LE) is based on Hooke's law of simplified elasticity. The elastic parameters are represented by Young's modulus (E) and Poisson's ratio (ν). It is not suitable for soil conditions since soils are highly non-linear and irreversible, therefore the model is mostly used for materials such as concrete. There is no limit to highest strength that can be applied, and therefore care has to be taken when modeling materials close to their maximum strength.

2.3.2 Mohr-Coulomb model

The Mohr-Coulomb model (MC) is a simple constitutive model in which many of the soil characteristics are not accounted for (PLAXIS, 2016). However, it provides a good basis for materials such as concrete and as a first analysis. With this model a linear elastic perfectly plastic relationship is assumed, see Figure 2. The increase of stress with strain indicates the elastic part and when the stress remains constant, it is behaving perfectly plastically.

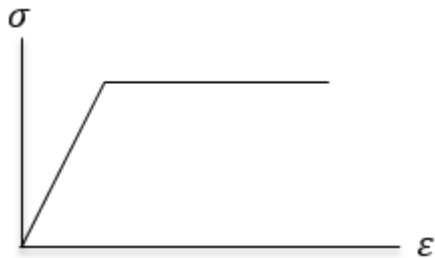


Figure 2: Elastic-perfectly plastic behavior.

The failure is based on the Mohr-Coulomb failure criteria, where failure occurs when the circle touches the failure envelope, see Figure 3 (Knappett & Craig, 2012).

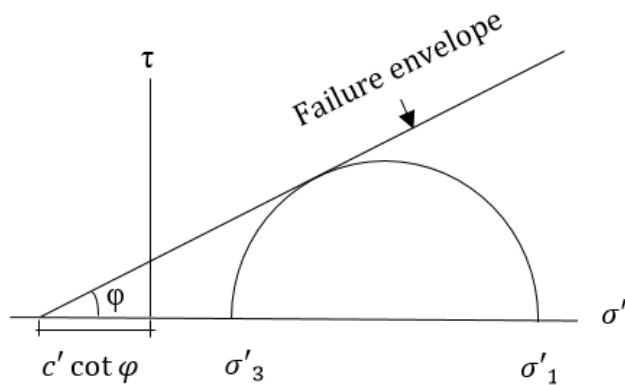


Figure 3: Mohr-Coulomb failure criterion.

The failure envelope is described by equation (1), where c' and φ' are the effective cohesion and the effective friction angle respectively.

$$\tau_f = c' + \sigma' \tan \varphi' \quad (1)$$

A yield surface (f) is used to define when the soil is behaving elastically or plastically. The stresses inside the yield surface have an elastic behavior and those which are on the surface have a perfectly plastic behavior. It is not possible to be outside the yield surface. When f is equal to zero a fixed hexagonal cone is presented in the principal stress space, see Figure 4.

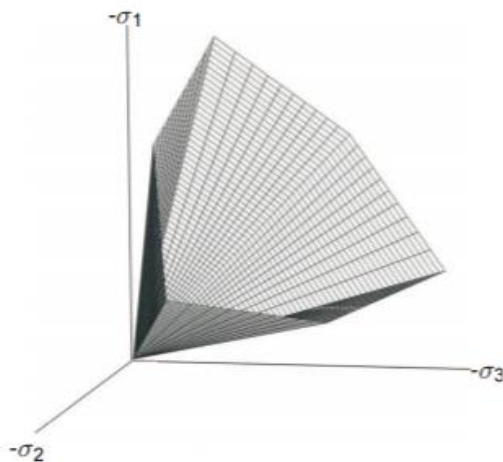


Figure 4: The Yield surface in the principal stress space (PLAXIS, 2010).

The direction of the plastic strains is defined with a flow rule, i.e. a plastic potential function (g). If they are perpendicular to the yield surface, i.e. associated plasticity, the dilatancy will be overestimated.

With this model, tensile stresses are modelled if the cohesion is not zero. However, in reality soils cannot carry tensile stresses so a tensile cut-off point is introduced.

2.3.3 Soft Soil model

The Soft Soil model (SS) is based on the MC failure criterion (PLAXIS, 2016). The main characteristics are that the model is based on a logarithmic relation between volumetric strain (ε_v) and effective stress (p') in the elastoplastic region. There are two different stiffnesses, one for primary loading and unloading/reloading. Additionally, the soil does not have infinite strength and the preconsolidation stress is taken into account.

This model is suitable for near-normally consolidated clays, clayey silts and peat. It is particularly suitable for very soft soil with a high compressibility. The explanation of the SS model can be found below.

The logarithmic stress strain behavior and the introduction of two stiffness parameters are obtained from the oedometer test (see Figure 5).

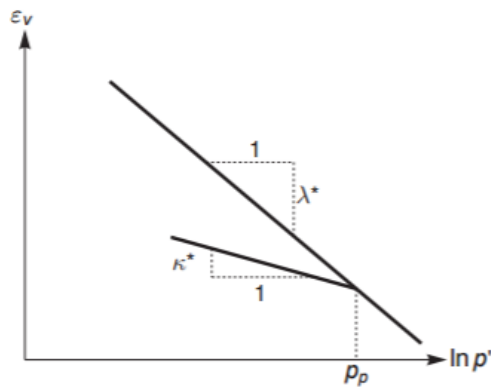


Figure 5: Logarithmic stress-strain relationship (PLAXIS, 2016).

The virgin compression, i.e. primary compression is represented by equation (2), where (λ^*) is the modified compression index. During compression the soil exhibits a plastic behavior.

$$\varepsilon_v - \varepsilon_v^0 = -\lambda^* \ln\left(\frac{p' + c \cot \varphi}{p^0 + c \cot \varphi}\right) \quad (2)$$

For the case of isotropic unloading and reloading, the soil is assumed to behave elastically, equation (3) is used, where the parameter (κ^*) represents the modified swelling index.

$$\varepsilon_v^e - \varepsilon_v^{e0} = -\kappa^* \ln\left(\frac{p' + c \cot \varphi}{p^0 + c \cot \varphi}\right) \quad (3)$$

The yield surface changes non-linearly and has an elliptical shape. The shape is controlled by the parameter, M , which is dependent on K_0^{nc} , whereas the size is governed by the hardening parameter (p'_0), which defines the cap. The elastic stress is bounded by the Mohr-Coulomb criterion, and the cap is represented by the bold lines in Figure 6.

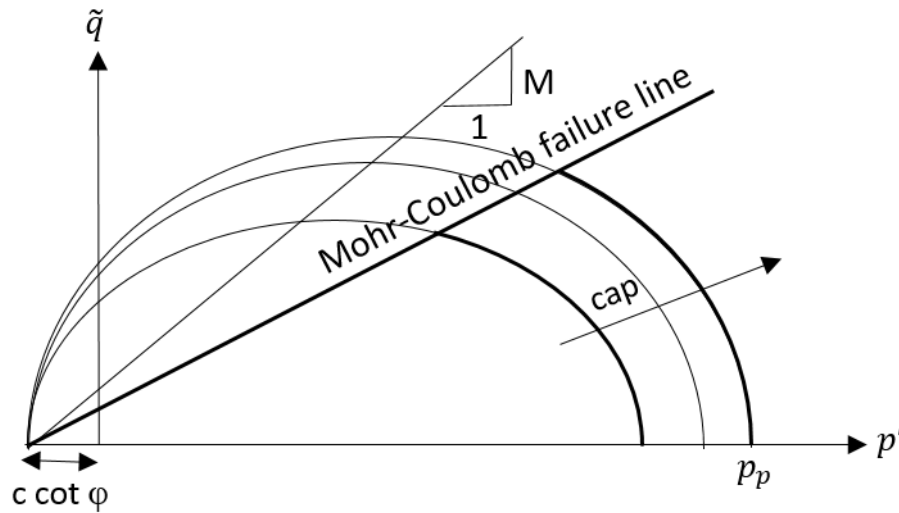


Figure 6: The yield surface, bounded by the Mohr-Coulomb failure line and the cap.

In terms of the direction of the plastic strains increments, it is assumed to be perpendicular to the yield surface, i.e. associated plasticity. This assumption has proven to be valid for clays. A 3D model of the yield surface in the principal stress space can be seen in Figure 7.

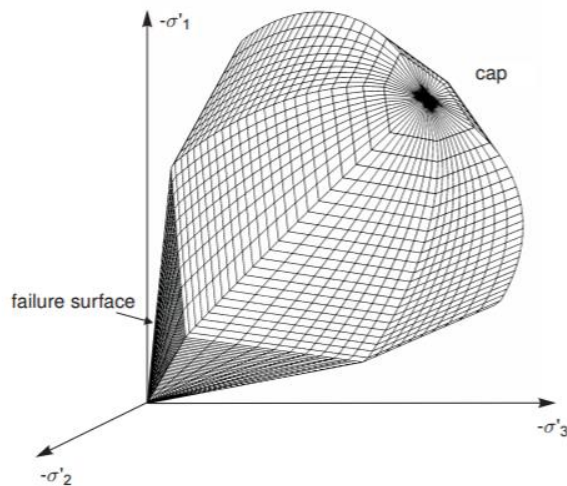


Figure 7: Yield surface in the principal stress space (PLAXIS, 2016).

2.3.4 Hardening Soil model with small-strain stiffness model

The Hardening Soil model with small-strain stiffness model (HSS) is an extension of the Hardening Soil model (HS), where the difference between the two models will be explained later in this chapter (PLAXIS, 2016). The principal difference between the HS and the SS model is that the former models a hyperbolic relationship between axial strain and deviatoric stress while the latter assumes a

logarithmic relationship. Both the models have unfixed yield surface with elliptical shape, but the HS model also has shear hardening, i.e. it is a double hardening model.

The model is based on three different stiffness to account for the stress dependency of soil stiffness. The first stiffness (E_{50}^{ref}) represents primary deviatoric loading and is obtained from drained triaxial test to describe plastic straining. The second stiffness (E_{oed}^{ref}) represents primary oedometer loading and also describes plastic straining. The last stiffness parameter (E_{ur}^{ref}) represents elastic unloading/reloading, is also evaluated from a drained triaxial test and describes elastic straining.

The different stiffnesses taken from the drained triaxial test are represented in Figure 8. The reference pressure is by default set to 100 kPa in PLAXIS.

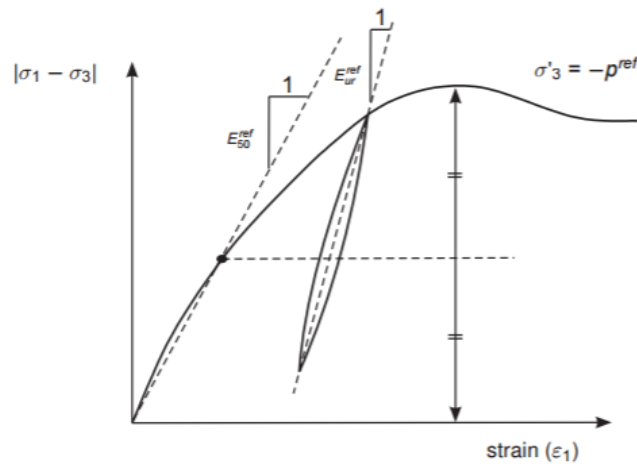


Figure 8: Stiffness's from the drained triaxial test (PLAXIS, 2016).

The primary loading is described by equation (4). Where m is normally equal to one when considering clay. This is due to the fact that clay exhibits a logarithmic relationship between stress and strain.

$$E_{50} = E_{50}^{ref} \left(\frac{c \cos \varphi - \sigma'_3 \sin \varphi}{c \cos \varphi + p^{ref} \sin \varphi} \right)^m \quad (4)$$

The unloading and reloading stiffness is described by equation (5).

$$E_{ur} = E_{ur}^{ref} \left(\frac{c \cos \varphi - \sigma'_3 \sin \varphi}{c \cos \varphi + p^{ref} \sin \varphi} \right)^m \quad (5)$$

The reference primary oedometer loading can be evaluated from an oedometer test, see Figure 9.

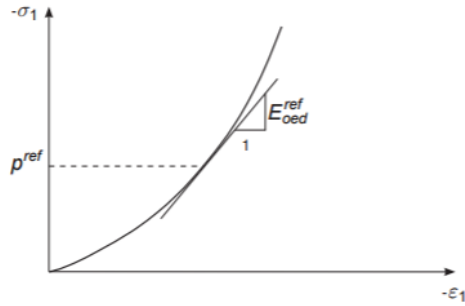


Figure 9: Determination of the reference primary oedometer stiffness modulus (PLAXIS, 2016).

The oedometric stiffness modulus can be calculated from equation (6).

$$E_{oed} = E_{oed}^{ref} \left(\frac{c \cos \varphi - \frac{\sigma'_3}{K_0^{nc}} \sin \varphi}{c \cos \varphi + p^{ref} \sin \varphi} \right)^m \quad (6)$$

The Hardening Soil (HS) model has two hardening processes, shear and volumetric hardening. Shear hardening has a hyperbolic shape and can occur until the Mohr-Coulomb failure criterion is reached, see Figure 10. The flow rule has a linear form and is based on the rate of plastic shear strain and plastic volumetric shear strain.

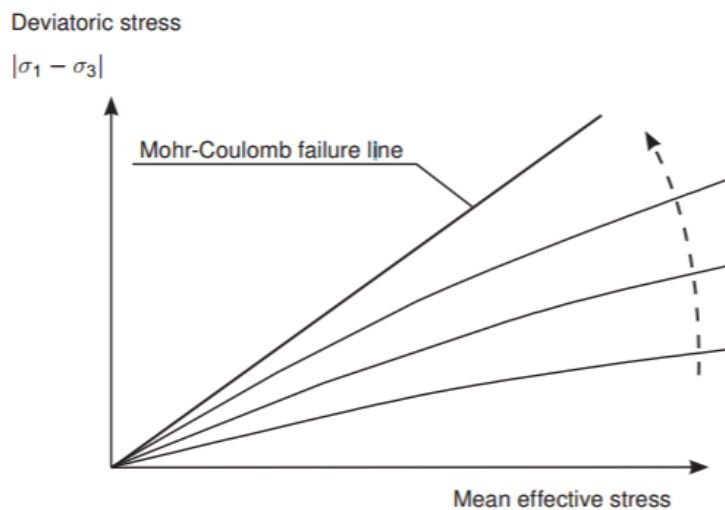


Figure 10: Shear hardening in the HS and HSs models (PLAXIS, 2016).

The other hardening, compression hardening is based on the oedometer modulus. The hardening defines the cap inside which the elastic region is found (see Figure 11) and is a function of the preconsolidation stress (p_p) and the M value.

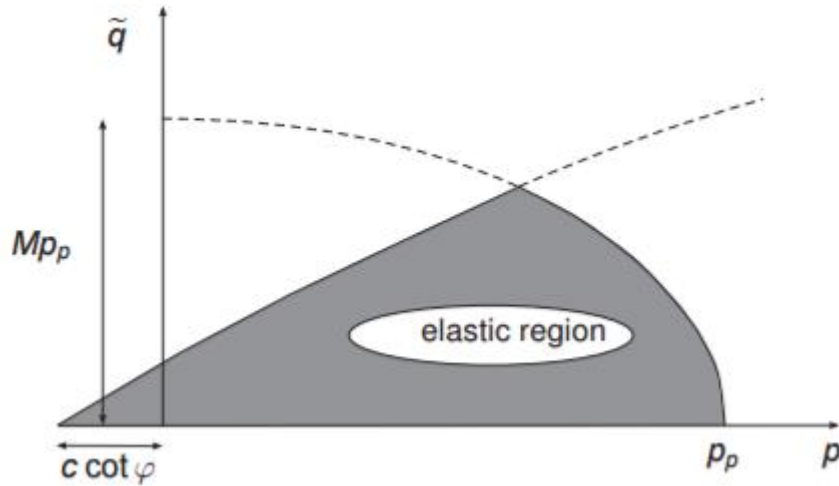


Figure 11: Yield surface of the HS and HSs models (PLAXIS, 2016).

A 3D model of the yield contours in the principal stress space can be seen in Figure 12. The locus cannot expand beyond the MC failure surface whereas the cap is dependent on the preconsolidation stress.

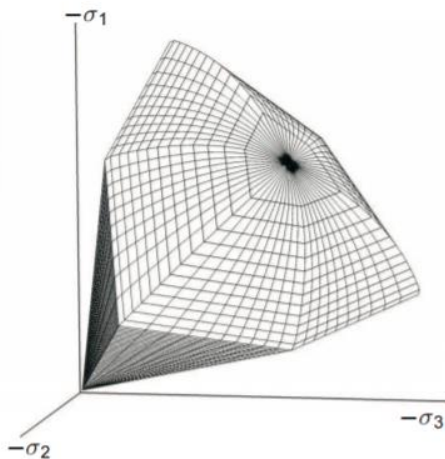


Figure 12: Yield contours in the principal stress space for cohesionless soils (PLAXIS, 2016).

The principal difference between the HS and the HSs models is that the HSs model only considers a small region of the unloading/reloading section to be fully elastic. Therefore, the HS model will lead to an overestimation of settlements, wall deflections, etc. The HSs model incorporates the very small strain stiffness and non-linear dependency of strain amplitude by the use of two further parameters. These are the small-strain shear modulus (G_0) and the strain level corresponding to approximately 70% of the very small-strain shear modulus ($\gamma_{0.7}$). These parameters are hard to measure in conventional tests and can be calculated by empirical relationships instead. According to SGI (2000) the small-strain shear modulus can be calculated by equation (7) when considering soft or medium stiff cohesive soils.

$$G_0 \approx 504 \frac{\tau_{fu}}{w_L} \quad (7)$$

The reference small-strain shear modulus can be calculated by equation (8) (PLAXIS, 2016).

$$G_0 = G_0^{ref} \left(\frac{c \cos \varphi - \sigma'_3 \sin \varphi}{c \cos \varphi + p^{ref} \sin \varphi} \right)^m \quad (8)$$

The threshold shear strain ($\gamma_{0.7}$), can be related to the plasticity index and the ratio of the initial and the shear modulus, that is by default set to 0.722, see Figure 13 (Vucetic & Dobry, 1991).

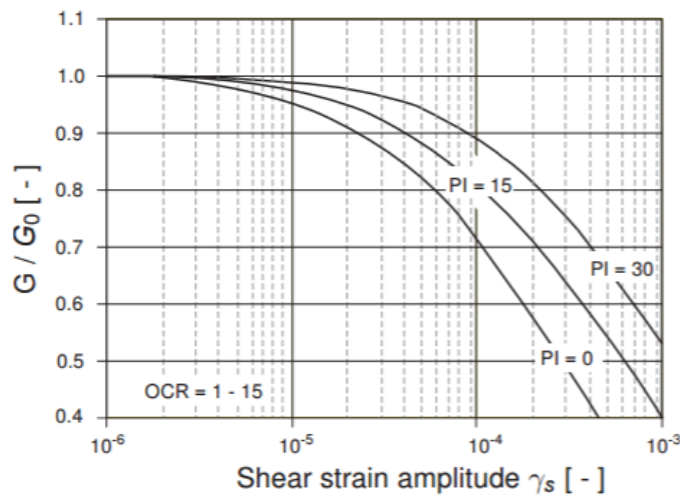


Figure 13: Graph in order to calculate the shear strain amplitude (PLAXIS, 2016).

2.4 Analytical safety calculations

The safety factor against basal heave can be analytically calculated by different conventional methods. In this study, two of the most common analytical calculations will be performed: Terzaghi's and Bjerrum and Eide's methods (Do, et. al, 2013).

The principal difference between the analytical calculations and PLAXIS is that the former is based on an assumed failure surface, where the safety factor is calculated by the resistance force divided by the driving force. In PLAXIS the safety factor is calculated by the phi-c reduction method where the strength is reduced until failure is obtained. The safety factor is equal to the available strength divided by the strength at failure. The calculations performed by PLAXIS also consider the effects of retaining system, excavation wall, horizontal strut, piles, etc.

2.4.1 Terzaghi's method

This is based on Terzaghi's bearing capacity theory and is appropriate for shallow excavations, i.e. when the excavation depth is smaller than the width (Ou, 2016). The model does not take into account the penetration of the wall below the excavation bottom. However, the shear strength is represented in two layers, where the upper layer represents the shear strength of the soil above

excavation (s_{u1}) and the lower layer represent the shear strength below the excavation (s_{u2}). Furthermore, the excavation is assumed to be infinitely long. As mentioned earlier, the critical failure surface is not known. An assumption is made about where it is located which is 0.7 times the width of the excavation ($0.7B$). Failure occurs when the weight of the soil above the excavation is greater than the bearing capacity. The profile of the excavation with the parameters is presented in Figure 14.

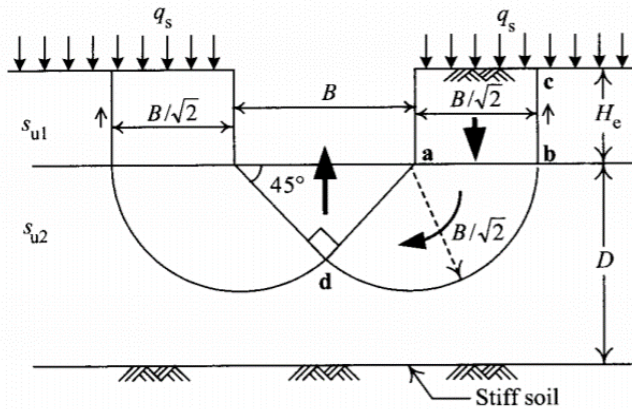


Figure 14: One possible failure mechanism for basal heave according to Terzaghi's method (Ou, 2016).

Depending on the distance between the excavation bottom and the stiff layer, different equations are used to calculate the safety factor. This is due to the fact that the resistant force is partially obtained from the shear resistance of the soil or the stiff layer depending on the depth to the stiff layer. When the distance to the stiff layer is greater than or equal to 0.7 times the width, equation (9) is used. Where $5.7s_{u2}$ is the bearing capacity of the soil, H_e is the length of the excavation, γ is the unit weight of the soil, q_s is the surcharge on the ground, $\frac{s_{u1}}{0.7B}$ is the shear strength of the soil.

$$F_b = \frac{1}{H_e} \cdot \frac{5.7s_{u2}}{\gamma + \frac{q_s}{H_e} - \frac{s_{u1}}{0.7B}} \quad (9)$$

When the distance to the stiff layer is less than 0.7 times the width, equation (10) should be used. Where $\frac{s_{u1}}{D}$ is the resistant force provided by the stiff layer.

$$F_b = \frac{1}{H_e} \cdot \frac{5.7s_{u2}}{\gamma + \frac{q_s}{H_e} - \frac{s_{u1}}{D}} \quad (10)$$

The safety factor should be equal or greater than 1.5 (JSA, 1988; Mana & Clough, 1981).

2.4.2 Bjerrum and Eide's method

Bjerrum and Eide's method is also referred to as the negative bearing capacity method and can be used for both shallow and deep excavations (Ou, 2016).

The failure mode is assumed to be similar to that of a deep foundation when it is loaded in the upward direction where the failure surface is a circular arc with radius $0.7B$. In this method the safety factor is equal to the ultimate unloading pressure divided by the existing unloading pressure. The ultimate unloading pressure is determined by using the bearing capacity equation for deep foundations. The profile of the excavation with the parameters is presented in Figure 15.

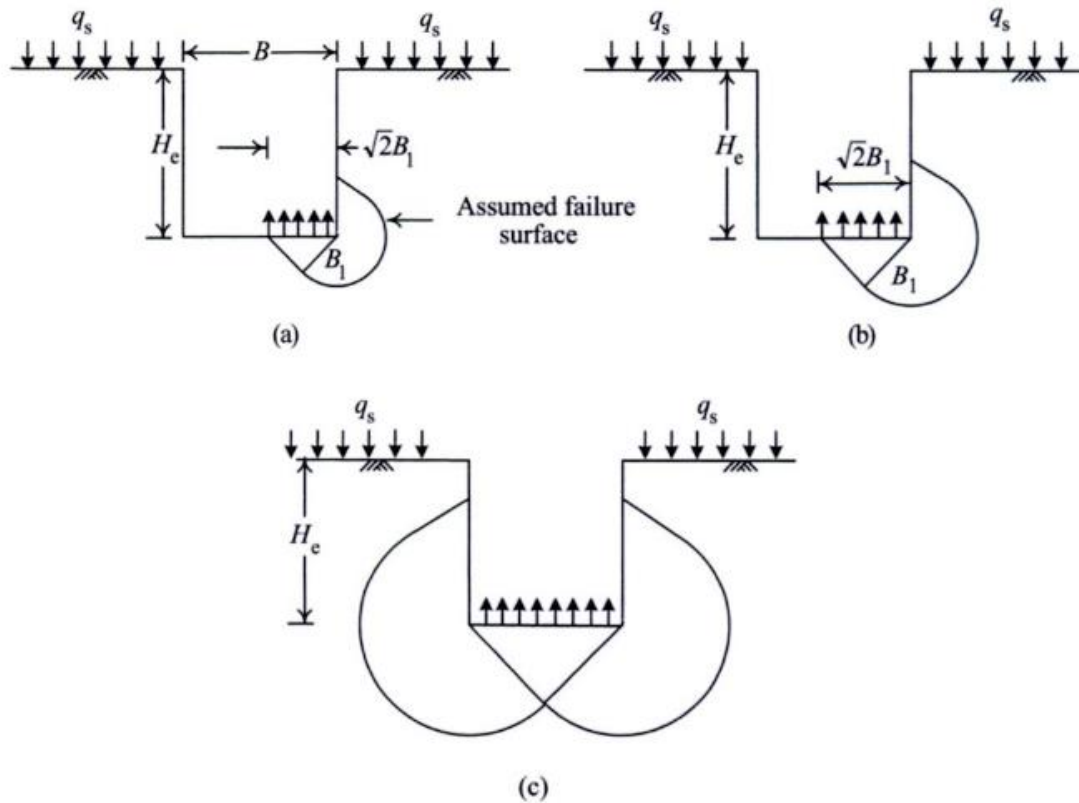


Figure 15: Analysis of basal heave according to Bjerrum and Eide's method: (a) and (b) represent wide failure surface, (c) failure surface extends across the entire bottom of the excavation (Ou, 2016).

The safety factor (F_b) is calculated by equation (11). Where s_u is the shear strength at the toe of the wall, N_c is the of the soil, H_e is the length of the excavation, γ is the unit weight of the soil and q_s is the surcharge load.

$$F_b = \frac{N_c s_u}{\gamma H_e + q_s} \quad (11)$$

The bearing capacity factor (N_c) is calculated from Skempton's bearing capacity factor, see Figure 16.

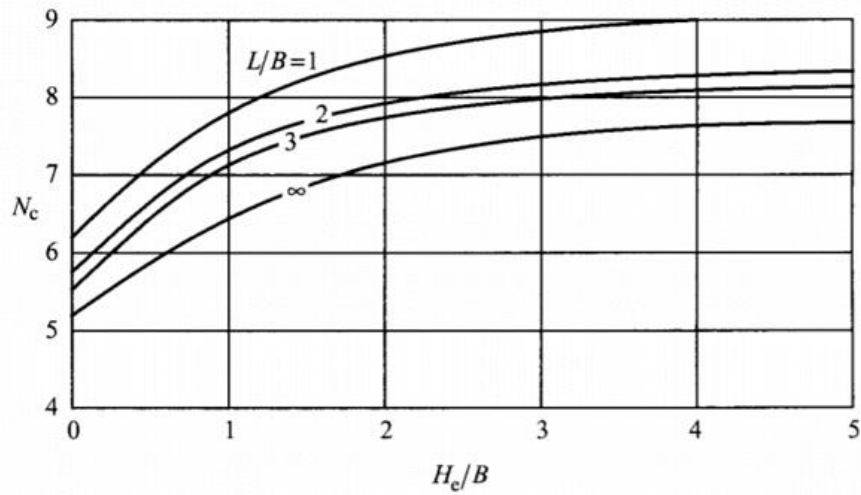


Figure 16 Skempton's bearing capacity factor (Skempton, 1951).

This method is an improvement of Terzaghi's method since the effect of the wall depth is accounted for. The safety factor obtained should be equal or larger than 1.2 (JSA, 1988).

3 Background

In the following subchapters the area description, geology of the area, dimensions of the dry dock, and description of the existing and the lime cement columns construction will be presented.

3.1 Area description

In Gothenburg there are four connections points between the mainland and the island Hisingen. Today there are approximately 130 000 inhabitants at Hisingen where several industries and the Gothenburg port are located. The ongoing Marieholm tunnel project is to be constructed on the southern part of Göta älv river, about 600 m north from the existing Tingstad tunnel (see Figure 17).



Figure 17: Location of the construction site (Google maps, 2017a).

A closer view of the area can be seen in Figure 18 where the white and red line indicates the placement of Marieholms tunnel. Close to the dry dock, two buildings and highly trafficked roads can be found.

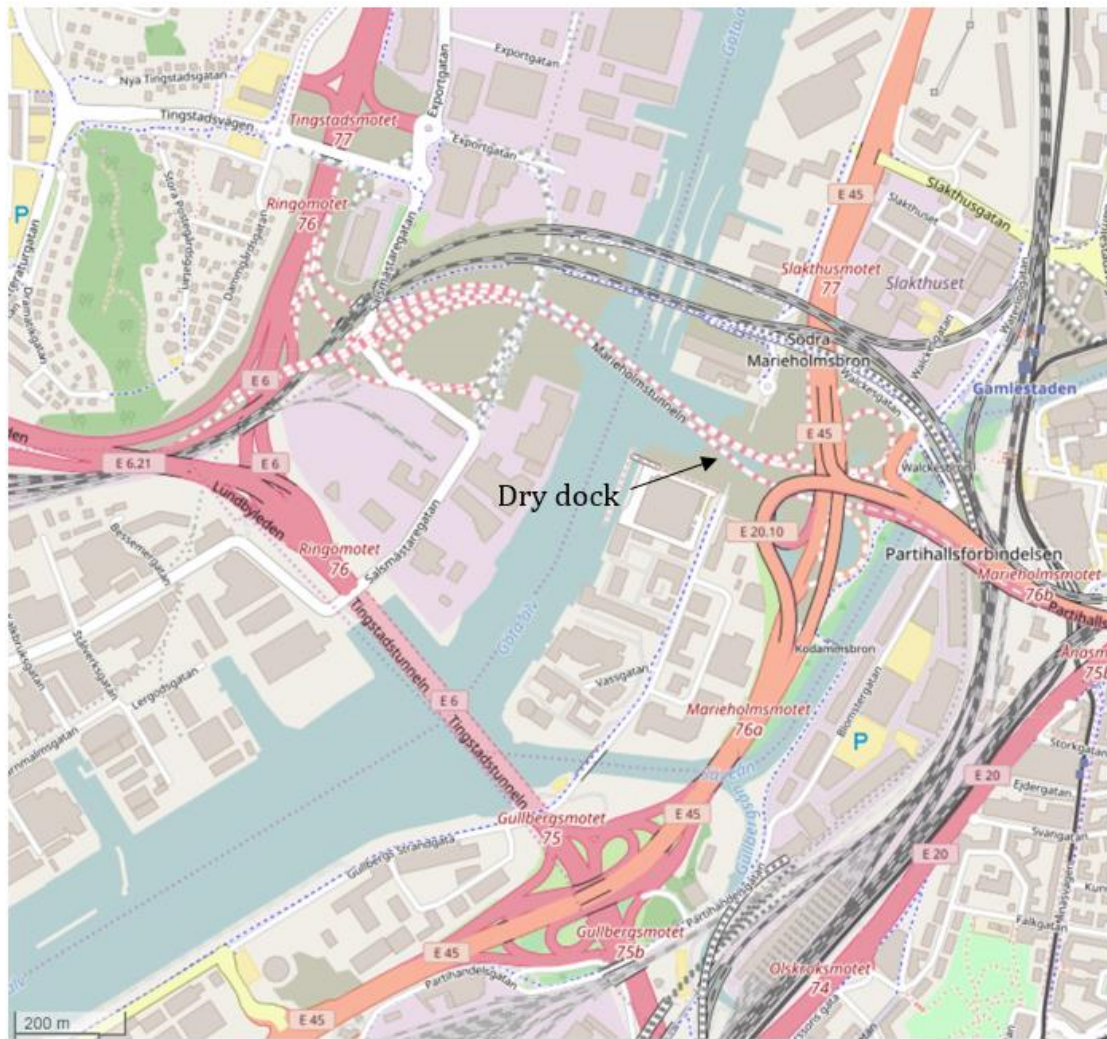


Figure 18: Mariefholms tunnel and surrounding area (OpenStreetMap contributors, 2017).

3.2 Geology of the area

The geology of the area is composed of homogeneous soil layers which were deposited after the last ice age in saline water conditions. The soil of the area is mainly comprised of clay with a thickness of around 100 m (Zublin, 2015a). The thickness of the clay decreases in the west direction. Overlying the clay is a fill layer which is composed of dredged material which thickness is difficult to determine but it is assumed to be 2.4 m. Underlying the clay there is a frictional layer with thickness ranging from 0 to 15 m, composed of sand gravels which is underlain by granite or rhyolite bedrock. A schematic representation of the ground profile can be found in Figure 19.

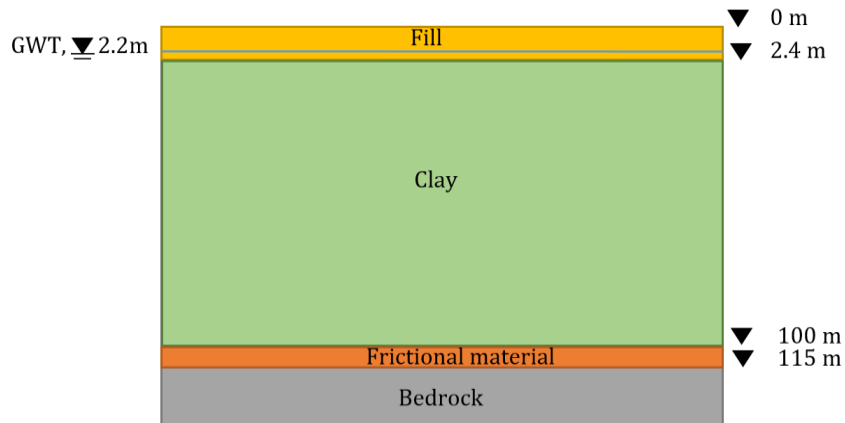


Figure 19: Schematic representation of the ground profile at Marieholm.

3.3 Dry dock

The Marieholm tunnel will be built in three segments, that are about 100 m long, 30 m wide, 10 m high and weigh about 25 000 tonnes. The segments will be built in a dry dock, a 15 m deep excavation, with a pipe-to-pipe retaining wall. After each segment is constructed, the wall beside the river will be removed and thereafter the segment will be floated out in the river and sunk in to place.

A plan view of the dry dock can be seen in Figure 20, it is about 120 m long and the width of the dock varies from approximately 40 to 60 m. In this project section A-A has been chosen to analyse, which is located close to Göta älv river. This was chosen since it is a representative section and possible to model in 2D as a plain strain model was assumed.

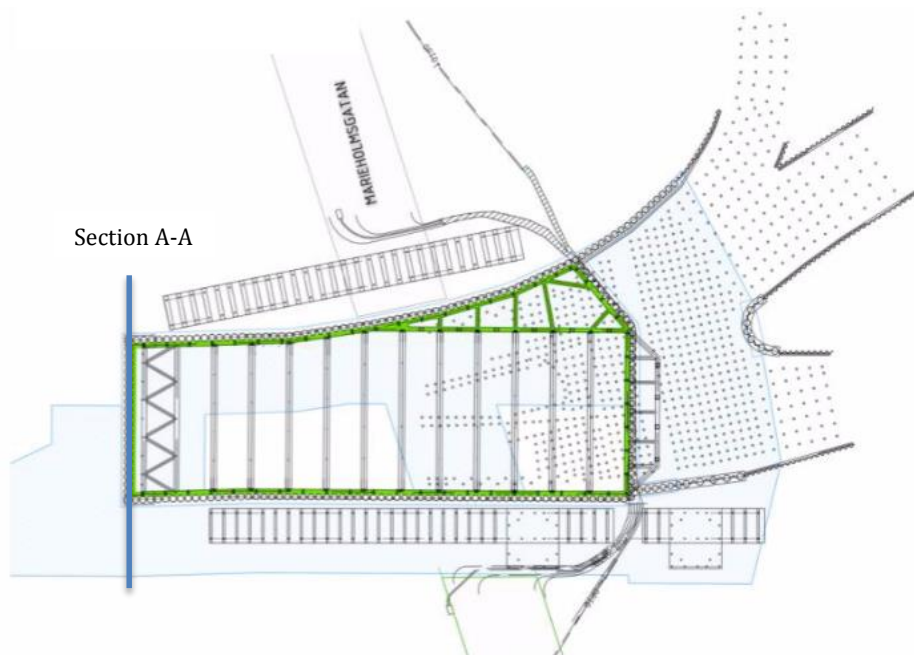


Figure 20: Plan view with the cross section modelled. Adapted from Trafikverket, Design torrdocka, 2017-01-19.

3.4 Description of the planned construction

The construction sequence of the existing dry dock is the following (Trafikverket, 2017a):

1. As heavy machinery was used for construction, a working platform consisting of a 1.5 m gravel layer and a geotextile were first installed. Thereafter, the pipe-to-pipe retaining wall was placed in the ground by vibration. The length of the pipe-to-pipe retaining system is 39 m. This retaining wall is to be 1.5 m above the surface.
2. Waler of concrete and steel.
3. A dry shaft in the form of a bench, i.e. the soil immediately adjacent to the pipe-to-pipe retaining wall will not be dug, will be excavated down to the water table.
4. Tubular steel struts will be placed.
5. Bench removal and excavation to three meters depth.
6. Fill the dock with water to 0.4 m depth.
7. Underwater (UW) excavation in three meters steps. This is done to monitor the construction. If there are deviations from what is expected, remedial actions will be taken.
8. A drainage layer 600 mm thick is to be placed at the bottom of the excavation.
9. A one meter thick slab of concrete will be placed underwater.
10. The water needs to be lowered to avoid overloading the UW concrete slab.
11. Emptying the water from the dock.
12. Replacing in 5 m sections the ballast with 0.7 m thick reinforced concrete.. There will be direct contact with the pipe-to-pipe wall. Shear dowels will be placed in between to reduce differential deflection and injection pipes so that cracks can be sealed when necessary. Furthermore, where there are openings in the UW slab also need to be in this layer. The reinforcement will be in 2.3 m cages. In this way piles can be placed between the cages. The reinforced concrete slab and the UW slab should act as one so shear connectors will be used.
13. Emptying the water to be able to begin the construction of the tunnel sections.

4 Parameters

In the following subchapters parameters that will be used for the analytical calculations and for modelling in PLAXIS are described. The parameters are based on field investigations that have been performed on the site, empirical data and data estimated by Zublin. The location of the field investigations is presented in Appendix A.

The parameters were calibrated by using the setting SoilTest in PLAXIS and the parameters for the lime-cement columns have been evaluated and it is described how they have been model in PLAXIS.

4.1 Structure and fill parameters

The concrete, strut, piles and retaining wall parameters were obtained from the Method Statement (4K394901) document of Zublin (2015d). For the underwater concrete different tensile strengths were used. It was assumed that when the reinforced concrete plate is placed the tensile strength of the underwater concrete will be significantly reduced since it will be reinforced concrete which carries most of the tensile strength. The parameters can be found in Appendix B.

Given that there were no tests carried out on the fill layer, the values were taken from Zublin report (4K284902) (Zublin, 2015c). Given the lack of data, this layer was modelled with the Mohr-Coulomb model. The parameters are presented in Appendix B.

The properties for the drainage layer was taken from Zublins report (4K284902), the values can be found in Appendix B (Zublin, 2015c).

4.2 Lime-cement columns parameters

In order to model lime-cement columns in the passive zone of the excavation in a 2D model in PLAXIS, simplifications have to be made. One way in which LCC panels can be modelled in PLAXIS is by modelling the columns as one block and use the homogenization technique based on linear elasticity. Since the block comprises the LCC columns and the existing soil, representable parameters for the block have been evaluated. An equivalent stiffness (E'_{equi}) for the two materials based on the area ratio can be calculated with equation (12). This is possible as the deformation is assumed to be the same for the whole homogenous block.

$$E'_{equi} = \frac{A_c}{A_T} E'_{col} + \frac{A_s}{A_T} E'_{soil} \quad (12)$$

The stiffness of the soil (E'_{soil}) is obtained from the oedometer modulus, M_0 . The stiffness of the columns (E'_{col}) is determined according to TK GEO 13 (Trafikverket, 2014). The characteristic undrained shear strength is calculated by equation (13) where c_{crit} , can be maximum 100 kPa for soft columns according to TK GEO 13.

$$c_u = c_{crit} \quad (13)$$

Since the shear strength of the columns is lower than 100 kPa the columns can be assumed to have an ideal elastic plastic behavior and follow Mohr-Coulomb criteria. Following the stiffness of the columns can be calculated by equation (14).

$$E'_{col} = 13c_{crit}^{1.6} \quad (14)$$

To calculate the area of LCC panels, the area is assumed to be a rectangle, and the equivalent width (d_e) is smaller than the diameter, a schematic plan view of the area of block and the columns is represented in Figure 21.

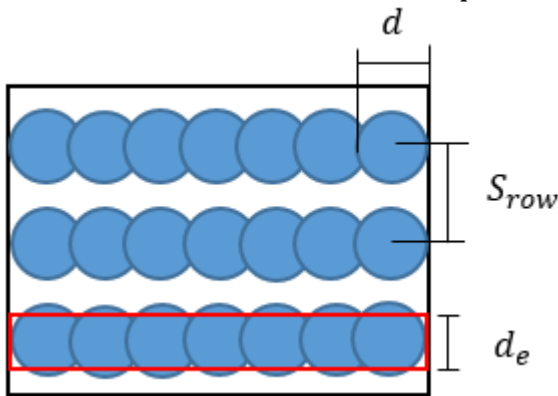


Figure 21: The red rectangle showing the area of the block and the black rectangle showing the area of the rows, seen from above.

According to TK GEO 13 the strengthened soil cohesion should be set equal to zero if they are placed in the passive zone (Trafikverket, 2014). Additionally, the permeability and Poisson's ratio are assumed to be the same as for the soil and the coefficient of lateral earth pressure (K_0) is set to automatic, determined by PLAXIS. All the evaluated values can be found in Appendix C.

Another way in which LCC can be modelled in 2D is by using the method proposed by Ignat et al (2015). The 2D model takes into consideration the 3D effect by assuming two different materials. The blue lines in Figure 22 represent the properties of the columns and the white lines represent the weaker overlapping zones between the columns. The distance between the column rows (see Figure 23) is taken into account on both the white and blue lines. Equations and a more detailed description of the 2D model can be found in Appendix D.

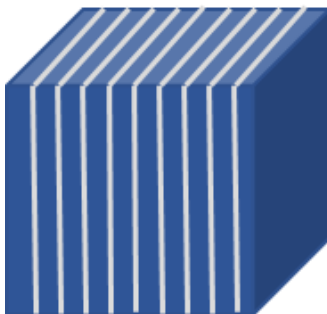


Figure 22: 2D model as per Ignat et al (2015) suggestion.

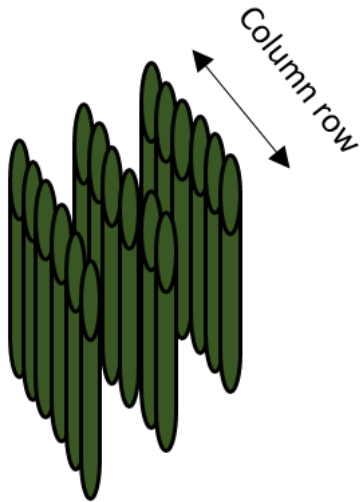


Figure 23: Picture of the column rows, in a 3D model.

4.3 Clay parameters

The density of the clay was obtained from piston samplings, carried out in the Marieholm area. Given that there is a variation in results a representative value was determined (see Appendix E). Since it could be seen from the test that density increases with depth it was decided to model two clay layers, see Table 1.

Table 1: Density for the two clay layers.

Depth	Density	Units
2.4 m to 22.5 m	16	kN/m ³
22.5 m to 102.1 m	16.5	kN/m ³

The effective cohesion was evaluated by making a linear interpolation of the evaluated diagrams from the vane test, cone test and direct shear strength, see Appendix E. They all correlate well to each other. Therefore, it is assumed that it is a reasonable value. The effective cohesion was then calculated by equation (15) (Trafikverket, 2011).

$$c' = 0.1c_u \quad (15)$$

The effective friction angle equal to 30, was taken from TK Geo 11 (Trafikverket, 2011). The dilatancy angle can then be calculated by equation (16).

$$\psi = \varphi' - 30 \quad (16)$$

The permeability was assumed to be equal in the horizontal and vertical directions. The values of the permeability were taken from the CRS test at Marieholm, see Appendix E. Furthermore, given that it has been decided to have two clay layers, two values of permeability were selected and can be seen in Table 2.

Table 2: Permeability for the two clay layers.

Depth	Permeability	Units
2.4 m to 22.5 m	$6.48 \cdot 10^{-5}$	m/day
22.5 m to 102.1 m	$4.32 \cdot 10^{-5}$	m/day

To obtain the coefficient of earth pressure (K_0) value Jaky's empirical relationship was used, see equation (17).

$$K_0 = 1 - \sin \varphi \quad (17)$$

Another method, used in Sweden, to determine the lateral earth pressure coefficient for normally consolidated soils is with equation (18) (Larsson, 2008).

$$K_0^{NC} = 0.31 + 0.71(w_L - 0.2) \quad (18)$$

The preconsolidation pressure was evaluated from the CRS test. A graph of the preconsolidation pressure versus depth and effective stress versus depth can be found in Appendix E.

The OCR was determined by dividing the preconsolidation pressure obtained from the CRS by the in situ effective stresses for the two clay layers. The values obtained are presented in Table 3.

Table 3: The OCR, evaluated from the CRS tests.

Clay layer	OCR	Unit
First layer (2.4 m to 22.5 m)	1.15	-
Second layer (22.5 m to 102.1 m)	1.18	-

The values of the modified compression and the swelling indices were determined from the odometer tests carried out at two different depths in the borehole T1206 (the boreholes can be found in Appendix A). To ensure that they are of good quality a check was carried out based on the initial change of strain. The allowed change of strain is dependent on the water content. The water content varies between 60 and 100% which means that the maximum allowable change in strain is approximately 4% (See Appendix E for more detailed graphs).

The parameters were then calculated by plotting the volumetric strain against the natural logarithmic effective stresses. The modified compression index (λ^*) is the gradient of the line after the preconsolidation pressure, i.e. it represents an increase in loading. This is calculated by equation (19). The modified swelling index (κ^*) was calculated the same way (see equation (20)), except it is the unloading/reloading gradient loop, see Appendix F for graphs. However, the unloading/reloading loop is not a straight line, therefore the gradient should be taken from the part which is relevant to the problem being modelled. Since the problem involves unloading, the relevant part is the furthest part of the unloading line.

$$\lambda^* = \frac{\varepsilon_v - \varepsilon_v^0}{\ln\left(\frac{p' + c \cot \varphi}{p^0 + c \cot \varphi}\right)} \quad (19)$$

$$\kappa^* = \frac{\varepsilon_v^e - \varepsilon_v^{e0}}{\ln\left(\frac{p' + c \cot \varphi}{p^0 + c \cot \varphi}\right)} \quad (20)$$

According to the graphs and equations the following values were obtained (Table 4).

Table 4: Unloading and reloading indices.

Depth	λ^*	κ^*	Unit
19.3 m	0.13	0.0022	-
25.3 m	0.19	0.003	-

Poisson's ratio is a pure elastic constant. The parameter is the ratio of the horizontal stress increment to the vertical stress increment in oedometer unloading and reloading, see equation (21).

$$\frac{v_{ur}}{1 - v_{ur}} = \frac{\Delta\sigma_{xx}}{\Delta\sigma_{yy}} \quad (21)$$

The Poisson's ratio is normally between 0.1-0.2, and is 0.15 by default in PLAXIS (2016).

The M-parameter is directly calculated, i.e. it is not user inserted, from the coefficient of lateral earth pressure, K_0^{nc} (PLAXIS, 2016).

Considering the Hardening Soil model, three stiffness parameters have been evaluated from drained triaxial and CRS tests. The triaxial tests have been evaluated from borehole 14 Z04, even if the sample quality was low, especially the second cycle was not considered reliable, it was used since it was the only test made. The CRS test was taken from borehole 11002, 11004 and 110. The quality seems to be acceptable (i.e. the change in volumetric strain before the preconsolidation stress is reached is less than 4%). In terms of the second clay layer, most of the CRS test were close to the 4% limit which led to some uncertainties. For the first layer, three of the best CRS test were evaluated and compared.

The secant stiffness in standard drained triaxial test (E_{50}^{ref}), the unloading/reloading stiffness (E_{ur}^{ref}) and the stiffness for primary oedometer loading (E_{oed}^{ref}) have been evaluated according to Chapter 2.3.4 Hardening Soil model with small-strain stiffness. This gives the following values according to Table 5 and the evaluated graphs can be found in Appendix G.

Table 5: Stiffness's modules for the HSs model.

Parameter	Depth	Value	Unit
E_{50}^{ref}	17.7 m	10 643	kN/m ²
	27.0 m	8105	kN/m ²
E_{oed}^{ref}	18.0 m	1465/2014	kN/m ²
	24.0 m	1823	kN/m ²
E_{ur}^{ref}	17.7 m	24 359	kN/m ²
	27.0 m	34 960	kN/m ²

Moreover, for the HSs model two further parameters need to be defined. These are the small strain shear stiffness (G_0) and the shear strain level ($\gamma_{0.7}$) at which the secant shear modulus is approximately 70% of the small strain shear stiffness. These were calculated by the equation and graphs given in Chapter 2.3.4 Hardening Soil model with small-strain stiffness. See Appendix H for detailed calculations and Table 6 for the calculated values.

Table 6: Small strain shear stiffness and shear strain at 70% of the small strain shear stiffness.

Parameter	Value	Unit
$\gamma_{0.7}$	0.004	-
G_0	21 600	kN/m ²

4.4 Calibration and validation of parameters

In order to get the most accurate model possible, the evaluated parameters from the field investigations have been calibrated. This was done by using the setting SoilTest in PLAXIS. Since the Soft Soil and the Hardening Soil small-strain stiffness models will be used to model the excavation, these were used to plot the graphs in the SoilTest. The aim of this calibration is to match the graphs in PLAXIS with the graphs evaluated from the field. This is done by changing the input parameters. However, given that it is not possible to obtain a perfect fit, it is important to calibrate the part which describes the relevant soil behaviour for unloading. In the case of the oedometer and the drained triaxial tests it is the unload/reload loop. In terms of the CRS tests it is the compression line before the preconsolidation stress has been reached.

4.4.1 Parameters for the Soft Soil model

The oedometer and the CRS tests at borehole T1206, at a depth 19.3 m and 25.3 m, have been used to calculate and calibrate the parameters for the Soft Soil model. However, for the CRS at a depth of 25.3 m, the borehole 110 at depth 24 m was used instead as the former is of bad quality (see Appendix F for quality chart). The preconsolidation for the oedometer test in PLAXIS was set to 90% of the preconsolidation from the CRS test due to the different strain rates which the tests were conducted at. The oedometer and CRS tests should have the same compression modulus (M_L) and can therefore be compared in order to determine if the quality of the tests are good. In Figure 24 and Figure 25 it can be seen that the compression modulus are not the same. It should be noted that the oedometer test was transported from Gothenburg to Linköping (approximately 280 km), where the test was performed. This could explain why the CRS and

oedometer tests did not have the same stiffness modulus, and also why the oedometer test should be evaluated with caution. Furthermore, in the oedometer test only one point after the unload/reload point was measured. The preconsolidation pressure lies somewhere between these two points.

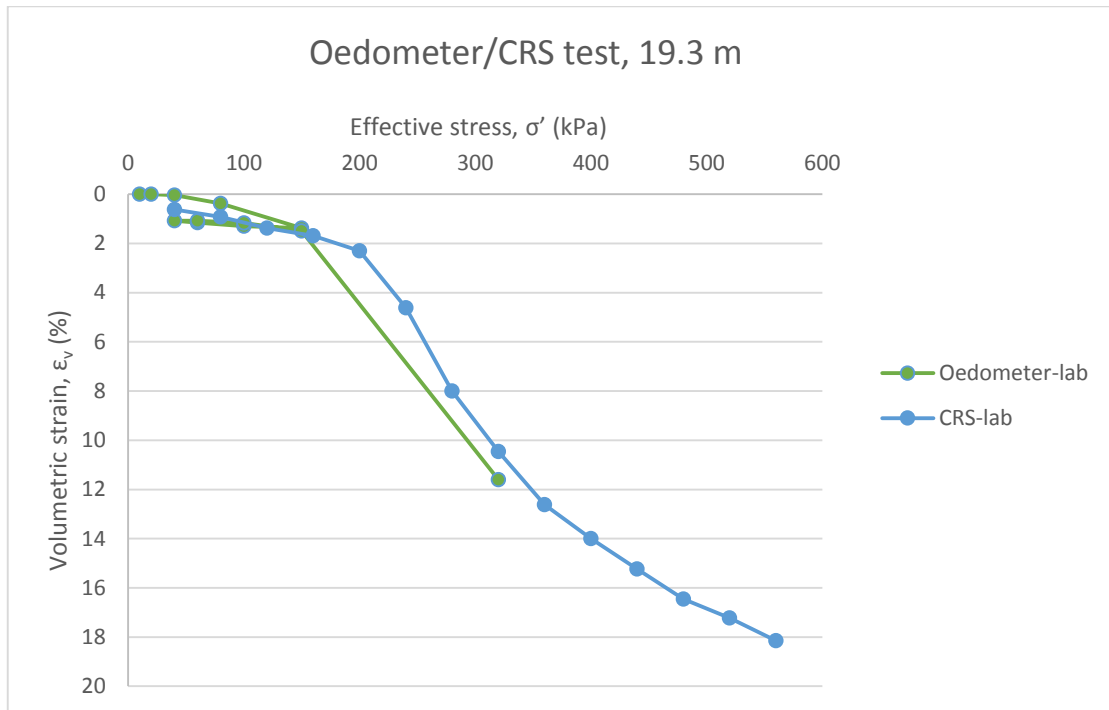


Figure 24: Comparison of the oedometer and CRS lab data at 19.3 m.

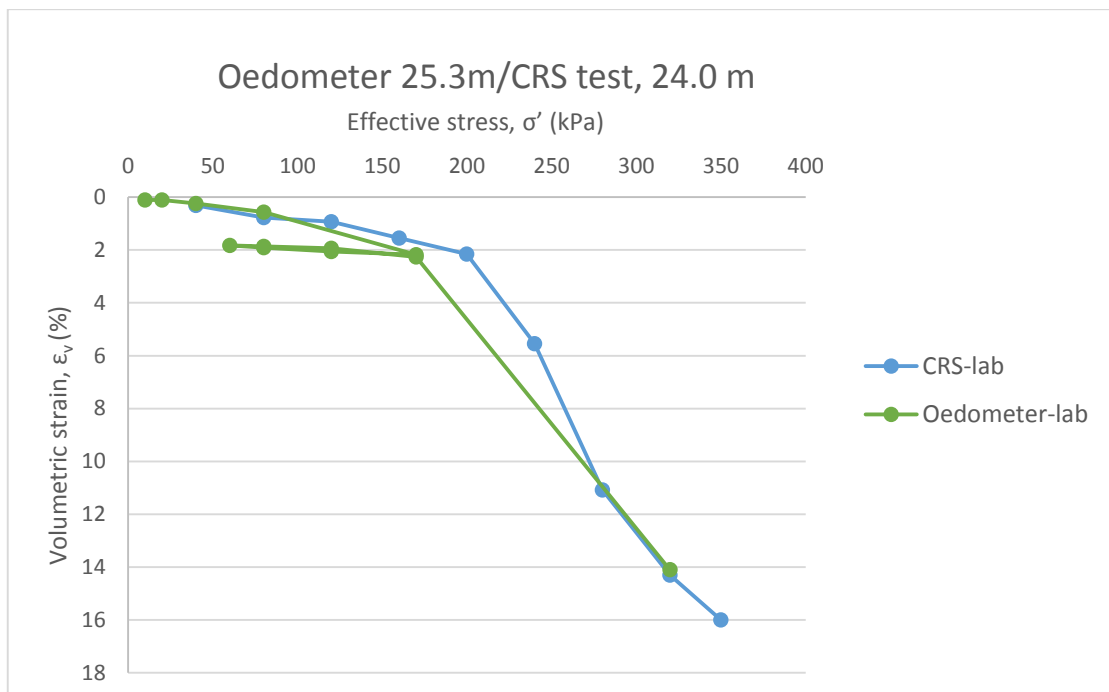


Figure 25: Comparison of the oedometer and CRS lab data at 25.3 m.

Since the oedometer test is not reliable, it was decided to firstly calibrate the CRS test and thereafter use the same values for the oedometer test. By increasing the modified swelling and the compression index, the result from SoilTest correlates

quite well with the lab result for the CRS test (see Table 7 for the values changed, and for all parameters and diagrams, see Appendix I).

Table 7: Evaluated and calibrated values for the soft soil model.

Parameters	Evaluated parameters		Calibrated values		Units
	19.3m	25.3m	19.3 m	25.3 m	
Modified compression index, λ^*	0.13	0.19	0.15	0.20	-
Modified swelling index, κ^*	0.0022	0.003	0.0082	0.007	-

Thereafter, the oedometer test was plotted with the same values as the CRS test, where the modelled phases can be found in Appendix I. The reason why no other parameter, apart from the modified swelling and compression indices, were changed was because they did not result in any significant changes. The graphs and used parameters can be found in Appendix I.

A comparison of the two tests can be seen in Figure 26 and Figure 27, where both test results are based on the calibrated CRS test.

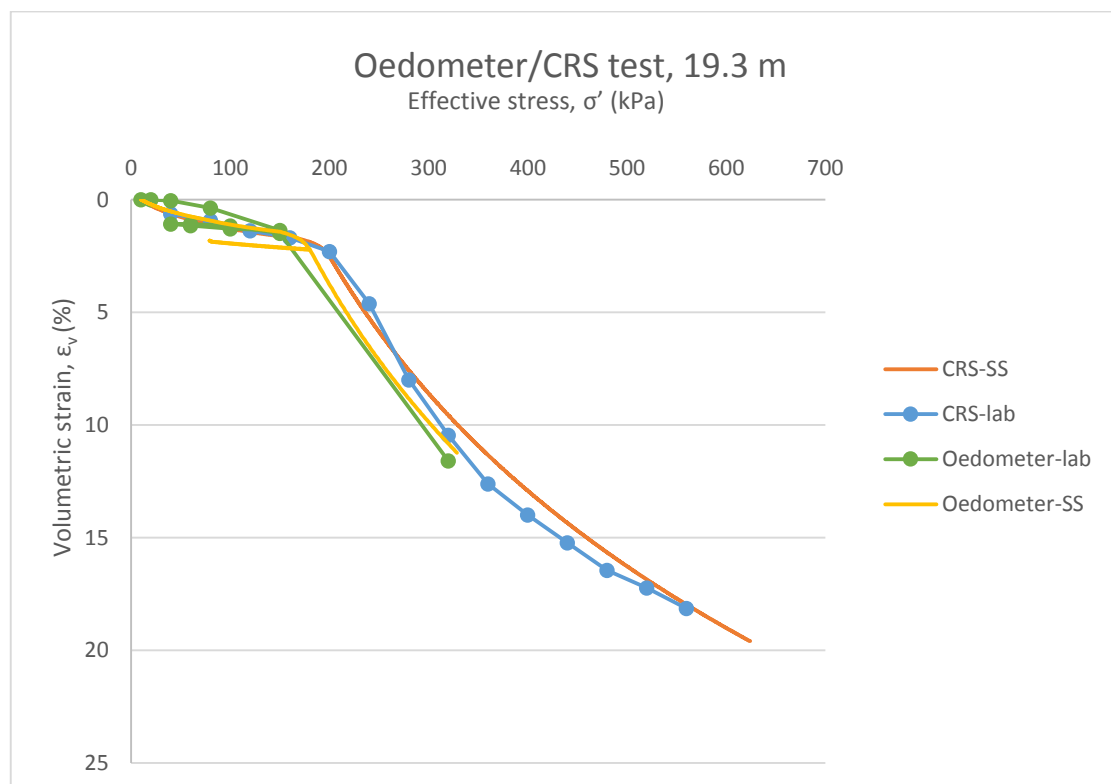


Figure 26: Comparison between the oedometer and CRS-test with the final calibrated values at 19.3 m.

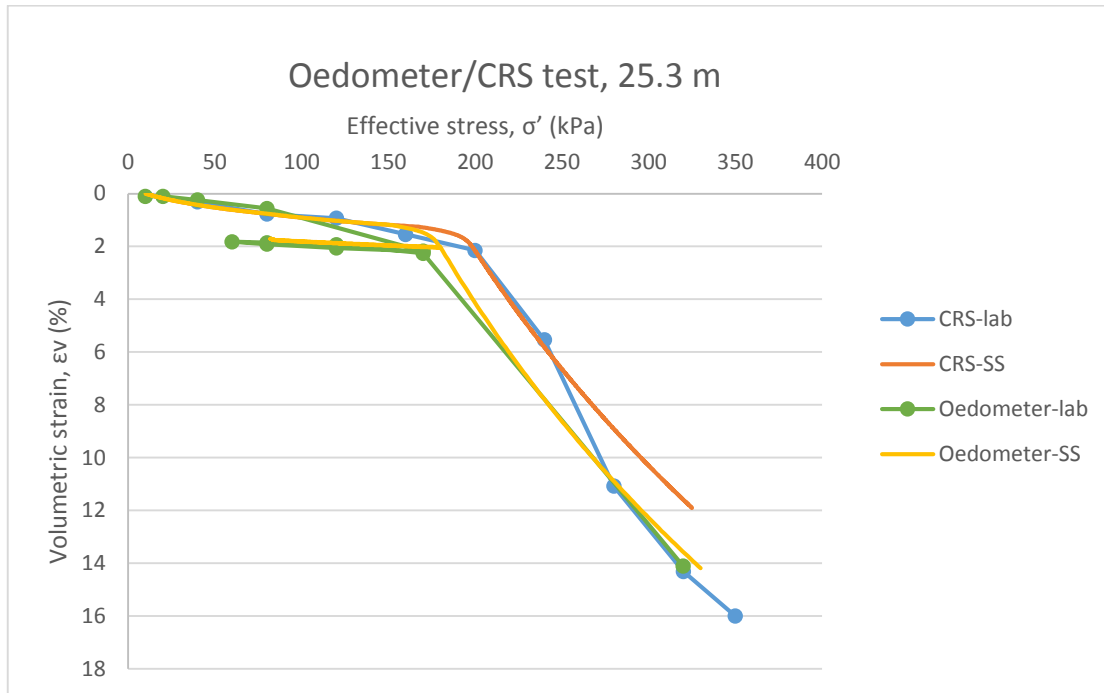


Figure 27: Comparison between the oedometer and CRS-test with the final calibrated values at 25.3 m.

Moreover, it should be noted that borehole T1206 is located in Göta älv river. Therefore, it was decided to evaluate CRS tests which are located close to the excavation. This was done in order to ensure that borehole T1206 is representative for the problem being modelled. The stiffness modulus, M_L , of the different boreholes are presented in Table 8.

Table 8: Stiffness modulus after the preconsolidation stress at different boreholes location.

Borehole number	M_L [kPa] at approx. 19m	M_L [kPa] at approx. 25 m
T1206	1160 (18 m, silty clay)	780
110	740 (18 m)	730 (24 m)
11002	830 (18 m)	820 (30 m)
11004	1080 (18 m, silty clay)	880 (27 m)
21015	730 (bad quality)	1270 (33 m bad quality)

As can be seen there is a variation in the stiffness modulus, especially at a depth of 19 m. This can be explained by the fact that the sample in Göta älv river contains silt. This results in a higher stiffness than if it was the sample just consisted of clay. However, for 25 m the values correlate quite well.

4.4.2 Parameters for the Hardening Soil model with small-strain stiffness

The stiffness parameters that were used in the Hardening Soil model with small-strain stiffness have been evaluated from the drained triaxial and CRS tests. The parameters have been set up in SoilTest and calibrated in order to get the best fit according to the lab data. The focus was to match the behavior before the preconsolidation pressure and for the unload/reload loop since it is impossible

to get a perfect fit and it is these behaviors which are relevant for the problem being analysed. Since the drained triaxial tests were not of good quality it was decided to have a better fit in the CRS test for the two relevant depths. The values which were altered were just the stiffness parameters since the others did not have such a great impact. A comparison of the lab data and the result from the SoilTest in PLAXIS can be found in Figure 28-Figure 31.

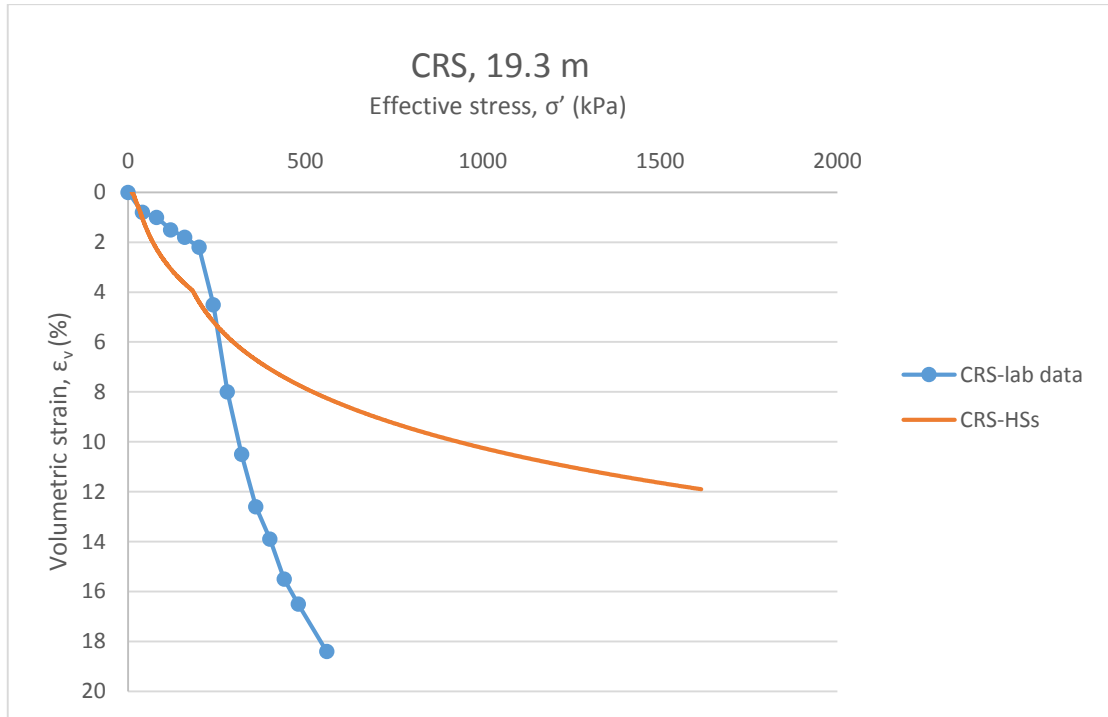


Figure 28: Comparisons between the lab data and data evaluated from SoilTest for the CRS test at 19.3 m.

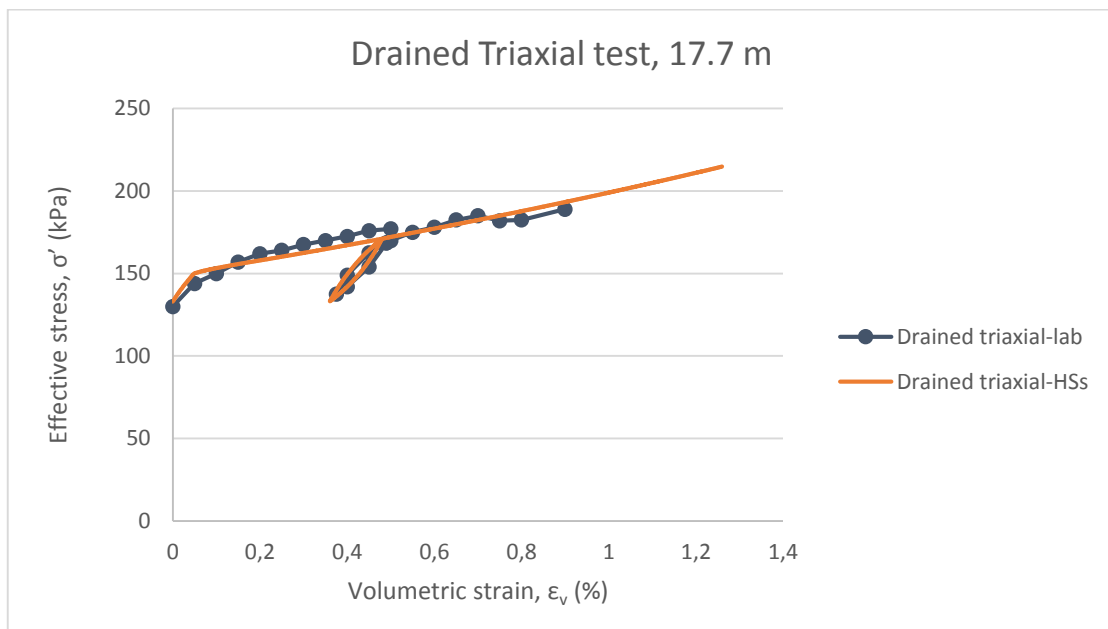


Figure 29: Comparisons between the lab data and data evaluated from SoilTest for the drained triaxial test at 17.7 m.

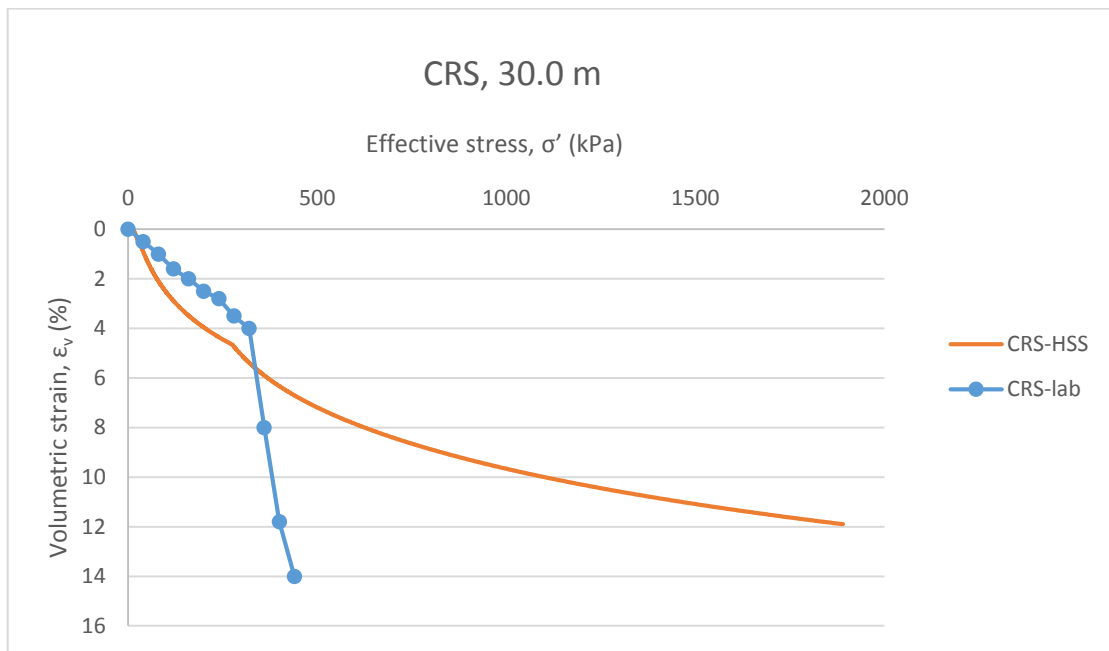


Figure 30: Comparisons between the lab data and data evaluated from SoilTest for the CRS test at 30.0 m.

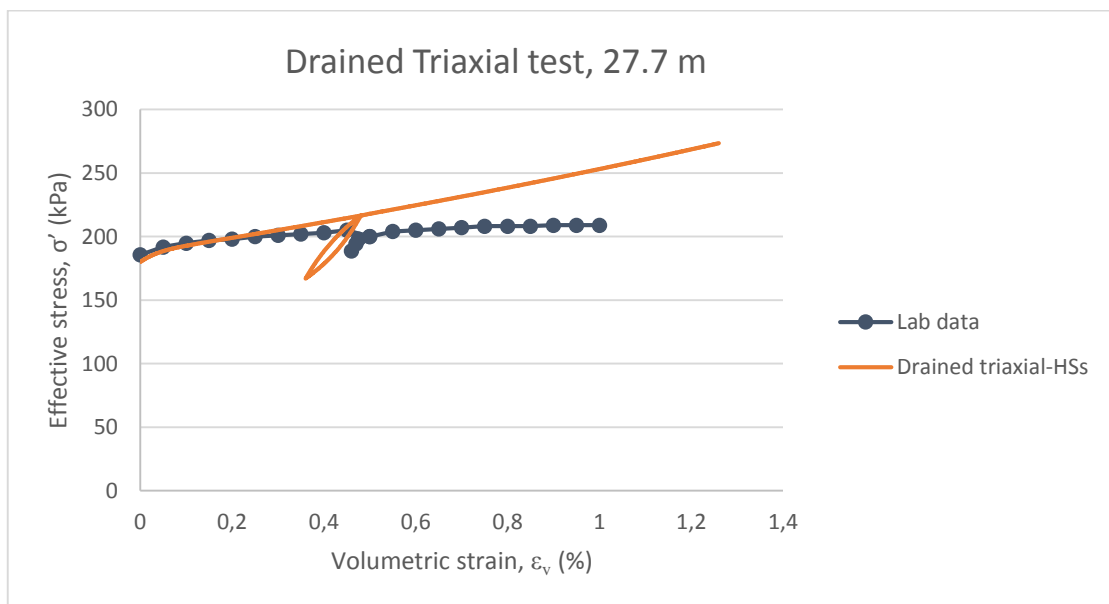


Figure 31: Comparisons between the lab data and data evaluated from SoilTest for the drained triaxial test at 27.7 m.

The drained triaxial test and the CRS test are not at the same depth due to lack of data. The drained triaxial test is from borehole 14Z04 and the CRS is from borehole T1206 for depth 19.3 m, and borehole 110 for depth 25.3 m. Furthermore, the CRS tests could not be matched perfectly. If the power (m) was reduced to 0.5 a better match was obtained. However, it was decided not to do this as clay has got a logarithmic stress-strain behaviour and therefore m should be equal to one.

In Table 9, both the initial and the calibrated values of the stiffness parameters can be found. A detailed table of all the input parameters can be found in Appendix J.

Table 9: Stiffness moduli.

Parameter	Depth	Initial values	Calibrated values	Unit
E_{50}^{ref}	17.7 m	10 643	5000	kN/m ²
	27.0 m	8105	5000	kN/m ²
E_{oed}^{ref}	19.3 m	1465/2014	2500	kN/m ²
	27 m	1823	2500	kN/m ²
E_{ur}^{ref}	17.7 m	24 359	15 000	kN/m ²
	27.0 m	34 960	15 000	kN/m ²

The value of E_{50}^{ref} is not realistic for 27 m and E_{ur}^{ref} for the same depth is too high. Furthermore, E_{oed}^{ref} was obtained from CRS tests in which the initial change in strain was approximately 4% and therefore the quality is not so good. In order to ensure that the stiffness chosen are realistic equation (22) and equation (23) were used as a guidance (PLAXIS, 2016).

$$E_{ur}^{ref} = 3E_{50}^{ref} \quad (22)$$

$$E_{50}^{ref} = 1.25E_{oed}^{ref} \quad (23)$$

4.4.3 Correlation between the Soft Soil and the Hardening Soil small-strain stiffness models parameters

The modified compression and swelling indices in the Soft Soil model are related to the stiffness parameters of the Hardening Soil model with small-strain stiffness model by equation (24) and equation (25).

$$E_{oed}^{ref} = \frac{p^{ref}}{\lambda^*} \quad (24)$$

$$E_{ur}^{ref} \approx \frac{2p^{ref}}{\kappa^*} \quad (25)$$

However, given that the relationship between the stiffness must be within certain limits it is not possible to use the modified compression and swelling indices simultaneously to calculate E_{oed}^{ref} and E_{ur}^{ref} . Therefore, firstly the oedometer stiffness moduli, E_{oed}^{ref} , was estimated based on λ^* . Thereafter, E_{50}^{ref} and E_{ur}^{ref} were calculated by equation (26) and equation (27).

$$E_{ur}^{ref} = 3E_{50}^{ref} \quad (26)$$

$$E_{50}^{ref} = 1.25E_{oed}^{ref} \quad (27)$$

The same procedure was used to estimate E_{ur}^{ref} according to κ^* . The values obtained are presented in Table 10.

Table 10: Stiffness moduli values according to the Soft Soil and the Hardening Soil model with small-strain stiffness.

Parameter	Depth	Values according to λ^* from SS	Values according to κ^* from SS	Calibrated values according to tests	Unit
E_{50}^{ref}	17.7 m	833	8130	5000	kN/m ²
	27.0 m	625	9524	5000	kN/m ²
E_{oed}^{ref}	18.0 m	667	6504	3051	kN/m ²
	24.0 m	500	7619	3051	kN/m ²
E_{ur}^{ref}	17.7 m	2500	24 390	15 000	kN/m ²
	27.0 m	1875	28 571	15 000	kN/m ²

As can be seen these differ significantly from those calibrated according to lab tests. Furthermore, when using the values from the SS model, the small shear stiffness is too high. It had to be reduced to $10.4 \cdot 10^3$ kN/m² for PLAXIS to be able to model it. Moreover, the graphs were an even worse fit with these values (see Appendix K). Therefore, it was decided to use the calibrated values from the tests instead.

5 Calculations

In the following subchapters, analytical calculations are presented together with description of how the calculation in the program PLAXIS has been performed. These include description of phases that have been modelled in PLAXIS, the effect of loads, piles and lime-cement columns, and an explanation of how the parametric studies have been performed.

5.1 Analytical safety calculations

The safety factor against basal heave for both the concrete slab and the LCC was calculated with Bjerrum and Eide's method, and additionally the Terzaghi's method was used for the concrete slab.

5.1.1 Terzaghi's method

The safety factor was calculated according to Chapter 2.4.1 Terzaghi's method. For this project the depth to the stiff layer is greater than $0.7B$ and therefore equation (28) was used to calculate the safety factor (F_b).

$$F_b = \frac{1}{H_e} \cdot \frac{5.7s_{u2}}{\gamma + \frac{q_s}{H_e} - \frac{s_{u1}}{0.7B}} \quad (28)$$

For the structure to be considered safe the safety factor should be equal to or higher than 1.5.

5.1.2 Bjerrum and Eide's method

The safety factor was calculated according to Chapter 2.4.2 Bjerrum and Eide's method. For the structure to be considered safe, the safety factor should be equal to or higher than 1.5, according to equation (29). The shear strength for the LCC was set to 100 kPa (Trafikverket, 2016).

$$F_b = \frac{N_c s_u}{\gamma H_e + q_s - q_c} \quad (29)$$

5.2 PLAXIS

The PLAXIS version 2015 is used to model a plane-strain model with 6-Noded elements. Given that there is no impermeable layer in the model and the water is able to flow freely, all boundaries were set to open apart from the symmetry line which was set to closed.

5.2.1 Model 1-Concrete slab

In Table 11 the description of the different stages for modelling the concrete slab in PLAXIS can be found. The loading type in all cases is staged construction. The excavation was modelled with both Soft Soil and Hardening Soil small-strain stiffness models. It should be noted that when the excavation was carried out, water entered from the Göta älv river into the excavation and therefore it was

decided to refill the dock with water. In order to compare the models with the measurements taken, the refilling of the dock after the placement of the reinforced concrete was modelled.

Table 11: Description of the phases used in the PLAXIS model.

Phase	Description	Calculation type	Duration (days)
0	Initial phase	K0 procedure	-
1	Piles installation	Consolidation	50
2	Crane deck construction	Consolidation	21
3	Retaining wall installation	Consolidation	139
4	Excavation of a dry shaft	Consolidation	7
5	Strut installation	Consolidation	16
6	Dry excavation and bench removal, 2.0 m deep	Consolidation	16
7	Underwater excavation, 6.6 m deep	Consolidation	16
8	Underwater excavation, 12.0 m deep	Consolidation	17
9	Underwater excavation, 16.7 m deep	Consolidation	16
10	Drainage layer	Consolidation	17
11	Underwater concrete	Consolidation	17
12	Ballast and lowering the water inside the dock	Consolidation	19
13	Emptying of the dock	Consolidation	10
14	Replacement of ballast to reinforced concrete	Consolidation	48
15	Fill the dock with water	Consolidation	10
16	Consolidation	Consolidation	74
17	Emptying of the dock	Consolidation	10

5.2.2 Model 2-Lime-cement columns

In Table 12 the description of the different stages for modelling the lime-cement columns in PLAXIS can be found. The loading type in all cases is staged construction. The excavation was modelled with both Soft Soil and Hardening Soil small-strain stiffness models. Given that it is not known what caused water to flow into the dock, it has been assumed that after the concrete plate is installed, the dock will be filled with water.

Table 12: Description of the phases used in the PLAXIS model for the LCC.

Phase	Description	Calculation type	Duration (days)
0	Initial phase	K0 procedure	-
1	Piles installation	Consolidation	50
2	Crane deck construction	Consolidation	21
3	Retaining wall installation	Consolidation	139
4	Excavation of a dry shaft	Consolidation	7
5	Strut installation	Consolidation	16
6	Dry excavation and bench removal, 2.0 m deep	Consolidation	16
7	Excavation 1, 2.4 m deep	Consolidation	16
8	Excavation 2, 6.4 m deep	Consolidation	16
9	Excavation 3, 8.4 m deep	Consolidation	16
10	LCC installation (15.8-33.4m deep)	Consolidation	28
11	Excavation 4, 15.8 m deep	Consolidation	17
12	Concrete	Consolidation	20
13	Fill the dock with water	Consolidation	10
14	Consolidation	Consolidation	74
15	Emptying of the dock	Consolidation	10

Figure 32 represents phase 10 in the PLAXIS model. After the LCC is installed (the grey area), the soil above will be excavated.

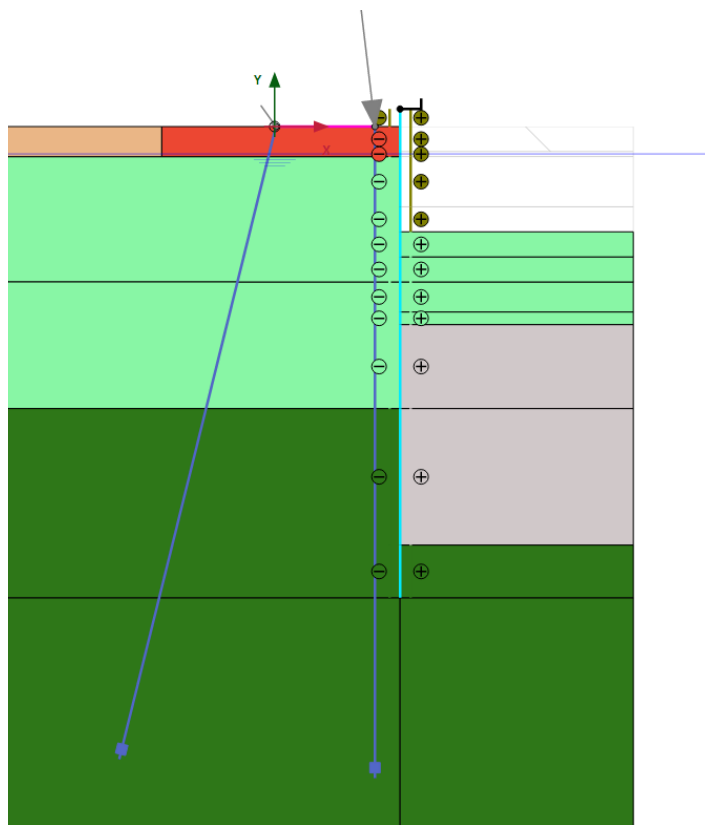


Figure 32: Picture showing how it will look after phase 10, where the grey area represents the LCC.

5.2.2.1 Modelling LCC with Ignat's method

The effect of modelling LCC as a block or as a composite material as suggested by Ignat (2015) was investigated in the Soft Soil model. It was only investigated in this constitutive model as it is assumed that there would be the same variations for the Hardening Soil with small-strain stiffness model. The model had the same construction stages as for the lime-cement columns, the only difference is how the LCC have been modelled in PLAXIS, see Figure 33.

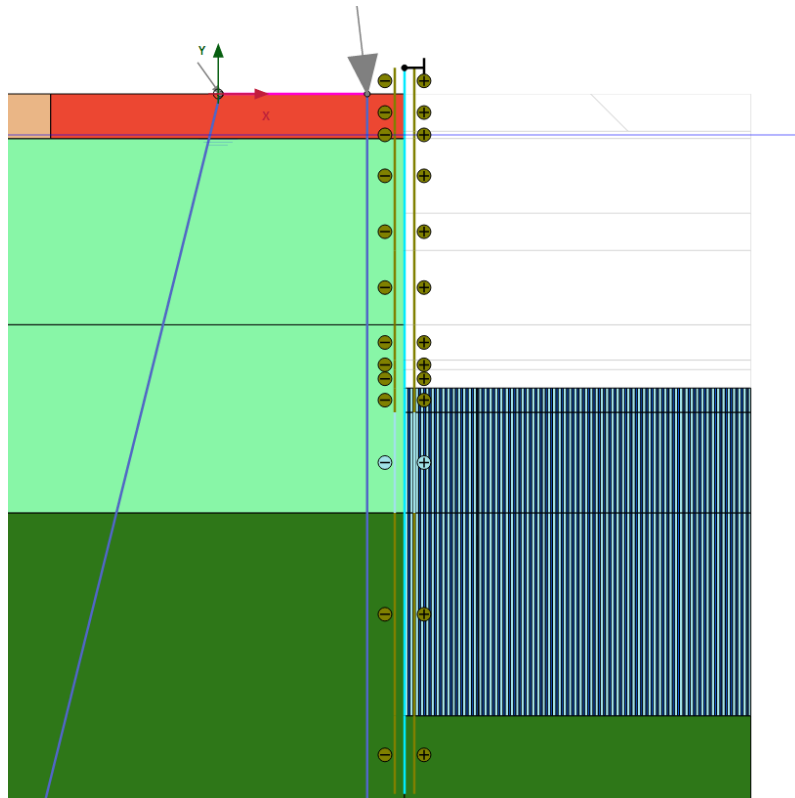


Figure 33: Picture showing how it will look after phase 11, where the dark and light blue represent the LCC according to Ignat's method.

5.2.3 Influence of load, piles and lime-cement columns

When an excavation is being carried out there will be live- and point loads due to the machinery being used to conduct the works. In the above models no loads have been accounted for. However, it is of interest to see the influence of loads. For this purpose, firstly two point loads (see Table 13) have been added when the retaining wall was installed, located close to the retaining wall. Secondly, a live load of 10 kN/m/m was added when the retaining wall was installed (see Appendix M for location of the loads). Finally, the influence of both loads simultaneously was investigated. Moreover, since the influence should be the same for both models, only the Soft Soil model with the concrete plate was used to investigate the differences at 30 m depth at the middle of the excavation.

Table 13: Point loads.

	Vertical component	Horizontal component	Units
Point load 1	106.2	12.54	kN/m
Point load 2	17.54	12.54	kN/m

During the excavation, two piles close to the excavation were installed in order to decrease the settlements for heavy machinery (see Appendix B for dimension and Appendix M for location of piles). In order to understand the piles effect of the excavation, the model was also calculated without piles for the Soft Soil model for the concrete slab.

Additionally, in order to investigate further about the lime-cement columns behaviour, modelled as a block, the columns length was increased to 40 m for the Soft Soil model, which is the maximum length according to EuroStab (EuroSoilStab, 2002).

5.2.4 Parametric studies- Model 1

Parametric studies were carried out for both the Soft Soil and Hardenig Soil with small-strain stiffness models for the concrete slab. Only the clay paramters were modified since they have the greatest effect of the basal heave. Furthermore, the parameters of the structures were not modified as their values are given. The parametric studies are carried out by changing one parameter per comparison, but the same parameters were changed for the both clay layers at the same time. Additionally it should be noted that in the HSs model it is required in occasions to change more than one parameter per occasion as certain parameters need to be within a range of each other.

5.2.4.1 Soft Soil- parametric studies

For the Soft Soil model it was decided to investigate how the modified compression index (λ^*), modified swelling index (κ^*), coefficient of earth pressure at rest for normally consolidated soils (K_0^{nc}), Poisson's ratio for unloading/reloading (ν'_{ur}), effective cohesion (c'), effective friction angle (ϕ') and OCR influence the result. These values were chosen as they are the ones which contain most uncertainty.

For the modified compression and swelling indices the values were reduced to those obtained from the graphs, see Chapter 4.4.1 Parameters for the Soft Soil model. It was decided to not increase the parameters further as it would not be realistic.

Given that the coefficient of earth pressure at rest for normally consolidated clays can be calculated with two different equations (see equation (17) and (18)) it was investigated the effect of using these two different values had on the excavation.

The effective Poisson's ratio for unloading and reloading for Gothenburg clay is normally between 0.1-0.3. Therefore, 0.3 was used as an upper value.

In terms of the effective cohesion, an approximation was made from the scattered data and therefore a lower and an upper bound value was chosen.

The effective friction angle of clay is normally around 30, this value was changed by +/- one degree.

The OCR of Gothenburg clay is normally 1.25 and given that the data exhibits scatter a range of 1.1 to 1.25 would be reasonable to be expected. Therefore, this variation was studied.

In summary, the values for the parameter variation for clay 1 and clay 2 are presented in Table 14 and Table 15 respectively.

Table 14: Parameter variation for the first clay layer - Soft Soil model.

Clay 1	Minimum	Reference	Maximum
Modified compression index, λ^*	0.13	0.15	0.15
Modified swelling index, κ^*	0.0022	0.0082	0.0082
Coefficient of earth pressure at rest for normally consolidated clay, K_0^{nc}	0.5	0.6	0.67
Effective Poisson's ratio for un/reloading, v'_{ur}	0.15	0.15	0.3
Effective cohesion, c'	0.7	0.8	1.3
Effective friction angle, φ'	29	30	31
Over Consolidation Ratio, OCR	1.1	1.15	1.25

Table 15: Parameter variation for the second clay layer - Soft Soil model.

Clay 2	Minimum	Reference	Maximum
Modified compression index, λ^*	0.19	0.20	0.20
Modified swelling index, κ^*	0.003	0.007	0.007
Coefficient of earth pressure at rest for normally consolidated clay, K_0^{nc}	0.5	0.6	0.67
Effective Poisson's ratio for un/reloading, v'_{ur}	0.15	0.15	0.3
Effective cohesion, c'	2.9	3.1	3.7
Effective friction angle, φ'	29	30	31
Over Consolidation Ratio, OCR	1.1	1.18	1.25

5.2.4.2 Hardening Soil with small-strain stiffness- parametric studies

For the Hardening Soil with small-strain stiffness model the secant stiffness in standard drained triaxial test (E_{50}^{ref}), tangent stiffness for primary oedometer loading (E_{oed}^{ref}), unload/reload stiffness (E_{ur}^{ref}), coefficient of earth pressure at rest for normally consolidated clay (K_0^{nc}), effective Poisson's ratio for unloading/reloading (v'_{ur}), effective cohesion (c'), effective friction angle (φ') and OCR were changed. These values were chosen as they contain uncertainty.

As mentioned above, more than one parameter needs to be changed per occasion. This is because the stiffnesses need to be within certain ranges of each

other. Furthermore, even though the undrained initial shear modulus at reference pressure (G_0^{ref}) was not included in the parametric study it needed to be changed along with the stiffnesses variation. Moreover, the effective cohesion and its increase with depth are dependent on each other and therefore should be changed simultaneously.

In terms of the stiffnesses for the minimum values it was decided to use those derived from the modified compression index (λ^*). For the maximum values they were derived from the modified swelling index (κ^*) (see Chapter 4.4.3 Correlation between the Soft Soil and the Hardening Soil small-strain stiffness models parameters for more details). The remaining of the parameters were changed in the same manner as 5.2.4.1 Soft Soil- parametric studies.

The values for the parameter variation for clay 1 and clay 2 are presented in Table 16 and

Table 17 respectively.

Table 16: Parameter variation for the first clay layer- Hardening Soil with small-strain stiffness model.

Clay 1	Minimum	Reference	Maximum
Secant stiffness in standard drained triaxial test at reference pressure, E_{50}^{ref}	833	5000	8130
Tangent stiffness for primary oedometer loading at reference pressure, E_{oed}^{ref}	667	3051	6504
Unload/reload stiffness at reference pressure, E_{ur}^{ref}	2500	15 000	24 390
Coefficient of earth pressure at rest for normally consolidated clay, K_0^{nc}	0.50	0.60	0.67
Effective Poisson's ratio for un/reloading, ν'_{ur}	0.15	0.15	0.30
Effective cohesion, c'	0.70	0.80	1.3
Effective cohesion increase, c'_{inc}	0.091	0.114	0.138
Effective friction angle, φ'	29	30	31
Over Consolidation Ratio, OCR	1.1	1.15	1.25

Table 17: Parameter variation for the second clay layer- Hardening Soil with small-strain stiffness model.

Clay 2	Minimum	Reference	Maximum
Secant stiffness in standard drained triaxial test at reference pressure, E_{50}^{ref}	625	5000	9524
Tangent stiffness for primary oedometer loading at reference pressure, E_{oed}^{ref}	500	3051	7619
Unload/reload stiffness at reference pressure, E_{ur}^{ref}	1875	15 000	28 571
Coefficient of earth pressure at rest for normally consolidated clay, K_0^{nc}	0.50	0.60	0.67
Effective Poisson's ratio for un/reloading, ν'_{ur}	0.15	0.15	0.30
Effective cohesion, c'	2.9	3.1	3.7
Effective cohesion increase, c'_{inc}	0.091	0.114	0.138
Effective friction angle, ϕ'	29	30	31
Over Consolidation Ratio, OCR	1.1	1.18	1.25

5.2.5 Parametric studies- Model 2

Parametric studies were carried out for the Soft Soil for the lime-cement columns since similar result was assumed to be obtained for the HSs. The permeability of lime-cement columns has been modelled due to uncertainties in its determination. According to Minna Karstunen¹, lime-cement columns do not increase the permeability of the soil. However, according to TK Geo 11, the permeability should be increased by 500 times the permeability of the soil, and according to Broms by 40 times (Trafikverket, 2011; Broms, 2004). Since the model fails with 500 times the permeability of the soil, and that the updated version of TK Geo no longer has this recommendation, it was decided to model an increase permeability of the lime-cement columns by 40. The area replacement ratio of columns was calculated to be 0.4 according to Chapter 4.2 Lime-cement columns parameters and thereby give a maximum permeability of $0.717 \cdot 10^{-3}$ m/day. The minimum value is equal to the reference since it is assumed that the permeability of the lime-cement columns cannot be lower than in the soil (Trafikverket, 2014).

Additionally, a parametric study was carried out for the equivalent stiffness. The equivalent stiffness was firstly based on the undrained shear strength for the soft columns according to TK GEO 13, with a value 100 kPa (Trafikverket, 2014). Since Larsson (2006) refers to soft columns up to 150 kPa, this was also tested.

¹Minna Karstunen (professor, Chalmers University of Technology) interview by writer 4 April 2017

6 Result

Results from the analytical calculations and the PLAXIS analyses are presented in the following subchapters. The result for the PLAXIS analyses include a comparison between the two different models (concrete slab and lime cement column), how the model is affected by piles, load and length of the lime-cement columns. Furthermore, the result from the parametric studies and corroboration with measured data for the basal heave are presented.

6.1 Analytical safety calculations

In Table 18 the safety factor against basal heave for two conventional methods is presented. A more detailed description of the calculations can be found in Appendix L. It can be seen that according to Bjerrum and Eide's equation the safety factor is acceptable for the concrete slab, but for the LCC and for the concrete slab according to Terzaghi's equation the safety factor is too low.

Table 18: Safety factor according to analytical calculations.

Calculation method	Factor of safety	Minimum allowable Factor of Safety
Terzaghi, concrete slab	1.25	1.5
Bjerrum and Eide, concrete slab	1.69	1.2
Bjerrum and Eide, LCC	1.17	1.2

6.2 PLAXIS

In the following subchapters the results for the two construction methods from the two different constitutive models are presented. These include maximum retaining wall bending moment, maximum strut force, basal heave and safety factor.

All models used 6-noded elements and fine mesh. According to calculations performed by Zublin (2015c) the maximum allowable bending moment of the retaining wall is approximately 3100 kNm/m and the maximum strut force is 6000 kN. To analyze the basal heave, points in the middle of section A-A, were chosen at depths of around 21, 30 and 39 m. These depths were chosen since measurements were taken at these points. The allowable safety factor is set to 1.5 according TK GEO 13 (Trafikverket, 2014).

The safety factor in PLAXIS is calculated by the ϕ -c method, where the soil strength is reduced successively until convergence to numerical solutions no longer remains (Do. et. al, 2013). To model the safety factor against basal heave, the safety factor analysis is performed at the final stage of the excavation and after the first dewatering since these are the most crucial stages. The safety factor was calculated at the middle of the excavation at a depth of approximately 16 m. The safety factor graphs obtained from PLAXIS can be found in Appendix M. Moreover, the failure surface and mesh of the models can also be found in Appendix M.

6.2.1 Model 1-Concrete slab

In the following subchapters the results for the excavation with the concrete slab are presented for the Soft Soil and Hardening Soil model with small-strain stiffness models.

6.2.1.1 Soft Soil-Model 1

The model has 2278 elements and 4918 nodes. Thereafter, the maximum bending moment of the wall, the maximum strut force and the safety factor were calculated (Table 19). As can be seen, the maximum bending moment, strut force and the safety factor are within allowable range (see Appendix M for safety factor graphs).

Table 19: Bending moment, strut force and safety factor, allowable and measured for the Soft Soil model for the concrete slab.

		Measured	Allowable
Maximum bending moment (kNm/m)		2093	3100
Maximum strut force (kN)		3066	6000
Factor of Safety [-]	After dewatering	4.1	1.5
	Final	4.5	

As mentioned in Chapter 6.2 PLAXIS, basal heave was measured at depths 21, 30 and 39 m. However, it should be noted that those exact depths were not available as nodes in PLAXIS and therefore, in some cases, more than one point was chosen to give an approximation. The measurements of basal heave across the different stages is presented in Figure 34. As can be seen basal heave decreases with depth and the maximum value is **7.5 cm**.

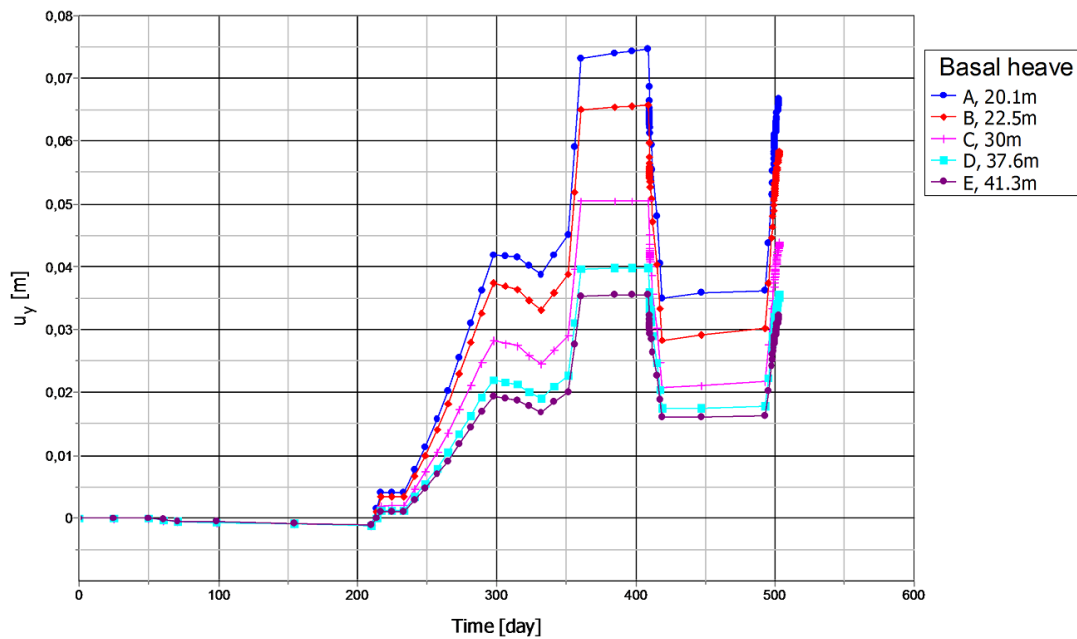


Figure 34: Change of basal heave versus time, model 1 -Concrete plate, Soft Soil.

6.2.1.2 Hardening Soil model with small-strain stiffness-Model 1

The model has 2278 elements and 4918 nodes. Thereafter, the maximum bending moment of the wall, the maximum strut force and the safety factor were calculated (Table 20). As can be seen the maximum bending moment, strut force and safety factor are within allowable range (see Appendix M for safety factor graphs).

Table 20: Bending moment, strut force and safety factor, allowable and measured for the Hardening Soil with small-strain stiffness model for the concrete slab.

		Measured	Allowable
Maximum bending moment [kNm/m]		2049	3100
Maximum strut force [kN]		2908	6000
Factor of Safety [-]	After dewatering	4.2	1.5
	Final	4.1	

The measurements of basal heave across the different stages is presented in Figure 35. As can be seen basal heave decreases with depth and the maximum value is **7.2 cm**.

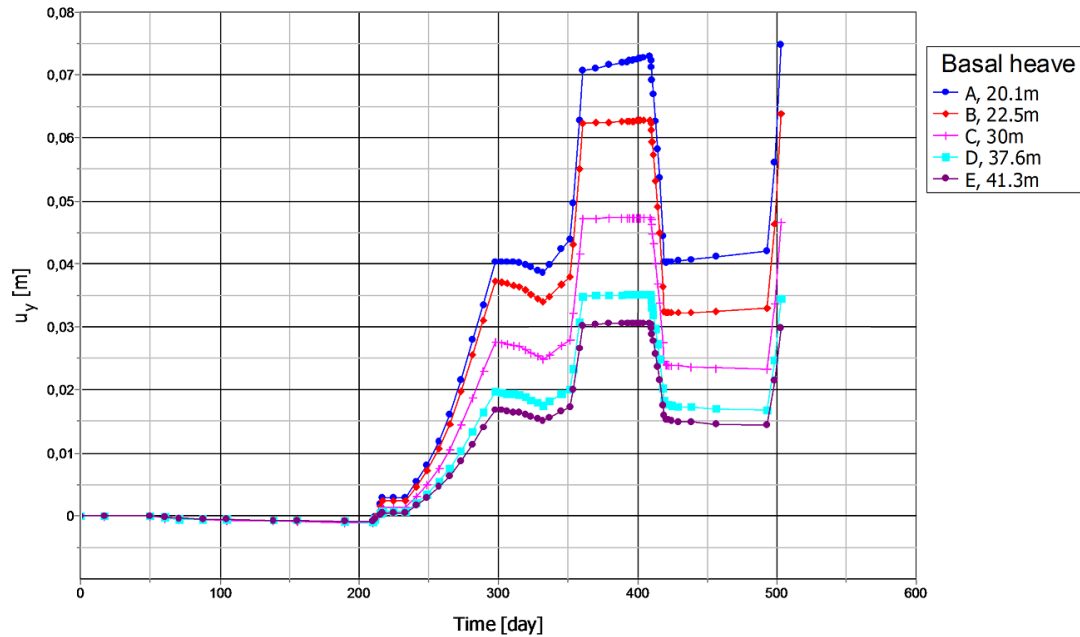


Figure 35: Change of basal heave versus time, model 1 –Concrete plate, Hardening Soil model with small-strain stiffness.

6.2.2 Model 2-Lime-cement columns

In the following subchapters the results for the excavation with the lime-cement columns are presented for the Soft Soil and Hardening Soil small-strain stiffness models.

6.2.2.1 Soft Soil-Model 2

The model has 2088 elements and 4524 nodes. Thereafter, the maximum bending moment of the wall, the maximum strut force and the safety factor were checked, see Table 21. As can be seen the maximum bending moment is higher than the allowable, but the strut force and the safety factor are within allowable range (see Appendix M for safety factor graphs).

Table 21: Bending moment, strut force and safety factor, allowable and measured for the Soft Soil model for the lime-cement columns.

		Measured	Allowable
Maximum bending moment [kNm/m]		5138	3100
Maximum strut force [kN]		5033	6000
Factor of Safety [-]	After 3 rd excavation	4.1	1.5
	Final	3.9	

The change of basal heave during the different stages is presented in Figure 36. As can be seen basal heave decreases with depth and the maximum value is **10.7 cm**.

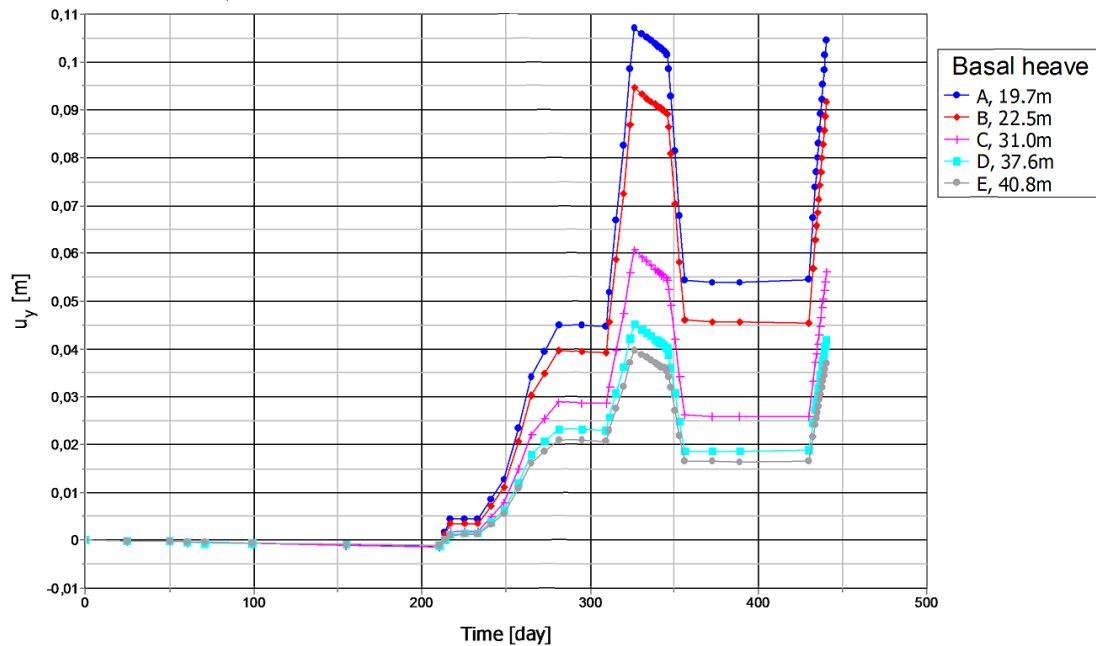


Figure 36: The change of basal heave versus time, model 2 –Lime-cement columns, Soft Soil.

6.2.2.1.1 Modelling LCC with Ignat’s method

The model has 13 882 elements and 28 298 nodes. With Ignat’s method the maximum basal heave increased by approximately three cm compared to the homogenous LCC block, for the Soft Soil model. The maximum bending moment, strut force and safety factor decreased compared to modelling LCC as a block, see Table 22 (see Appendix M for safety factor graphs).

Table 22: Bending moment, strut force and safety factor, allowable and measured for the Soft Soil model for the lime-cement columns according to Ignat’s method.

		Measured	Allowable
Maximum bending moment [kNm/m]		5107	3100
Maximum strut force [kN]		4978	6000
Factor of Safety [-]	After 3 rd excavation	3.8	1.5
	Final	3.6	

6.2.2.2 Hardening soil model with small-strain stiffness-Model 2

The model has 2088 elements and 4524 nodes. Thereafter, the maximum bending moment of the wall, the maximum strut force and the safety factor were calculated, see Table 23. As can be seen, the maximum bending moment and the strut force are too high but the safety factor are within allowable range (see Appendix M for safety factor graphs).

Table 23: Bending moment, strut force and safety, allowable and measured for the Hardening Soil model with small-strain stiffness for the lime-cement columns.

		Measured	Allowable
Maximum bending moment [kNm/m]		6450	3100
Maximum strut force [kN]		6018	6000
Factor of Safety [-]	After 3 rd excavation	4.1	1.5
	Final	3.6	

The change of basal heave during the different stages is presented in Figure 37. As can be seen basal heave decreases with depth and the maximum value is **15.2 cm**.

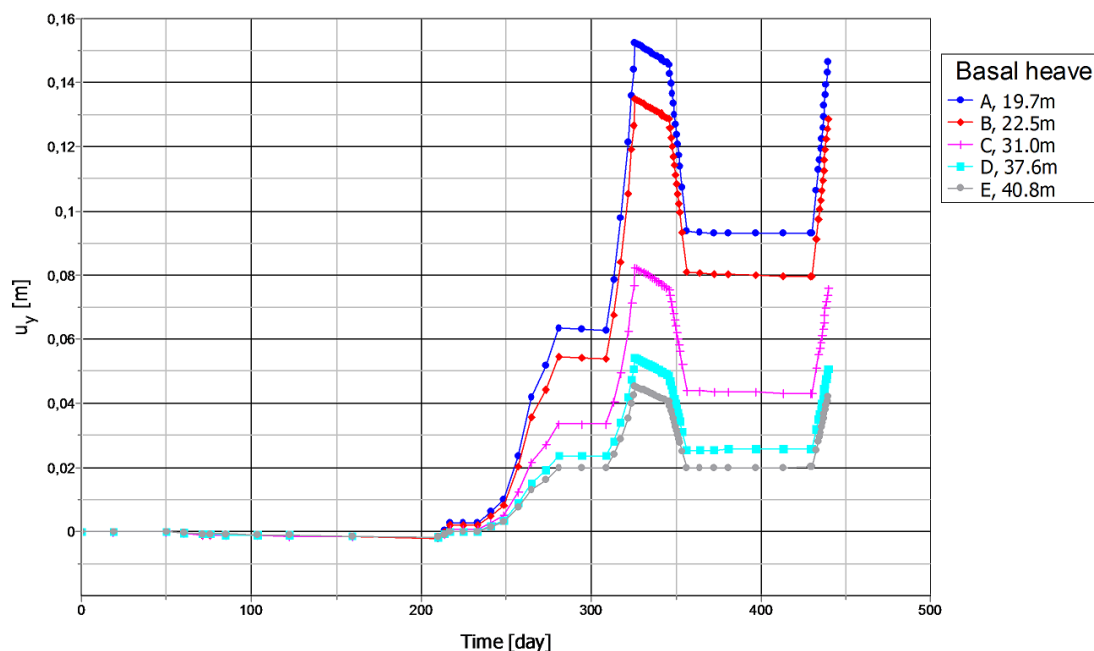


Figure 37: The change of basal heave versus time, model 2 –Lime-cement columns, Hardening Soil model with small-strain stiffness.

6.3 Comparison of model 1 and model 2

As the basal heave at different depths change similarly, it was decided to present a comparison of basal heave at 30 m depth. Figure 38 shows that the basal heave is larger for the LCC model. It is also clear that the HSs model gives larger basal heave for the LCC model. The opposite is true for the concrete slab model.

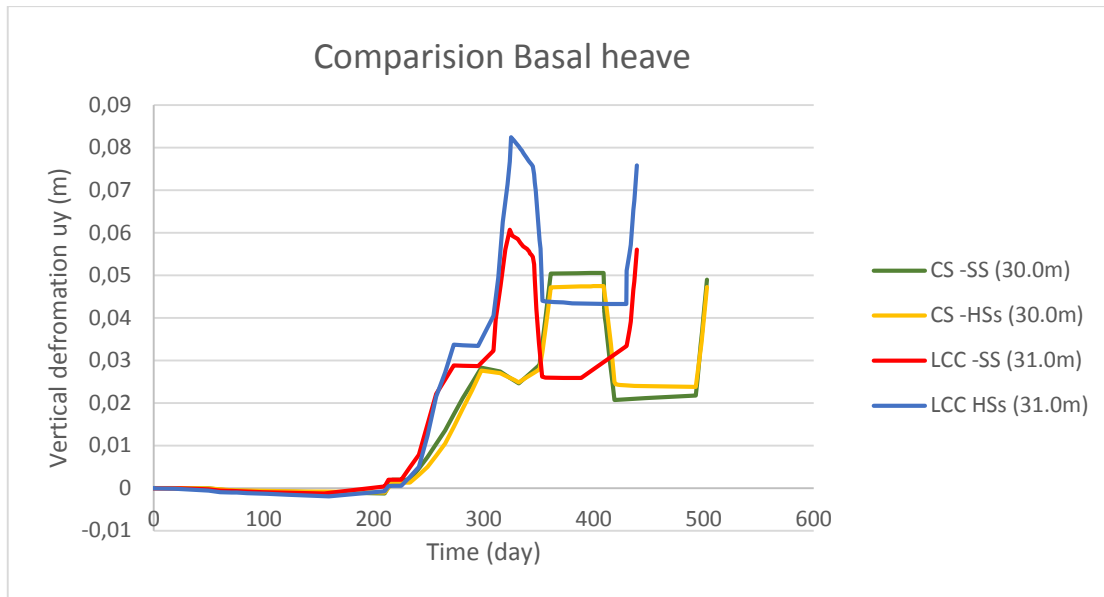


Figure 38: Comparison of basal heave for the different models. Note that the LCC have a different construction period.

In Table 24, a comparison of the safety factor, maximum bending moment and maximum strut force can be found. The first number in the safety factor is after the 3rd excavation and the second number is after the construction is finished. The bending moment and the strut force for model 2, with lime-cement columns gives an overall a higher bending moment and strut force. The safety factor is overall lower for model 2, with lime-cement columns.

Table 24: Comparison of the result for model 1-concrete slab and model 2 -Lime-cement columns.

	Max. bending moment [kNm/m]	Max. strut force [kN]	Factor of Safety [-]
Model 1 -Concrete slab, SS	2093	3066	4.1/4.5
Model 1-Concrete slab, HSs	2049	2908	4.2/4.1
Model 2 -LCC, SS	5138	5033	4.1/3.9
Model 2 -LCC,HSs	6450	6018	4.1/3.6

6.4 Influence of load, piles and lime-cement columns

The influence of load and piles was only modelled for the concrete plate for the Soft Soil model, and the effect of length of lime-cement columns for the Soft Soil model. When point or live loads are modelled the basal heave does not differ significantly. The biggest differences are found up to the point where the retaining wall is installed. However, the variations are of one millimeter when compared to the reference model. When modelling the point and live load simultaneously the basal heave is the same. The maximum bending moment, maximum strut force and the safety factor did not vary (see Appendix N for graphs).

Without piles, the basal heave had the same result as before. However, the maximum bending moment and the maximum strut increased by about 300 kNm/m and 600 kN respectively. The safety factor was about the same.

The lime-cement columns were increased to a length of 40 m instead of 25 m. The safety factor, bending moment and the strut force were almost the same. The basal heave increased by approximately **2 cm**.

6.5 Parametric studies- Model 1

In the subchapters below the parametric studies are presented for model 1- concrete slab, for both the Soft Soil and Hardening Soil with small-strain stiffness models.

6.5.1 Soft Soil

In the Soft Soil model, the parameters which have the highest influence on the excavation are the effective Poisson's ratio for unloading/reloading (v'_{ur}) and the modified swelling index (κ^*), see Figure 39. A detailed result of the parametric studies can be found in Appendix O.

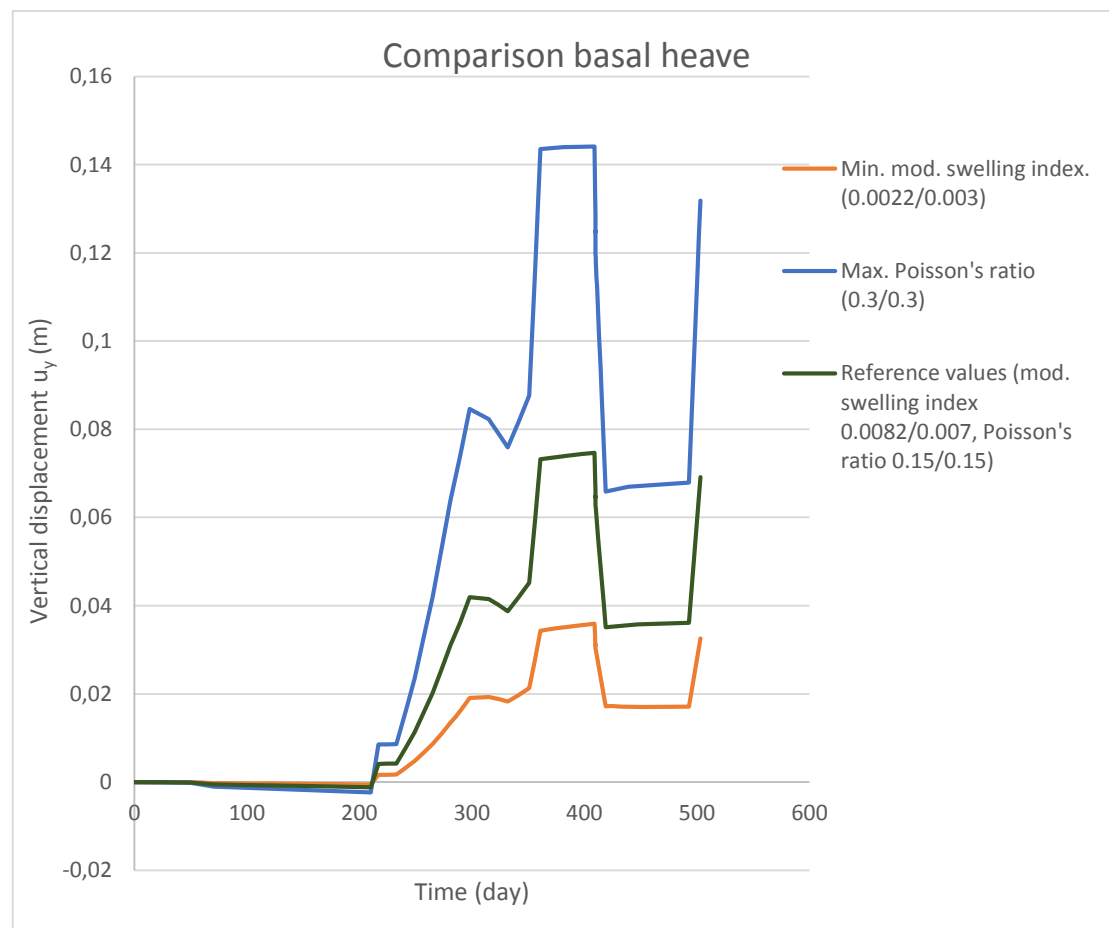


Figure 39: Comparison of basal heave for 20.1m depth for different values, Soft Soil mode, the first number refers to the first clay layer and the second one to the second clay layerl.

6.5.2 Hardening Soil with small-strain stiffness

In the Hardening Soil with small-strain stiffness model, the parameters which have the highest influence on the excavation are the stiffnesses (E_{50}^{ref} , E_{oed}^{ref} & E_{ur}^{ref}), the coefficient of earth pressure at rest for normally consolidated clays (K_0^{nc}) and the effective friction angle (φ'). How the remaining values influence the excavation can be found in Appendix O.

However, it should be noted that the minimum stiffnesses used are not realistic. When the SoilTest are performed with those values the graphs are not closely related to the lab graphs. Therefore, it was decided to also see the influence of the stiffnesses would have on the result if they were reduced by 10%. As can be seen in Figure 40, the 10% reduction will not have much of an impact on the basal heave. The reference values for the stiffnesses, coefficient of earth pressure and effective friction angle are the same for both clay layers.

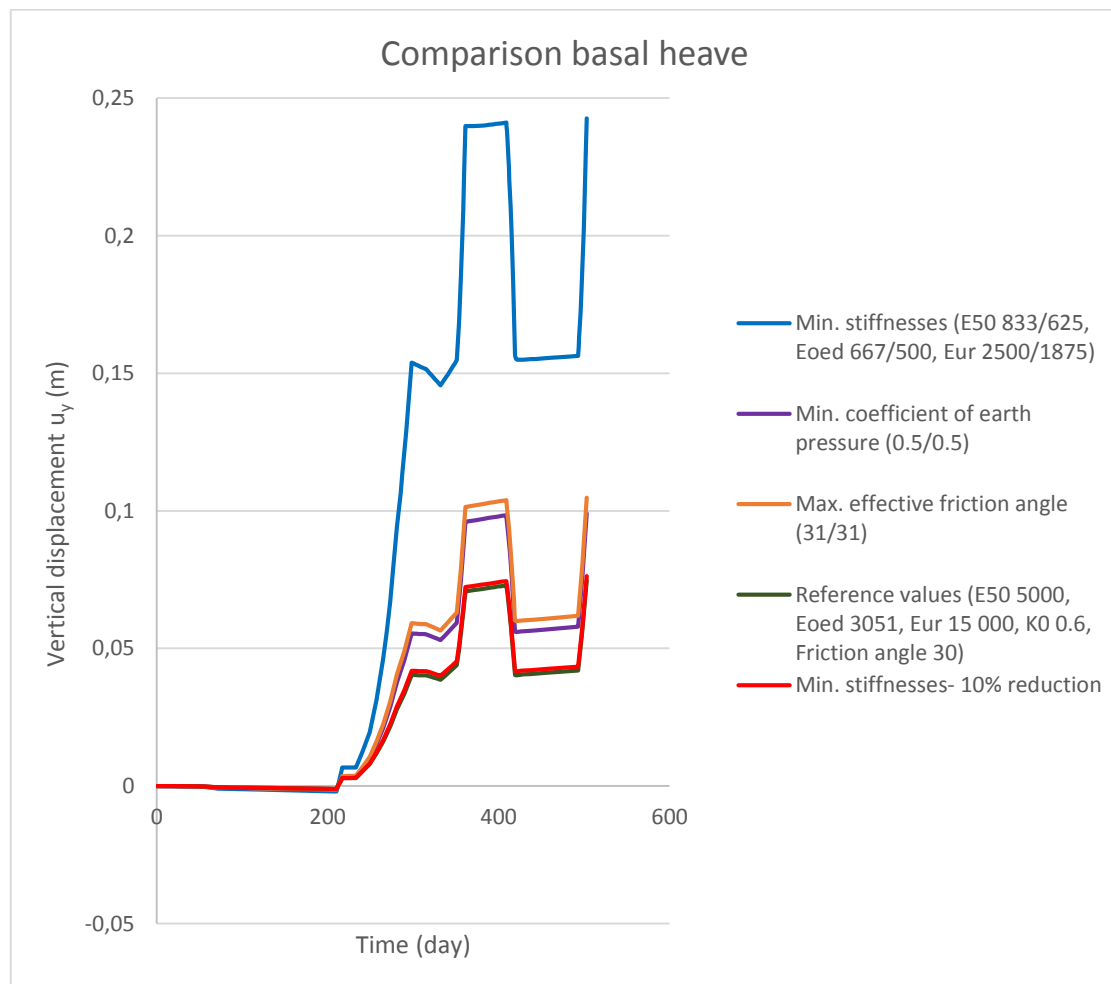


Figure 40: Comparison of basal heave for 20.1 m depth for different values, Hardening Soil with small-strain stiffness, the first number refers to the first clay layer and the second one to the second clay layer.

6.6 Parametric studies- Model 2

With an increased permeability (from $0.0432 \cdot 10^{-3}$ to $0.717 \cdot 10^{-3}$ m/day) for the LCC, the safety factor remains the same and the basal heave increases approximately **3 cm** for depth 19.7 m. Additionally, it can be seen in Table 25 that the bending moment has decreased and that the maximum strut has increased.

Table 25: Comparison of permeability, Soft Soil model.

		Reference permeability	Maximum permeability	Units
Basal heave	19.7 m	10.6	14.0	cm
	31.0 m	6.0	6.0	cm
	37.6 m	4.5	4.5	cm
Max. bending moment		5138	4639	kNm/m
Max. strut force		5033	5511	kN

An increased undrained shear strength from 100 to 150 kPa resulted in a decrease of basal heave of **0.5 cm** for 19.7 and 22.5 m depths. The safety factor and the maximum bending moment and strut force remains the same.

6.7 Corroboration with measured data

To validate the model, the basal heave obtained was compared to measurements. Since it could be seen that the basal heave at different depths changed about the same, it was chosen to present a comparison of basal heave for one point, that have nodes close to each other (at depth of around 30 m). In the Figure 41, it can be seen that the basal heave for the concrete slab is about **1 cm** higher than the measurements (ME1).



Figure 41: Comparison of calculated and measured basal heave.

7 Discussion

In the following subchapters, the reliability of the parameters and the constitutive models will be discussed. Furthermore, a discussion of the result of the analytical and PLAXIS calculations, for both models, concrete slab and lime-cements columns is presented. Lastly, it will be discussed if it is feasible for LCC to be used in the passive zone of excavations in Sweden.

7.1 Parameters

There are several aspects that can explain the difference between the modelled basal heave for the concrete slab and the measurements. The same reasons would probably apply if the LCC had been constructed and measurements have been taken. One important factor is the quality of the evaluated field and lab data. Unfortunately, much of the lab data was disturbed and therefore did not capture accurately the soil behavior. The soil samples used for oedometer testing were transported from Gothenburg to Linköping. Therefore, many of the samples were probably of bad quality. Additionally, the sample quality of the triaxial tests was low. This meant that the CRS tests were firstly used to calibrate the parameters. However, the curves did not match perfectly. Since the CRS, oedometer and triaxial tests were used to calculate the stiffness parameters for the SS and HSs models it will have an impact on the reliability of the result. When calibrating the HSs parameters, the m value was kept as one. However, if a value of 0.5 would have been used, a better fit would have been obtained. This was not done since clay has a logarithmic stress-strain behavior, and it should therefore be equal to one.

It can also be seen in Chapter 4.4.3 Correlation between the Soft Soil and the Hardening Soil small-strain stiffness models parameters, the stiffness parameters for the two constitutive models do not correlate. It was not possible to use the modified compression and swelling indices simultaneously to correlate the HSs and the SS models. If two correlations were done to the SS model, i.e. one for the modified swelling index and one for the modified compression index, the stiffness values for the HSs model would have not been realistic and the PLAXIS graphs would be of an even worse fit. This will affect the reliability of the result.

For the parametric studies for concrete slab modelled with SS, the parameters which had the highest impact were the minimum modified swelling index and the maximum Poisson's ratio. For clay layer one the minimum modified swelling index was almost 4 times lower the reference value whereas the Poisson's ratio was doubled for the parametric studies. An accurate value of Poisson's ratio is of vital importance for excavations since a higher Poisson's ratio will result in a considerably larger basal heave. If the minimum modified compression index would have been used, the predictions of the basal heave would have been more accurate to reality. However, it was not used since the stress paths modelled in PLAXIS would have not been close to the test ones. However, since the lab data is not of good quality, it is not known which stress paths should be modelled.

For the parametric studies for concrete slab modelled with HSs, the parameters which had the biggest impacts were the minimum stiffness, minimum coefficient of earth pressure and maximum effective friction angle. The minimum stiffnesses were obtained from the modified compression index used for the SS model. Even though this value should be related, the results from the two different models do not agree. The stiffnesses obtained from the modified compression index were unrealistically low and thereby resulted in quite large basal heave predictions. The minimum coefficient of earth pressure and the maximum effective friction angle did not vary much from the reference value but even so had a considerable effect on the basal heave.

Since not many studies have been performed using LCC in the passive side of the excavation, several assumptions had to be made in order to evaluate these parameters. For the LCC-block, the major assumption was that the soil and the LCC act as a fully composite material. The parameters were therefore derived from the average of the two materials based on the area. The ground settlements will be the same for the whole block, and an equivalent E-modulus is calculated. Additionally, the permeability of the LCC-block is assumed to be the same as for clay layer one, and the specific weight is assumed to be the same as for clay layer two. Moreover, it is assumed that the LCC-block has no cohesion. This is a conservative assumption. The effect of cohesion on the behavior of the excavation should be investigated.

7.2 Constitutive model

There is no constitutive model which captures all aspects of soil behavior and the choice of model used affects the result. In this case, the Soft Soil and the Hardening Soil with small-strain stiffness models were used. Moreover, for the LCC and the fill layer the Mohr-Coulomb model was used since there was not sufficient data to use a more advanced model.

The HSs model was developed for sands and therefore is not ideal to use for soft clay. However, it accounts for the non-elastic behavior for unloading/reloading, which is a desirable property to have when modelling excavation problems. The HSs model requires three stiffness parameters that are connected to each other and need to be within a certain range. This means that not all stiffness defined will be ideal. In order to model a deep excavation the E_{50}^{ref} and the E_{ur}^{ref} have to be prioritized, and therefore it leads to unrealistic high values of the E_{oed}^{ref} . Given that a better fit was obtained for the SS graphs and measured data, and the fact that it is suitable for soft soils, it can be deduced that in this case the SS model is more suitable for modelling the excavation.

Even though these models do not account for all soil behavior, such as anisotropy, it was decided to use them since more complex models would require more input parameters which would have been difficult to estimate. Moreover, it is always advisable to start with simpler models and progress to more complicated ones as the model is only as good as the input parameters are. Given the drawbacks of the current models used, it could be advantageous to use another constitutive model, for example S-CLAY 1S. This model takes into

account anisotropy and destructuration, two vital properties that depict the behavior of soft soil. However, this model does not take into account rate dependency.

7.3 Analytical calculations

The analytical calculations are only a rough simplification of the reality, and can only estimate the safety factor at a defined yield surface. Therefore, no predicted basal heave settlement can be calculated analytically. According to Bjerrum and Eide's equation the safety factor is acceptable for the concrete slab, but for the LCC and for the concrete slab according to Terzahi's equation the safety factor is too low. The lower value of Terzahi's equation can be explained by the fact that it does not take into account the penetration of the wall. With PLAXIS an overall higher safety factor, between 3.6-4.5, was obtained. The major advantage of using PLAXIS is that the most critical failure surface is determined whereas for the analytical calculations it is assumed. It can therefore be seen that in order not to be too conservative, PLAXIS calculations are required. However, analytical calculations should always be performed first since they are relatively quickly to do and modelling in PLAXIS will not be required if the structure is deemed to be safe or the determination of basal heave is not considered relevant for the problem.

7.4 Result

For the comparison of basal heave, for the two models, it could be seen that the LCC-block had about one centimeter higher basal heave for the SS model but 3.5 cm higher for the HSs model. The bending moment, strut force and the safety factor are more favorable for the concrete slab. These could be explained by several assumptions and simplifications had to be made in order to model the LCC-block but also the LCC may require stiffer structural elements. Additionally the change of result between the two constitutive models could be explained by that the stiffness parameters did not correlate and the fact that they take into account different aspects of the soil behavior.

As mentioned previously, the LCC-block is assumed to have an average E-modulus. With an increased undrained shear strength from 100 to 150 kPa, it did not have significant effect of the result. The only differences were of a reduction of 0.5 cm of basal heave close to the excavation bottom.

The specific weight of the LCC-block is assumed to be 16.5 kN/m³, which is the same as clay layer two, and only 0.5 kN/m³ higher than clay layer one. Since lime-cement has a higher density, it can be deduced that the block weight is conservative.

When modeling longer piles, 40 m compared to 25 m, the basal heave increased by 2 cm. This not realistic and can be explained by that the LCC-block was modeled with the Mohr-Coulomb model. This model does not give an accurate values for deformations and settlements. Additionally, the permeability of LCC is not agreed upon, it ranges between 1-500 times the soil permeability according to previous studies. With an increased permeability of 40 times the basal heave

close to the surface increased by 3.6 cm, whereas the maximum bending moment decreased by 10% and the maximum strut force increased by approximately 10%. Therefore it can be of interest to know what permeability should be used, because with 500 times of the soil permeability the model failed.

The measurements of basal heave are about one cm lower compared to the concrete slab model. As mentioned previously this could be effect of the parameter calibration, bad quality of lab data and the choice of constitutive models. Additionally, it can also be an effect of the piles and the load, which is discussed below.

When an excavation is being constructed there will be loads on the ground surface during certain times. These loads did not have any effect on the maximum basal heave, differences in basal heave were only observed until the retaining wall was constructed. However, even then the maximum difference in basal heave was of approximately one millimeter. This could be explained by the fact that the loads were not considerable.

In the result it could be seen that the piles on the side of the excavation did not have any effect on the basal heave. This could be explained by the fact that PLAXIS 2D does not take into account the lateral force of piles. Therefore, in reality basal heave will probably be lower since two piles are installed on the side of the excavation. Furthermore, it should be noted that the piles were installed to minimize ground settlements due to the use of heavy machinery, and the ground settlements should therefore be checked.

When comparing the LCC-block with the model based on Ignat's method, i.e. the weaknesses of the columns overlap were taken into account, for the Soft Soil model three centimeters lower basal heave was obtained. The Ignat's method will give a higher value of basal heave since with the homogenous block the weakness of the columns overlap were not considered and it therefore had an overall higher stiffness. Ignat proved that the weakness of overlap needs to be modelled, but this means that the PLAXIS model will have quite fine elements which makes it more computationally expensive and leads to more instability in the model.

Lastly, it should be highlighted that it is not easy to model a construction as there will always be deviations from reality. For example, for every stage of the excavation there were trigger points when remedial work should be done to minimize basal heave. It was assumed that such action was not taken. Moreover, the quality of workmanship has a high impact on the result.

7.5 LCC-Preventing basal heave?

The main focus of this report was to evaluate if LCC could be used instead of a concrete slab to prevent basal heave. As just discussed in the result, the LCC results in higher basal heave than the concrete slab, but this could be because of all the uncertainties and assumptions regarding modelling the LCC-block. There are some benefits of using LCC, the ability to choose the installation pattern, distance between columns, depth and diameter of columns. Additionally,

lower transportation and energy costs can be achieved and the excavation can be carried out dry.

However, there are uncertainties regarding the installation of the LCC. In order to get a strong LCC-block, there should not be any interruptions in the work to get a good overlapping zone. There is also a risk that columns that are damaged, or not good mixed columns, have weaker zones that affect the buckling strength, capacity against tension and bending stresses. This means that it is hard to know with certainty the properties of LCC, especially since the properties varies with depth. Another aspect to account for is the constructability of the LCC. The dock needs to be excavated to a certain depth before the LCC can be installed. Therefore, the machines will need to be placed at the excavation bottom and this may not be straightforward since there will be struts.

Regarding all the uncertainties of the properties of the LCC, and how they should be modelled in PLAXIS, it would be beneficial to investigate this further. With a more accurate model and parameters, the LCC could be used more in Sweden for preventing basal heave on the passive side of excavations. Moreover, it should be noted that even though the results were more unfavourable for the LCC, the safety factor was still adequate. Furthermore, once the excavation is completed, construction of the tunnel segments will begin. This will result in a reduction of basal heave as the tunnel segments will act as a counteracting weight. Therefore, even though higher basal heave is predicted for LCC it could still be used if it is proven to be a cheaper and/or easier alternative to construct.

7.6 Further studies

Currently there is no guideline how exactly the LCC columns should be designed when they are installed on the passive side of the wall. It could therefore be of interest to investigate this further. Ignat Razan developed a LCC model that takes into account the 3D effects in a 2D model in PLAXIS. However, the model is quite complex to analyze. By analyzing the LCC as a block instead, the analysis is easier to handle, but more simplifications must be made. Therefore it could be of interest to investigate further how well the LCC-block represents reality. This could be done on a test bank, so that field measurements of basal heave could be compared to results from PLAXIS. It would also be beneficial to measure the E-modulus of the LCC-block, and also measure and evaluate further what permeability should be used since there are no clear guidelines today.

In Sweden today the maximum length of the lime cement columns is set to 25 m. Even though the result showed higher basal heave for the 40 m long columns, this could be a misleading result as was discussed before. Therefore, it can be of interest to investigate further if implementing longer lime-cement columns in Sweden could be favorable, which could also be used in other geotechnics field areas.

To get a better correlation between the measured data and the result in PLAXIS a more advanced constitutive model, for example S-CLAY 1S, could be used. With better lab data, the parameters used would have less uncertainty.

Additionally, to get a more representable picture of using the dry dock, it would be beneficial to take into account the cyclic effect of reusing the dry dock to construct the three tunnel segments, and take into account the creep effects. Moreover, a section besides the water could be modelled. Finally, a 3D model could be used to determine the effect of using piles and take into account the corner effects.

8 Conclusion

The main focus of this report was to evaluate if lime-cement columns (LCC) could be used instead of a concrete slab in the Marieholm tunnel project to minimize basal heave. According to PLAXIS calculations it could be seen that LCC result in a larger basal heave, lower safety factor and higher bending moment and strut forces. This could be a result of several assumptions and simplifications that had to be made to model the LCC.

Firstly, the LCC was modeled as a homogenous block, and thereby an average E-modulus was assumed and the permeability was set equal to the permeability of clay layer one. When the LCC block was modelled according to Ignat's method, it led to higher basal heave. This is due to the fact that not only an average E-modulus was used but the weaknesses of the overlapping of the LCC was taken into account.

Even though the basal heave was larger for the LCC-block than the concrete slab, the safety factor of the LCC was acceptable. However, the bending moment should be further investigated and maybe the retaining wall need to be redesigned. Otherwise the LCC could be used if it is proven to be cheaper and/or easier to construct. It should also be noted that the tunnel segments will be constructed at the excavation bottom and help to prevent basal heave failure.

When comparing the concrete slab model with the measurement of basal heave it could be seen that it was about 1cm higher. This could be explained by several aspects that probably would be the same for the LCC model. The quality of the field and lab data were not of good quality, and no constitutive model captures all aspects of the soil behavior. It could be seen that the Soft Soil model (SS) captures the soil behavior better than the Hardening Soil with small-strain stiffness model (HSs). Additionally the S-Clay 1S model could be recommended to be used instead since it takes into account anisotropy and destructuration.

Currently there is no guideline on how to design the LCC in the passive side of the retaining wall. It could be interesting to investigate this further. Since Ignat's model is more computationally expensive, it can be preferable to compare the LCC-block model with measurements from a real excavation. Additionally guidelines should be made on how to evaluate the permeability and the E-modulus of the LCC-block.

Finally, to get a more representable model of the dry dock it would be beneficial to take into account the cycling effects of reusing the dry dock to construct the tunnel segments, account for creep and model more than one section, one section of the wall beside the water could be of interesting.

9 References

Broms, B. B. (2004): Lime and lime/cement columns. *Ground improvement*, 2nd edition. New York, Spoon press, pp.252-330.

Concrete Construction (1962): Tremie concrete. Available at: http://www.concreteconstruction.net/how-to/materials/tremie-concrete_o. [Accessed 2017-02-17].

Do, T.N., Ou, C.Y., Lim, A. (2013): Evaluation of Factors of Safety against Basal Heave for Deep excavations in Soft Clay Using the Finite-Element Method. *Journal of Geotechnical and Geoenvironmental Engineering*, Vol. 139, No. 23, December 2013, pp 2125-2135.

EuroSoilStab (2002): *Design Guide Soft Soil Stabilization: Development of design and construction methods to stabilize soft organic soils*. HIS BRE Press, 1 edition, November 2010, 96 pp.

Google maps, (2017a): Göteborg. *Google maps*. <https://www.google.se/maps/@57.7329606,11.9979757,13z>. [Accessed 2017-02-28].

Google maps, (2017b): Göteborg. *Google maps*. <https://www.google.se/maps/@57.7262013,11.9947296,389m/data=!3m1!1e3>. [Accessed 2017-02-28].

Ignat, R. (2015): *Files and Laboratory tests of laterally loaded rows of lime-cement columns*. Licentiate Thesis, Department of Civil and Architectural Engineering, KTH, Royal Institute of Technology at Stockholm, 69 pp.

Ignat, R., Baker, S., Larsson, S., Liedberg, S. (2015): Two- and three-dimensional analyses of excavation support with rows of dry deep mixing columns. *Computers and Geotechnics*, Vol. 66, May 2015, pp. 16-30.

Implemeteringskommission för Europastandarder inom Geoteknik, IEG (2010): *Geoteknisk undersökning och provning: Identifiering och klassificering av jord. Del 2: Klassificeringsprinciper: Tillämpningsdokument, SS-EN/ISO 14688-2:2004* (Implementation commission for European standards within geotechnics, Geotechnical investigation and testing: Identification and classification of soil, Part 2: Classification principles: Application document. In Swedish), Stockholm, Sweden, 2011, 28 pp.

JSA (1988): *Guidelines of Design and Construction of Deep Excavations*. Japanese Society of Architecture, Tokyo, Japan.

Karlsruud, K., Andresen, L. (2008): Design and Performance of Deep Excavations in Soft Clays. *International Conference on Case Histories in Geotechnical Engineering*. August 11-16 2008. Paper 9. Available at:

<http://scholarsmine.mst.edu/icchge/6icchge/session12/9/> [Accessed on 2017-01-13].

Knappett, J.A., Craig R.F. (2012): *Craig's Soil Mechanics*. Spon Press, Oxon, United Kingdom, 2012, 552 pp.

Larsson, R. (2006): *Djupstabilisering med bindemedels-stabiliserade pelare och masstabilisering- en vägledning*, Svensk Djupstabilisering, Rapport 17 (Deep mixing with binders stabilized columns and mass stabilization- A guide, Swedish Deep stabilization, Report 17. In Swedish), Linköping, Sweden, 386 pp.

Larsson, R. (2008): *Jords egenskaper*, Statens Geotekniska Institut (Soils properties, Governmental Geotechnical Institute. In Swedish), Linköping, Sweden, 62 pp.

Mana, A. I., Clough, G. W. (1981): Prediction of movements for braced cut in clay, *ASCE Journal of Geotechnical Engineering Division*, Vol. 107, No. 6, pp 759-777.

OpenStreetMap contributors. (2017) Marieholm tunnel, Göteborg. Available at: <https://www.openstreetmap.org> [Accessed on 2017-03-01]

Ou, C.Y., (2006): *Deep Excavation: Theory and Practice*. CRS Press, (2006) pp. 125-175.

Ou, C.Y., Wu T.S., Hsieh H.S. (1996): Analysis of deep excavation with column type of ground improvement in soft soil. *Journal of Geotechnical Engineering*, Vol. 122, No. 9, September 1996, pp. 709-716.

PLAXIS (2016): Material Models Manual. Available at: <https://www.plaxis.com/support/manuals/plaxis-2d-manuals/>

Schweiger, H.F., (2009): Influence of constitutive model and EC7 design approach in FEM analysis of deep excavations. *Proceedings of ISSMGE International Seminar on Deep Excavations and Retaining Structures*, Budapest, pp. 99- 114.

Statens Geotekniska Institut, SGI (2007): *Skjuvhållfasthet-utvärdering i kohesionsjord* (Governmental Geotechnical Institute, Shear strength-evaluation of cohesive soil. In Swedish), Linköping, Sweden.

Statens Geotekniska Institut, SGI (2000): *Geodynamik i praktiken* (Governmental Geotechnical Institute, Geodynamics in practice. In Swedish), Linköping, Sweden.

Statens Geotekniska Institut, SGI (2010a): *Sammanställning laboratorieresultat (rutinundersökning)*, Projekt Marieholmstunneln, Entreprenad Ed1, Markteknisk undersökningsrapport (Governmental Geotechnical Institute, Compilation of lab tests (routine examination) Project Marieholm tunnel, Contractor Ed1, Research report. In Swedish), Linköping, Sweden.

Statens Geotekniska Institut, SGI (2010b): *Sammanställning odränerade skjuvhållfasthet vid direkta skjuvförsök och aktiva odränerade triaxialförsök*, Projekt Marieholmstunneln, Entreprenad Ed1, Markteknisk undersökningsrapport (Governmental Geotechnical Institute, Compilation of undrained shear strength at direct shear test and active undrained triaxial test, Project Marieholm tunnel, Contractor Ed1, Research report. In Swedish), Linköping, Sweden

Statens Geotekniska Institut, SGI (2011a): *Sammanställning odränerad skjuvhållfasthet med vingförsök*, Projekt Marieholmstunneln, Entreprenad Ed1, Markteknisk undersökningsrapport (Governmental Geotechnical Institute, Compilation of undrained shear strength for vane test, Project Marieholm tunnel, Contractor Ed1, Research report), Linköping, Sweden.

Statens Geotekniska Institut, SGI (2011b): *sammanställning konsolideringsegenskaper enligt CRS- och stegvisa ödometerförsök*, Projekt Marieholmstunneln, Entreprenad Ed1, Markteknisk undersökningsrapport (Governmental Geotechnical Institute, Compilation of consolidation properties according to CRS and incremental loading oedometer tests, Project Marieholm tunnel, Contractor Ed1, Research report. In Swedish), Linköping, Sweden.

Svenska Geotekniska Föreningen, SGF (2000): *Kalk-och kalkcementpelare: Vägledning för projektering, utförande och kontroll* (Swedish Geotechnical Institute, Lime- and lime-cement columns: Guidance for projection, implementation and control), Roland Offset AB Linköping, Sweden, 2000 pp. 1-115.

Skempton, A.W., (1951): *The Bearing capacity of Clays*. Buildings Research Congress, Vol. 1, 1951, pp. 180-189.

Trafikverket (2011): *TK Geo 11: Trafikverkets tekniska krav för geokonstruktioner* (The road administration technical requirements for geoconstructions. In Swedish), Trafikverket, Sweden, 2011, 178 pp.

Trafikverket (2014): *TK Geo 13: Trafikverkets tekniska krav för geokonstruktioner* (The road administration technical requirements for geoconstructions. In Swedish), Trafikverket, Sweden, May 2014, 178 pp.

Trafikverket (2017a): *Marieholmsbron* (Marieholm tunnel. In Swedish). Available at: <http://www.trafikverket.se/nara-dig/Vastra-gotaland/projekt-i-vastra-gotalands-lan/Marieholmsforbindelsen/Marieholmstunneln/>. [Accessed 2017-01-30].

Trafikverket (2017b), *Design torrdocka* (Dry dock design. In Swedish), PowerPoint presentation.

Vucetic, M., Dobry, R. (1991): Effect of soil plasticity on cyclic response. *ASCE Journal of Geotechnical Engineering*, Vol. 117, No. 1, January 1991, pp. 89-107.

WSP (2009a): E6/E45/E20 Marieholmsförbindelsen i Göteborg, Arbetsplan Beskrivning (E6/E45/E20 Marieholms connection in Gothenburg. Work plan description. In Swedish). Available at: http://www.trafikverket.se/contentassets/07c8c0775bf0414284638e848fa90b8a/arbetsplan/0c050001_20091001_rev5_beskr_arbetsplan.pdf [Accessed 2017-01-12].

WSP (2009b): *Ödometerförsök CRS*, Projekt Marieholmstunneln, Entreprenad Ed1, Markteknisk undersökningsrapport (Oedometer test CRS, Project Marieholm tunnel, Contractor Ed1, Research report . In Swedish), Gothenburg, Sweden.

Wu, S.H., Ou C.H., Ching, J., Juang, H. (2012): Reliability-Based Design for Basal Heave Stability of Deep Excavations in Spatially Varying Soils. *Journal of Geotechnical and Geoenvironmental Engineering*, Vol. 138, No 5, May 2012, pp. 594-603.

Zublin (2015a): 4G130001, Geotechnical Interpretative Report.

Zublin (2015b): 4G130002, Försöksrapport- Geotekniska undersökningar (Test report- Geotechnical surveys. In Swedish)

Zublin (2015c): 4K284902, Structural design overall system & detailed design retaining wall.

Zublin (2015d): 4K394901, Method Statement.

Appendices

Appendix A- Borehole map

Appendix B- Structure, fill and drainage parameters

Appendix C- Lime-cement columns parameters

Appendix D- Properties of the Lime-cement according to Ignat's method

Appendix E- Properties of Clay layer

Appendix F- Compression and Swelling index

Appendix G- Evaluation of HSs-stiffnesses parameters

Appendix H- Calculation of the small strain shear stiffness (G_0) and the shear strain level ($\gamma_{0.7}$)

Appendix I- Calibration of the Soft Soil parameters

Appendix J- Calibration of the Hardening Soil model with small-strain stiffness parameters

Appendix K- Correlation between the Soft Soil and the Hardening Soil small-strain stiffness models parameters

Appendix L- Analytical calculations

Appendix M- Mesh, failure surface and safety factor

Appendix N- Influence of loads- Model 1

Appendix O- Parametric studies- Model 1

Appendix A- Borehole map

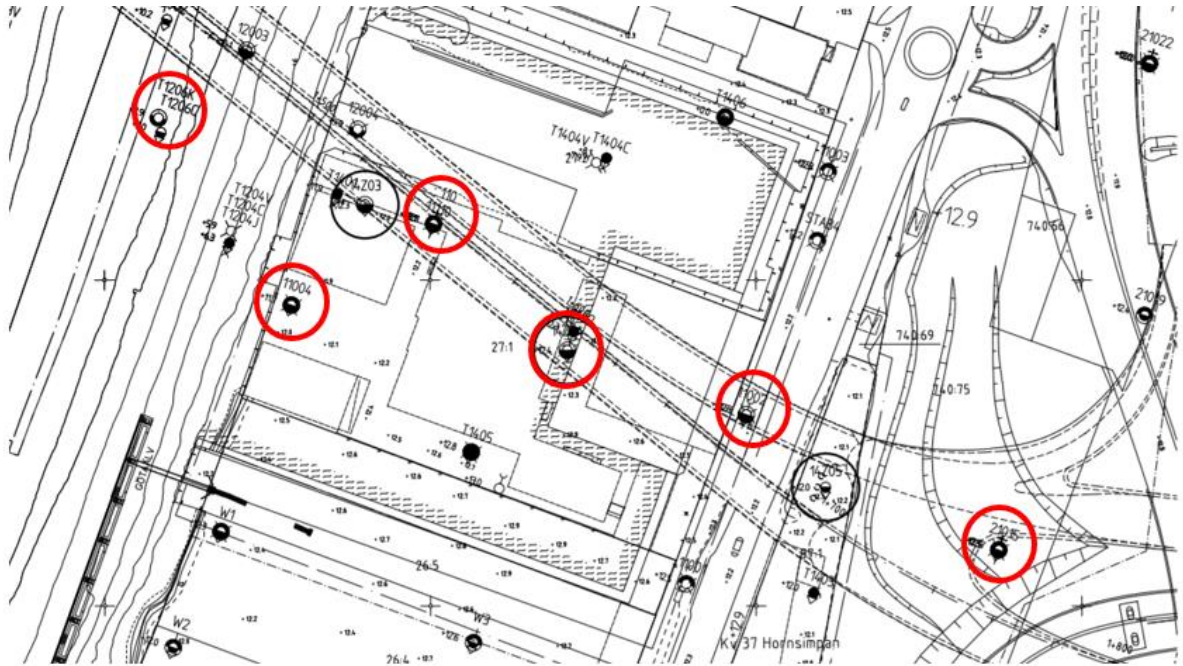


Figure 42: The boreholes that have been used is marked with a red circle, from left to right: T1206, 1104, 110, 14Z04, 1102, 21015 (Zublin, 2015a).

Appendix B- Structure, fill and drainage parameters

Properties of concrete, strut, piles and retaining wall

Table 26: Properties of underwater concrete after the reinforced concrete is placed, MC model.

Parameters	Value	Units
Unsaturated weight, γ_{unsat}	23	kN/m ³
Saturated weight, γ_{sat}	23	kN/m ³
Effective Young's Modulus, E'	$27.26 \cdot 10^6$	kN/m ²
Effective Poisson's ratio, ν'	0.2	-
Effective cohesion, c'_{ref}	7800	kN/m ²
Effective friction angle, ϕ'	35	°
Dilatancy angle, ψ	0	°
Tensile strength, σ_t	20	kN/m ²
Permeability, $k_x = k_y$	864	m/day
Interface, R_{inter}	0.71	-
Coefficient of lateral earth pressure at rest, K_0	1	-

Table 27: Properties of underwater concrete before the reinforced concrete is placed, MC model.

Parameters	Value	Units
Unsaturated weight, γ_{unsat}	23	kN/m ³
Saturated weight, γ_{sat}	23	kN/m ³
Effective Young's Modulus, E'	$27.26 \cdot 10^6$	kN/m ²
Poisson's ratio, ν'	0.2	-
Effective cohesion, c'_{ref}	7800	kN/m ²
Effective friction angle, ϕ'	35	°
Dilatancy angle, ψ	0	°
Tensile strength, σ_t	2020	kN/m ²
Permeability, $k_x = k_y$	864	m/day
Interface, R_{inter}	0.71	-
Coefficient of lateral earth pressure at rest, K_0	1	-

Table 28: Properties of reinforced concrete, LE model.

Parameters	Value	Units
Unsaturated weight, γ_{unsat}	25	kN/m ³
Saturated weight, γ_{sat}	25	kN/m ³
Effective Young's Modulus, E'	$19.44 \cdot 10^6$	kN/m ²
Effective Poisson's ratio, ν'	0.2	-
Permeability, $k_x = k_y$	864	m/day
Interface, R_{inter}	0.67	-
Coefficient of lateral earth pressure at rest, K_0	1	-

Table 29: Values between the underwater concrete and the retaining wall interface.

Parameters	Value	Units
Unsaturated weight, γ_{unsat}	23	kN/m ³
Saturated weight, γ_{sat}	23	kN/m ³
Effective Young's Modulus, E'	$27.26 \cdot 10^6$	kN/m ²
Poisson's ratio, ν'	0.2	-
Effective cohesion, c'_{ref}	7800	kN/m ²
Effective friction angle of soil, φ'	35	°
Dilatancy angle, ψ	0	°
Tensile strength	0	kN/m ²
Permeability, $k_x = k_y$	0	m/day
Interface, R_{inter}	0.2	-
Coefficient of lateral earth pressure at rest, K_0	0.56	-

Table 30: Parameters for the struts.

Parameters	Value	Units
Material Type	Elastoplastic	-
EA	$17.2 \cdot 10^6$	kN/m
Lspacing	9.0	m
F _{max, comp}	9616	kN

Table 31: Parameters for the 52m long piles.

Parameters	Value	Units
Young's Modulus, E	$30 \cdot 10^6$	kN/m ²
Specific weight, γ	24	kN/m ³
Width	0.27	m
Area	0.0729	m ²
Second moment of area, I	$0.4429 \cdot 10^{-3}$	m ⁴
Skin resistance	Linear	-
T _{top, max}	11	kN/m
T _{bot, max}	64	kN/m
T _{min}	0	kN/m
F _{max}	27	kN

Table 32: Parameters for the 39m long pipe-to-pipe wall.

Parameters	Pipe-to-pipe wall	Units
Material type	Elastic	-
Isotropic	Yes	-
End bearing	No	-
EA	$8.24 \cdot 10^6$	kN/m
EI	$2.03 \cdot 10^6$	kNm ² /m
D	1.719	m
Weight, W	3.06	kN/m/m
Poisson's ratio, ν	0.3	-
M_p	$1 \cdot 10^{15}$	kN m/m
$16N_g$	$1 \cdot 10^{10}$	kN/m

Table 33: Parameters for the crane slab.

Parameters	Crane Slab	Units
Material type	Elastic	-
Isotropic	Yes	-
End bearing	No	-
EA	$9 \cdot 10^6$	kN/m
EI	$67.5 \cdot 10^6$	kNm ² /m
D	0.3	m
Weight, W	7.5	kN/m/m
Poisson's ratio, ν	0.2	-
M_p	$1 \cdot 10^{15}$	kN m/m
$16N_g$	$1 \cdot 10^{10}$	kN/m

Properties of fill layer

Table 34: Properties of fill layer, MC model.

Parameters	Value	Units
Unsaturated weight, γ_{unsat}	17	kN/m ³
Saturated weight, γ_{sat}	17	kN/m ³
Young's Modulus, E	10 000	kN/m ²
Effective Poisson's Ratio, ν'	0.2	-
Effective cohesion c'_{ref}	0	kN/m ²
Effective friction angle of soil, ϕ'	30	°
Dilatancy angle, ψ	0	°
Permeability, $k_x=k_y$	$0.864 \cdot 10^{-3}$	m/day
Interface, R_{inter}	0.67	-
Coefficient of lateral earth pressure, K_0	0.5	-

Properties of drainage layer

Table 35: Properties of drainage layer, HSs model (used when the clay layers were modelled with HSs).

Parameters	Value	Units
Unsaturated weight, γ_{unsat}	19.5	kN/m ³
Saturated weight, γ_{sat}	19.5	kN/m ³
Secant stiffness in standard drained triaxial test at reference pressure, E_{50}^{ref}	10 000	kN/m ²
Tangent stiffness for primary oedometer loading at reference pressure, E_{oed}^{ref}	10 000	kN/m ²
Unload/reload stiffness at reference pressure, E_{ur}^{ref}	30 000	kN/m ²
Effective Poisson's ratio for un/reloading, ν'_{ur}	0.2	-
Effective reference cohesion, c'_{ref}	1	kN/m ²
Effective friction angle of soil, ϕ'	31	°
Dilatancy angle, ψ	0	°
Shear strain level when $G = 0.7G_0$, $\gamma_{0.7}$	$0.1 \cdot 10^{-3}$	-
Undrained initial shear modulus at reference pressure, G_0^{ref}	45 000	kN/m ²
Coefficient of earth pressure at rest for normally consolidated clay, K_0^{nc}	0.485	-
Tensile strength	0	kN/m ₂
Permeability, $k_x = k_y$	8.64	m/day
Interface, R_{inter}	0.67	-
Coefficient of lateral earth pressure at rest, K_0	Automatic	-

Table 36: Properties of drainage layer, MC model (used when the clay layers were modelled with SS).

Parameter	Value	Units
Unsaturated weight, γ_{unsat}	19.5	kN/m ³
Saturated weight, γ_{sat}	19.5	kN/m ³
Young's Modulus, E	30 000	kN/m ²
Effective Poisson's Ratio, ν'	0.2	-
Effective cohesion c'_{ref}	1.0	kN/m ²
Effective friction angle of soil, ϕ'	31	°
Dilatancy angle, ψ	1.0	°
Permeability, $k_x=k_y$	8.64	m/day
Interface, R_{inter}	0.67	-
Coefficient of lateral earth pressure, K_0	0.49 (Automatic)	-

Appendix C- Lime-cement columns parameters

In Table 37 the parameters that have been used to model the LCC box can be found.

Table 37: Parameters for the block consisting of the LCC columns and the existing soil.

Parameter	Value	Unit
Equivalent unsaturated weight, $\gamma_{\text{unsat, eq}}$	16.5	kN/m ³
Equivalent saturated weight, $\gamma_{\text{sat, eq}}$	16.5	kN/m ³
Equivalent effective Young's Modulus, E'_{eq}	15 450	kN/m ²
Equivalent effective Poisson's ratio, ν'_{eq}	0.15	-
Equivalent effective cohesion, c'_{eq}	0	kN/m ²
Equivalent effective friction angle, ϕ'_{eq}	30	°
Equivalent dilatancy angle, ψ_{eq}	0	°
Equivalent permeability, $k_x=k_y$	$4.32 \cdot 10^{-5}$	m/day
Interface, R_{inter}	0.8	-
Coefficient of lateral earth pressure, K_0	Automatic	-

Appendix D- Properties of the Lime-cement according to Ignats' method

The lime-cement columns will be placed as panels where the individual columns overlap each other. The geometry is presented in Figure 43, and the notations are explained in Table 38.

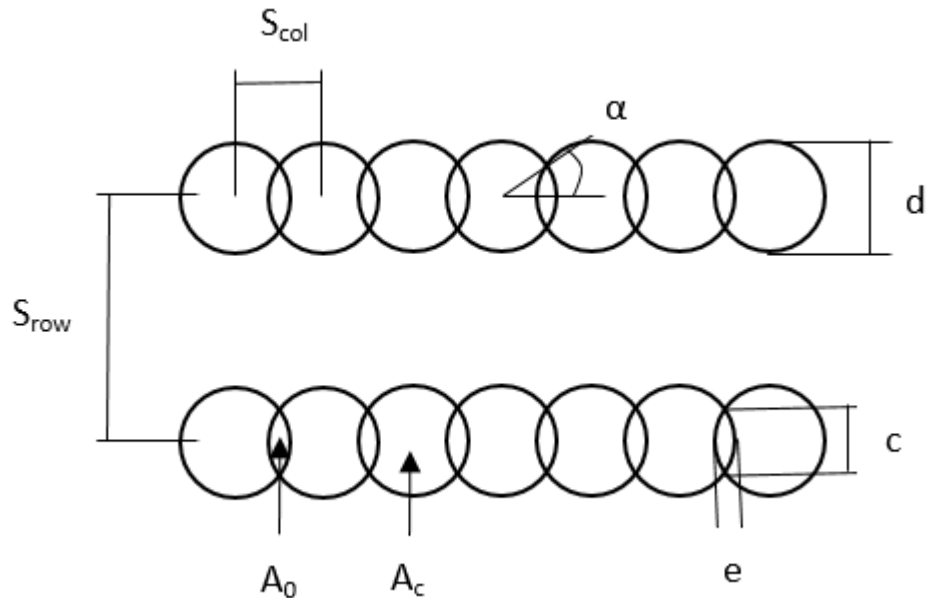


Figure 43: Geometry of the lime-cement columns.

Table 38: Parameters of the lime-cement columns.

Explanation of parameters	Value	Unit
Column diameter, d	0.6	m
Overlap distance between the columns, e	0.1	m
Chord length of the overlap, c	0.3	m
One half of the chord angle, α	0.6	rad.
Center distance between the column rows, S_{row}	1.0	m
Area of the overlap zone between columns, A_0	0.02	m ²
Area of columns without overlap, A_c	0.2	m ²
Effective width of overlap zone, i.e vertical joints, $b_{0,2D}$	0.04	m
Effective width of the columns, b_{c2D}	0.7	m
Area replacement ratio of overlap zone, a_{s0}	0.3	m ²
Area replacement ratio of columns, a_{sc}	0.5	m ²
Shear strength of overlap, s_{u0}	50	kPa
Shear strength of columns, s_{us}	100	kPa
Shear strength of soil between columns, s_{uc}	34.3	kPa
Composite shear strength of overlap, $s_{u,02D}$	51.4	kPa
Composite shear strength of columns, $s_{u,c2D}$	68.1	kPa

Equations (30) to equation (37) were used in order to simplify the geometry from a 3D to a 2D model in PLAXIS where the definition of the notations can be found in Table 38 above (Ignat, 2015).

$$A_0 = 2 \left[\alpha \left(\frac{d}{2} \right)^2 - \frac{(d-e)c}{4} \right] \quad (30)$$

$$A_c = \pi \left(\frac{d}{2} \right)^2 - 2A_0 \quad (31)$$

$$b_{0\ 2D} = \frac{A_0}{c} \quad (32)$$

$$b_{c\ 2D} = \frac{A_c}{c} \quad (33)$$

$$a_{s0} = \frac{c}{s_{row}} \quad (34)$$

$$a_{sc} = \left(\frac{A_c}{s_{row} (d - e - b_{0\ 2D})} \right) \quad (35)$$

$$s_{u,\ 02D} = s_{u,0} a_{s0} + s_{u,s} (1 - a_{s0}) \quad (36)$$

$$s_{u,\ 02D} = s_{u,0} a_{s0} + s_{u,s} (1 - a_{s0}) \quad (37)$$

Appendix E- Properties of clay layers

In the following chapter, the properties of the clay layers are presented.

Density

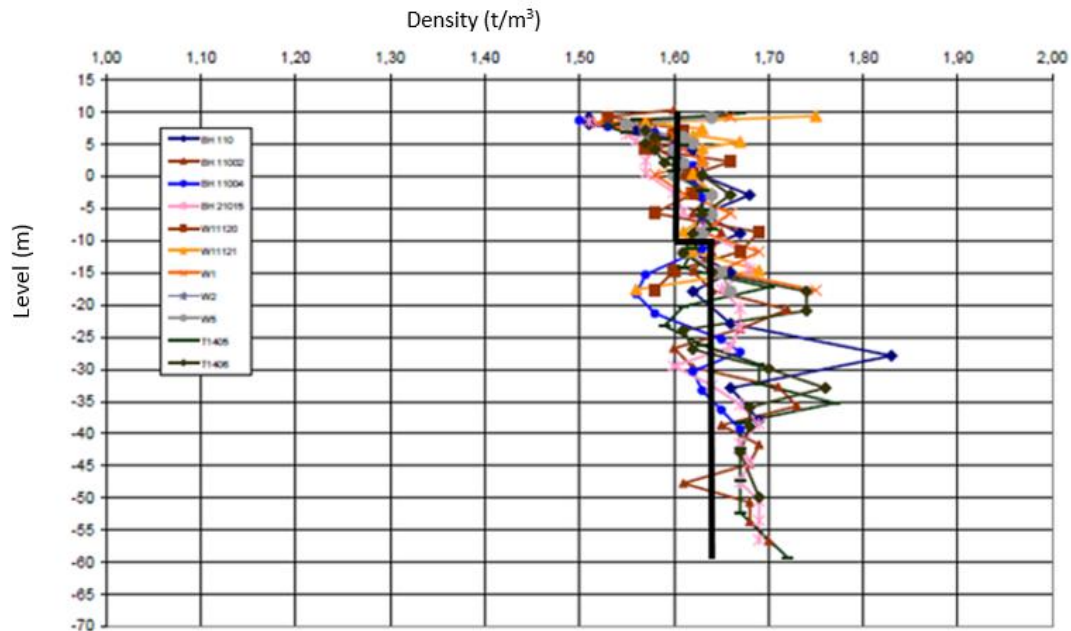


Figure 44: Diagram of the evaluated density from piston samples at the Marieholm side (SGI, 2010a).

Undrained Shear strength

The undrained shear strength is evaluated by interpolating the plotted values given from vane, cone and direct shear tests. Equation (38) represents the undrained shear strength, where x is the level. The level is equal to 12.4m minus the depth.

$$c_u = 20 - 1.14x \quad (38)$$

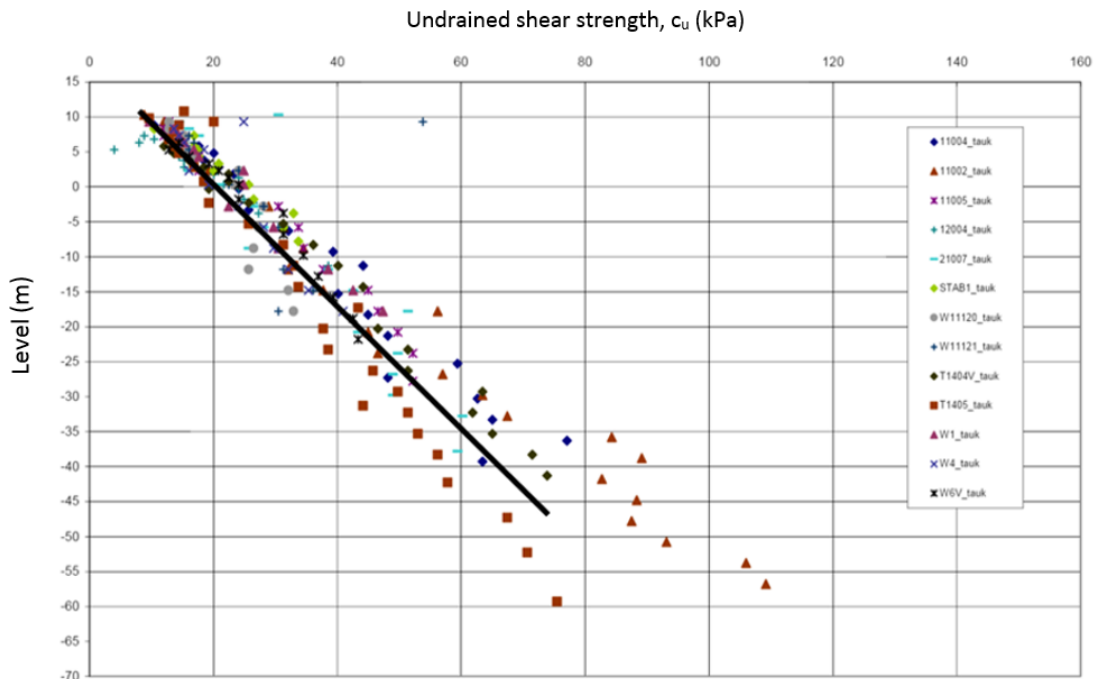


Figure 45: Undrained shear strength at Marieholm side, (vane test, corrected) (SGI, 2011a).

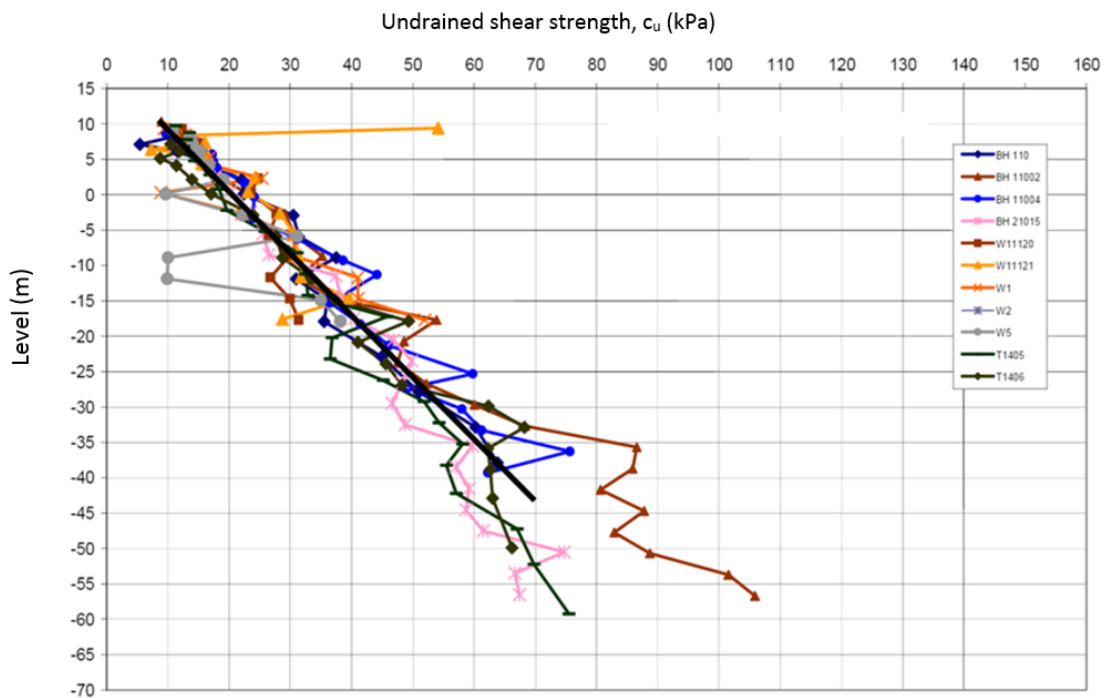


Figure 46: Undrained shear strength at Marieholm, (cone penetration test, corrected according to SGI 3) (SGI, 2010a).

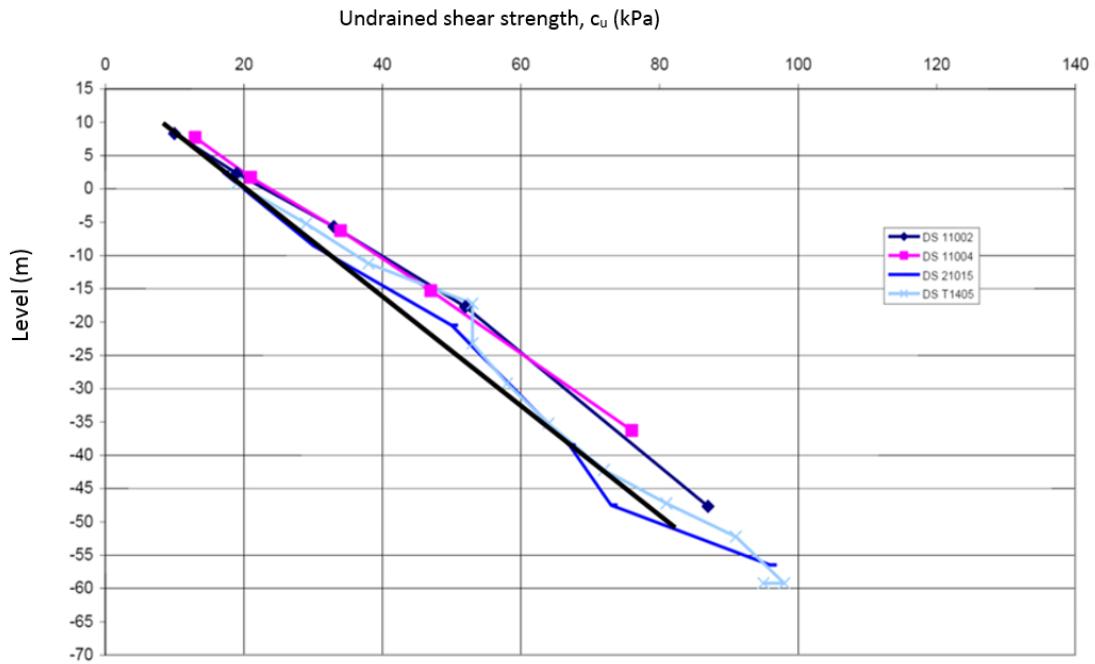


Figure 47: Undrained shear strength at Marieholm, (direct shear test) (SGI, 2010b).

Permeability

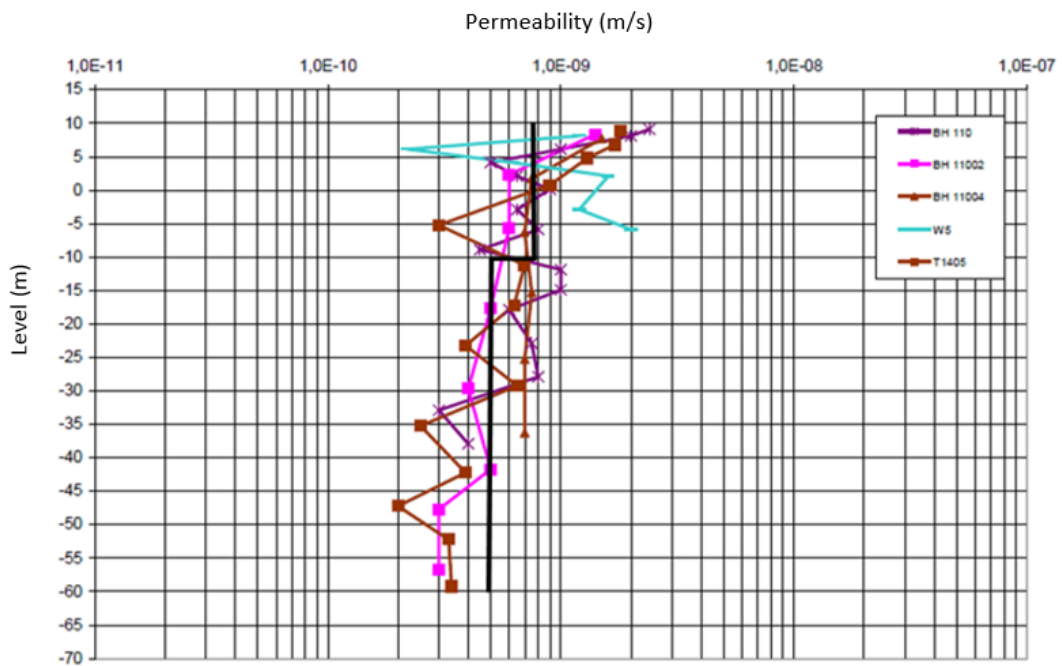


Figure 48: Evaluated permeability (SGI, 2011b).

Preconsolidation pressure

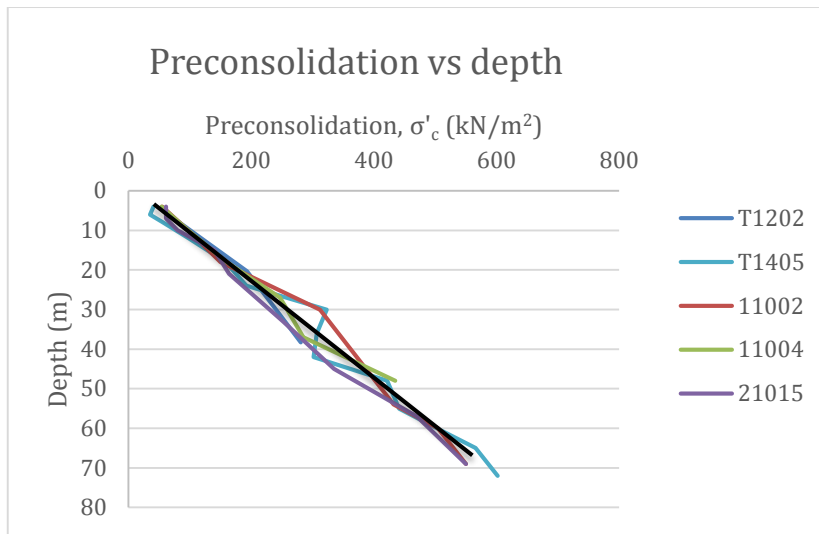


Figure 49: The preconsolidation pressure evaluated from CRS-test (WSP, 2009b).

OCR determination

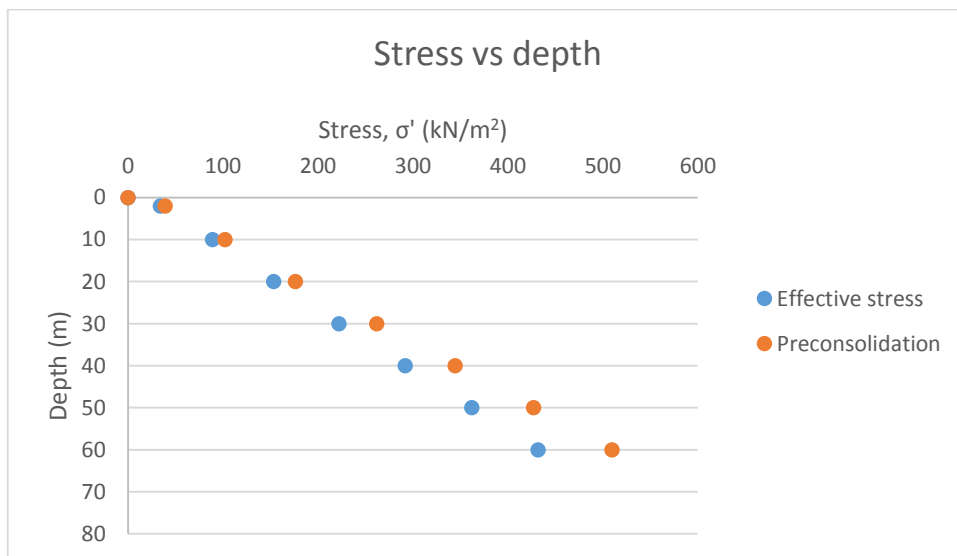


Figure 50: Effective stress and preconsolidation versus depth.

Appendix F- Compression and Swelling index

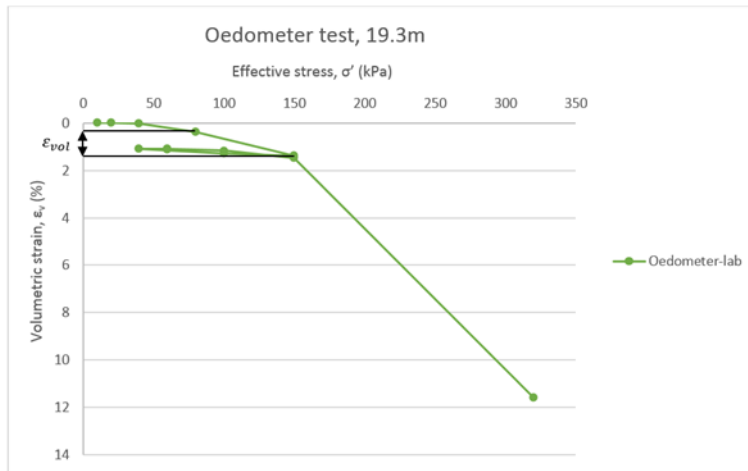


Figure 51: Showing the Volumetric strain change, which correspond to acceptable value according to SGI (2007).

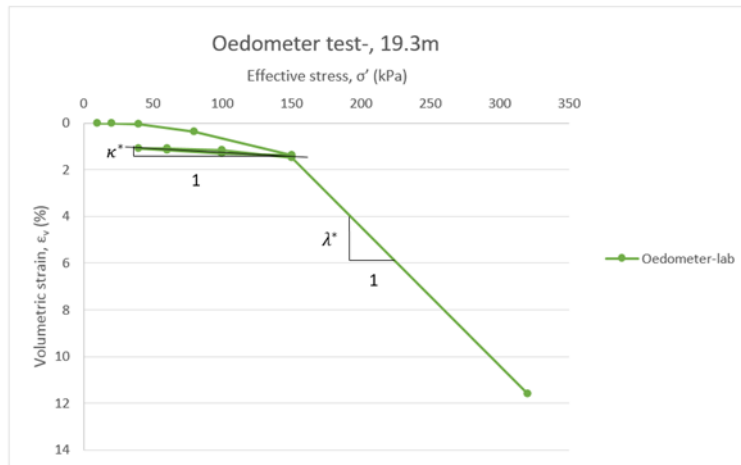


Figure 52: Lines in order to calculate the swelling index (κ^*) and the compression index (λ^*).

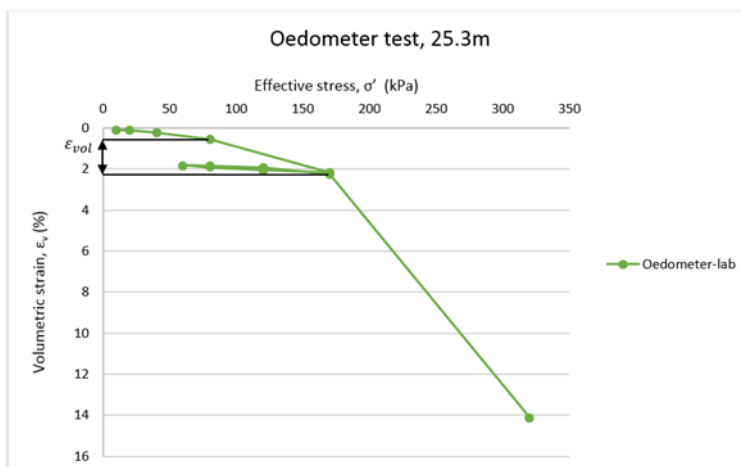


Figure 53: Showing the Volumetric strain change, which correspond to acceptable value according SGI (2007).

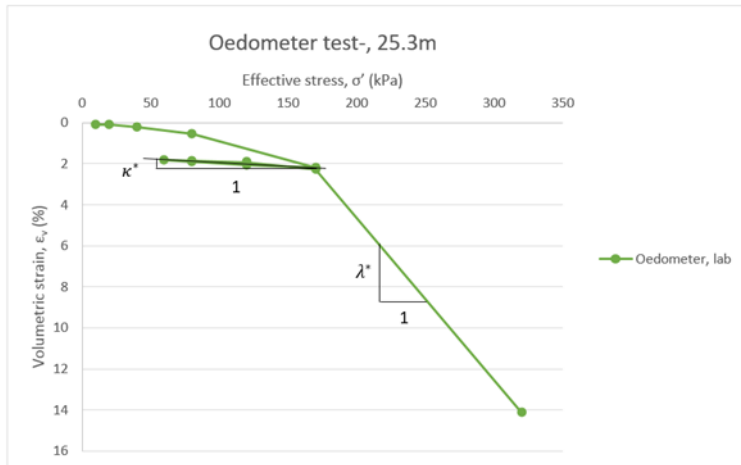


Figure 54: Lines in order to calculate the swelling index (κ^*) and the compression index (λ^*).

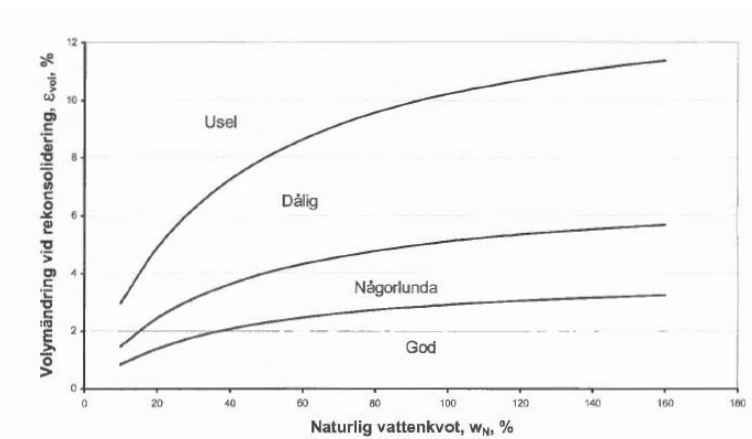


Figure 55: Chart showing how to judge the quality of saturated cohesive soils by looking at the change of volume with reconsolidation. Where "God" is equal to Good, "Någorlunda" is equal to acceptable, "dålig" is equal to bad and "usel" is equal to really bad (SGI, 2017).

Appendix G- Evaluation of HSs-stiffness parameter

The Drained Triaxial tests have been evaluated at two depths which represent the two different clay layers. The following graphs are from Zublin's report 4G130002 (Zublin, 2015b). However, the stiffnesses have been recalculated according to the values in Table 39 and Table 40 (the stiffnesses have been calculated according to chapter Hardening Soil model with small-strain stiffness).

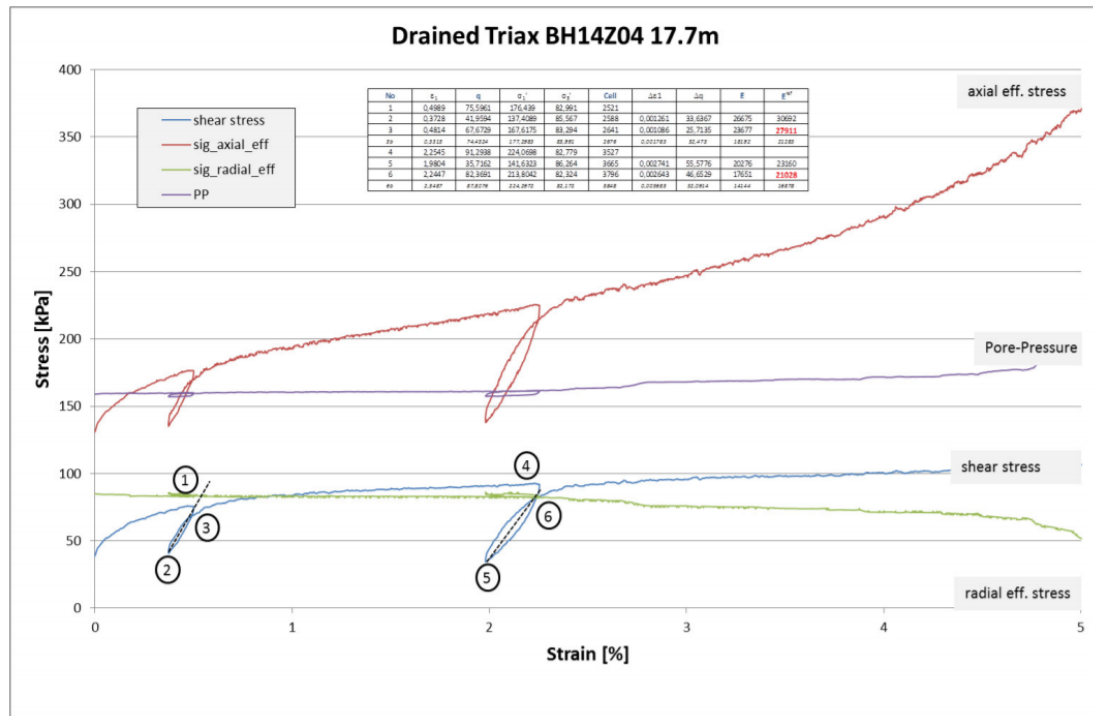


Figure 56: Drained Triaxial test, evaluate reload-unload stiffness parameter (Zublin, 2015b).

Table 39: Values in order to calculate the unload-reload stiffness.

No	ε_1	q	σ'_1	σ'_3	$\Delta\varepsilon_1$	Δq	E_{ur}	E_{ur}^{ref}
1	0.50	76	176	83				
2	0.37	42	137	86	0.001	34	26 667	
3	0.48	68	168	83	0.001	26	23 677	27 472
4	2.25	91	224	83				
5	1.98	36	142	86	0.003	56	20 276	
6	2.24	82	214	82	0.003	47	17 651	21 246

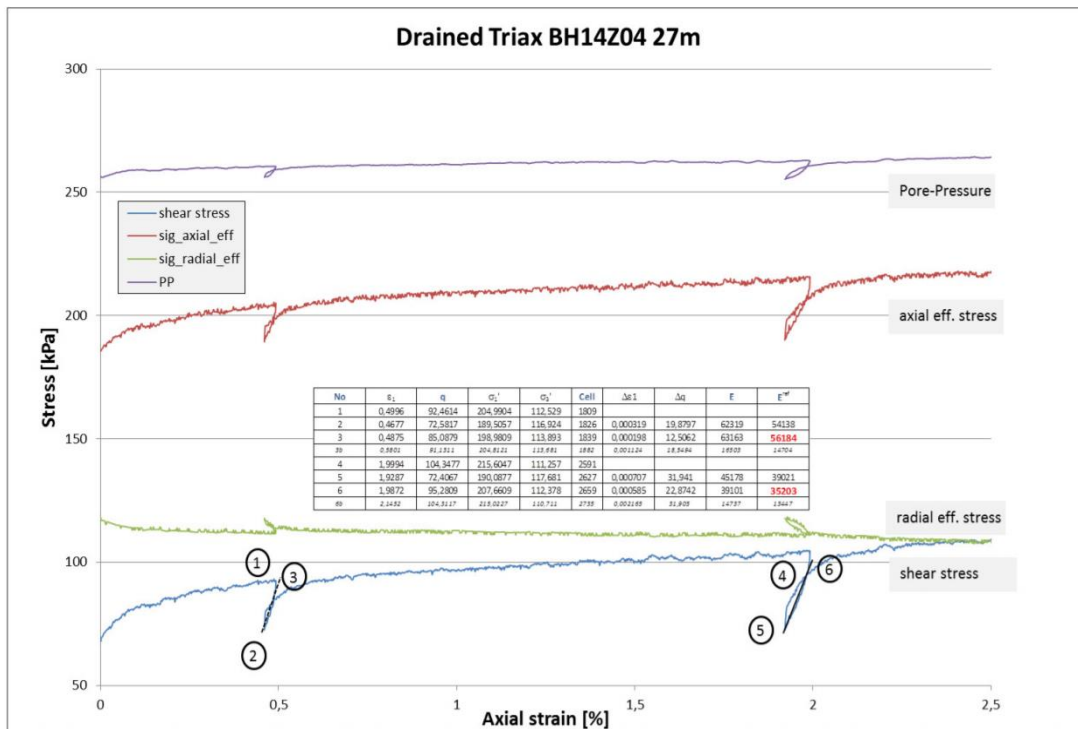


Figure 57: Drained Triaxial test, evaluate reload-unload stiffness parameter (Zublin, 2015b).

Table 40: Values in order to calculate the unload-reload stiffness.

No	ε_1	q	σ'_1	σ'_3	$\Delta\varepsilon_1$	Δq	E_{ur}	E_{ur}^{ref}
1	0.50	92	205	113				
2	0.47	73	190	117	0.0003	20	62 319	
3	0.49	85	199	114	0.0002	13	63 163	55 750
4	2.00	104	216	111				
5	1.93	72	190	118	0.0007	32	45 178	
6	1.99	95	214	112	0.0006	23	39 101	34 960

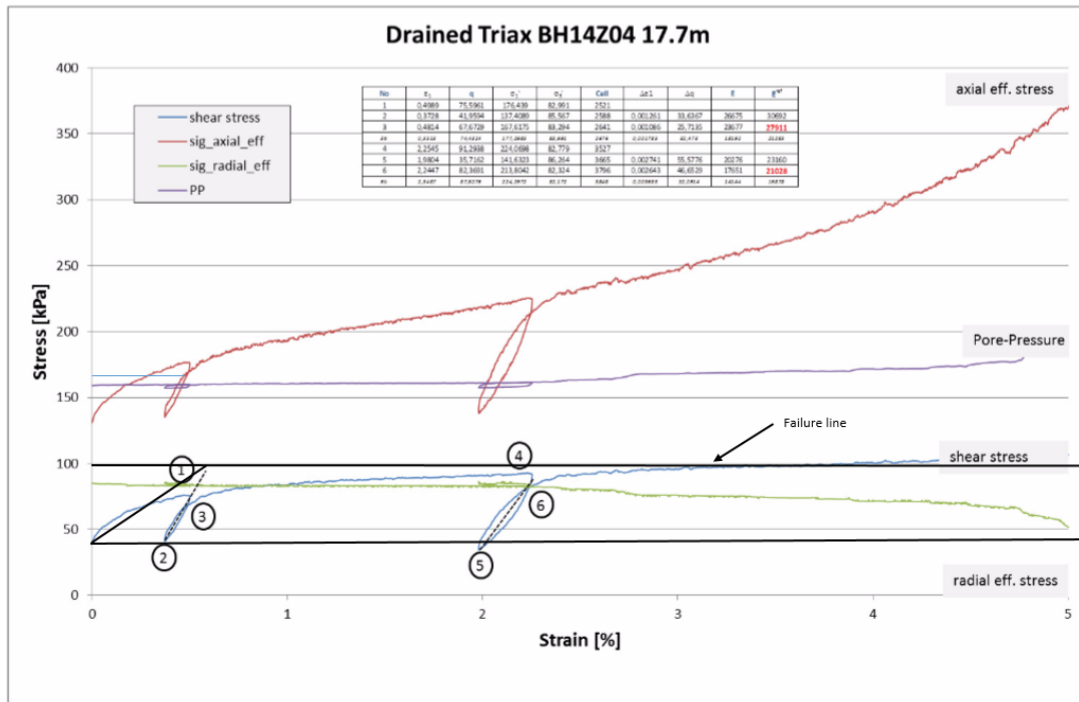


Figure 58: Evaluation of the primary stiffness (E_{50}) in Drained Triaxial test at a depth of 17.7 m (Zublin, 2015b).

Table 41: Calculation of E_{50}^{ref} from the drained triaxial test at 17.7 m depth.

$\Delta\epsilon_1$	Δq	E_{50}	E_{50}^{ref}
0.59	61	10 339	10 643

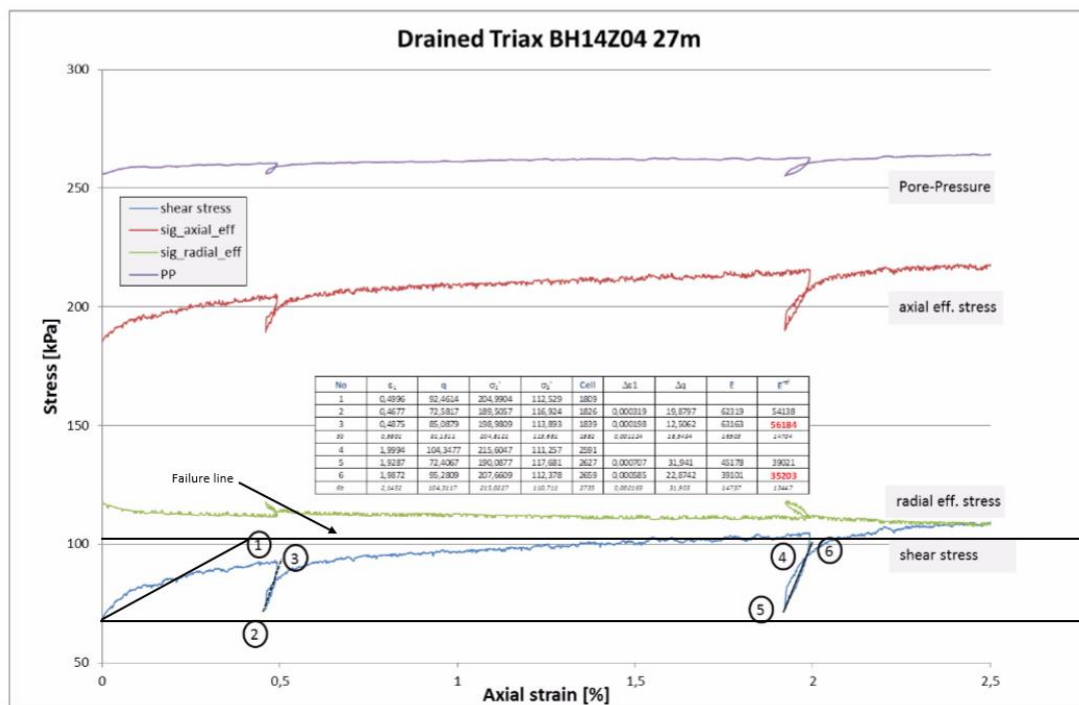


Figure 59: Evaluation of the primary stiffness (E_{50}) in Drained Triaxial test at a depth of 27.0 m (Zublin, 2015b).

Table 42: Calculation of E_{50}^{ref} from the drained triaxial test at 27.0 m depth.

$\Delta\varepsilon_1$	Δq	E_{50}	E_{50}^{ref}
0.4	36.7	9175	8105

To calculate the E_{oed}^{ref} firstly the E_{oed} needs to be calculated. This is determined by calculating the tangent stiffness in the compression line of the CRS test, see Figure 60. Thereafter, the E_{oed}^{ref} can be determined by using equation (39) .

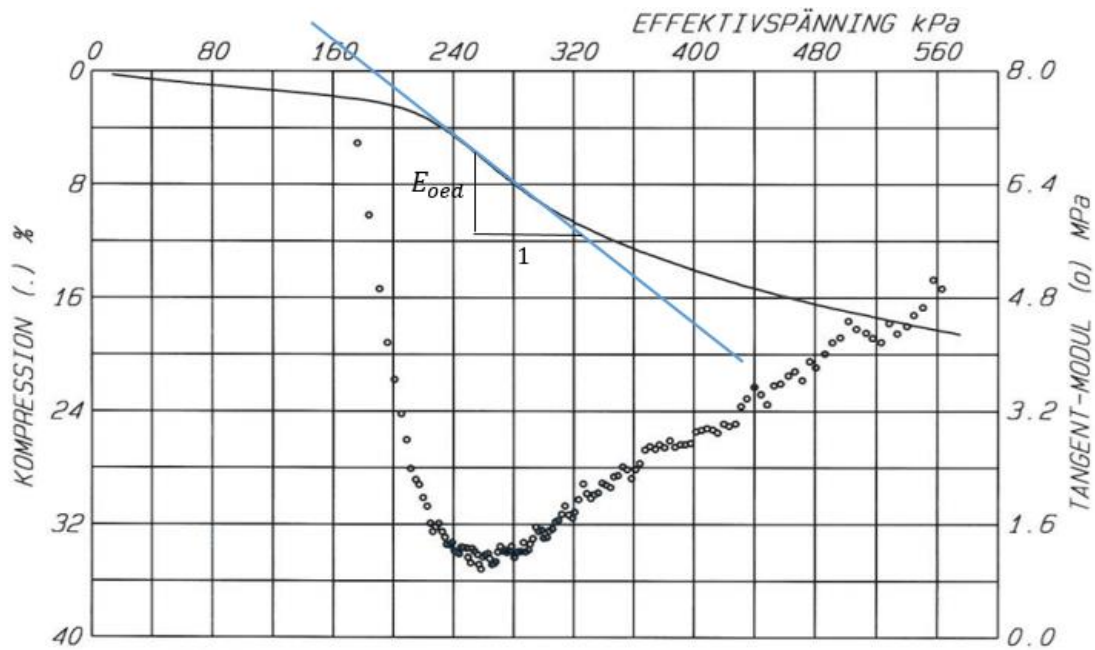


Figure 60: Evaluation of the tangent stiffness for primary oedometer loading, at borehole T1206, depth 19.3 m.

$$E_{oed}^{ref} = E_{oed} / \left(\frac{c \cos \varphi - \frac{\sigma'_3}{K_0^{nc}} \sin \varphi}{c \cos \varphi + p^{ref} \sin \varphi} \right)^m \quad (39)$$

Appendix H- Calculation of the small strain shear stiffness (G_0) and the shear strain level ($\gamma_{0.7}$)

The small strain shear stiffness and the reference small strain shear stiffness can be calculated by equation (40) and equation (41). The input values and the result can be seen in the Table 43. Since undrained tests were not available c and φ cannot be determined. Therefore to calculate G_0^{ref} , the shear strength should be taken from $\sigma'_3 = 100$ so equation (40) will be equal to G_0^{ref} .

$$G_0 \approx 504 \frac{c_u}{w_L} \quad (40)$$

$$G_0 = G_0^{ref} \left(\frac{c \cos \varphi - \sigma'_3 \sin \varphi}{c \cos \varphi + p^{ref} \sin \varphi} \right)^m \quad (41)$$

Table 43: Input values and result in order to calculate the small strain shear stiffness and the shear strain level.

Parameter	Value	Unit
Reference small strain shear stiffness, G_0^{ref}	21 600	kN/m ²
Small strain shear stiffness, G_0	21 600	kN/m ²
Shear strength, c_u	30	kN/m ²
Liquid limit, w_L	70	%
Horizontal stress, σ'_3	100	kPa
Power, m	1	-

The yield point that was used in the equation was obtained from the following graph (see Figure 61).

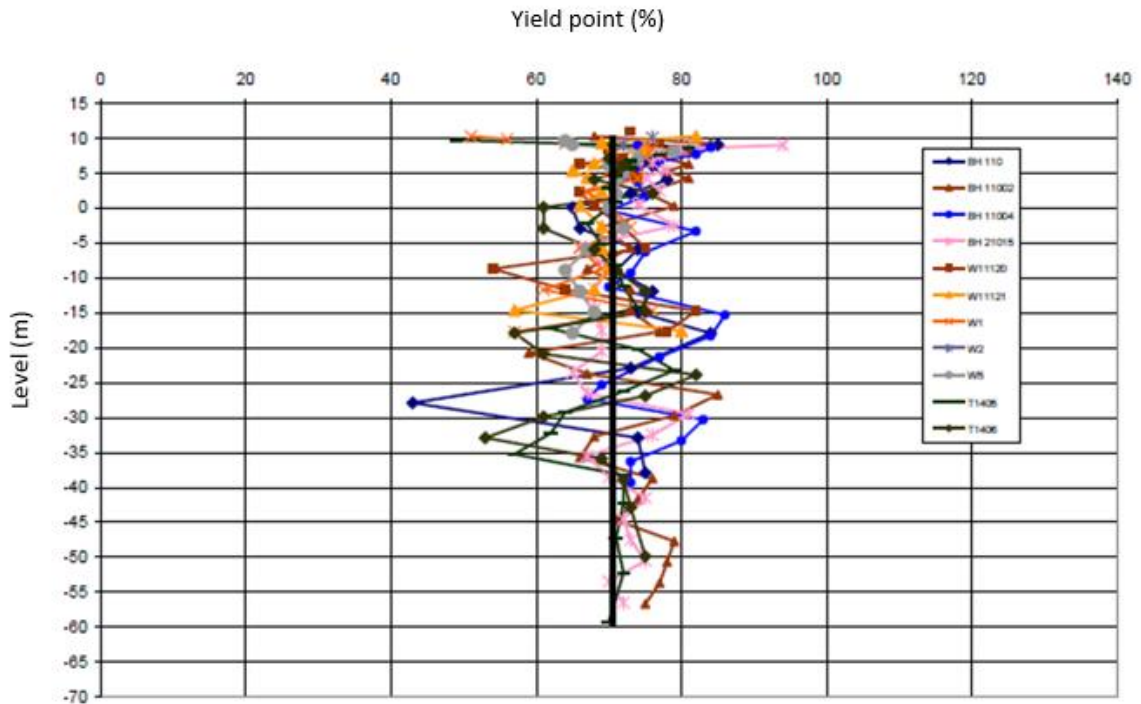


Figure 61: Measurement from the area showing the evaluated yield point from piston samples (SGI, 2010a).

The shear strain at 70% of G_0 , $\gamma_{0.7}$, was estimated from Figure 62. The exact value of the plasticity index is not known, therefore it is assumed to be 30 as the range is between 25-50 according to IEG 13:2010 (IEG, 2010).

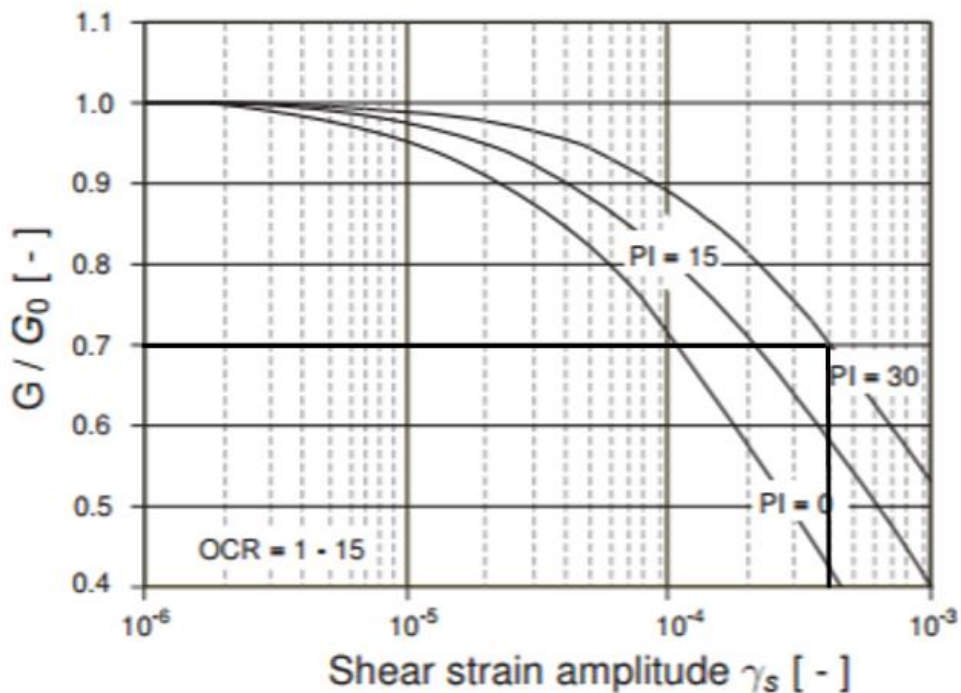


Figure 62: Estimation of shear strain at 70% of the initial small shear strain modulus (PLAXIS, 2016).

Appendix I- Calibration of the Soft Soil parameters

In Table 44 and Table 45 the phases modelled in PLAXIS in order to represent the behavior for the oedometer tests can be seen.

Table 44: Phases from the oedometer test of borehole T1206, at depth 19.3m.

Phase	Duration [days]	Steps	Stress increment [kN/m ²]
1	1	100	-10
2	1	100	-10
3	1	100	-20
4	1	100	-40
5	1	100	-70
6	1	100	50
7	1	100	40
8	1	100	20
9	1	100	-20
10	1	100	-40
11	1	100	-50
12	1	100	-170

Table 45: Phases from the oedometer test of borehole T1206, at depth 25.3m.

Phase	Duration [days]	Steps	Stress increment [kN/m ²]
1	1	100	-10
2	1	100	-10
3	1	100	-20
4	1	100	-40
5	1	100	-90
6	1	100	50
7	1	100	40
8	1	100	20
9	1	100	-20
10	1	100	-40
11	1	100	-50
12	1	100	-150

Figure 63-Figure 66 show the difference of the stress-strain curve between the evaluated and calibrated values from the oedometer test and the CRS test at the two evaluated depths. Additionally the evaluated and calibrated values can found in Figure 44.

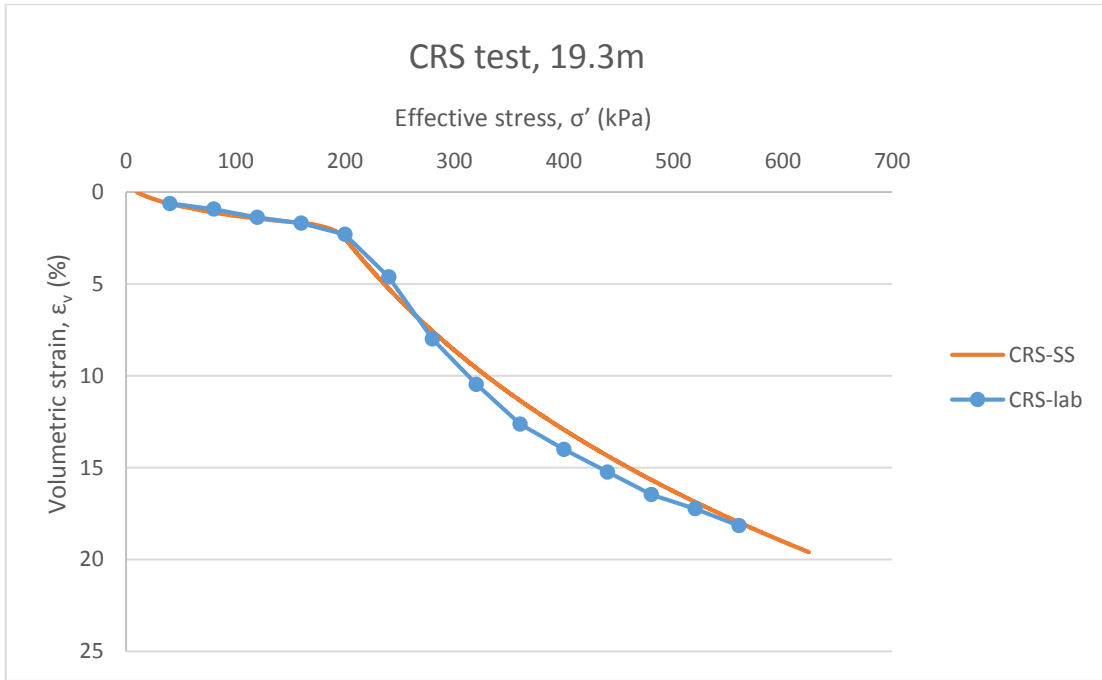


Figure 63: Comparison between the lab data and data evaluated from Soft Soil for the CRS test at 19.3 m.

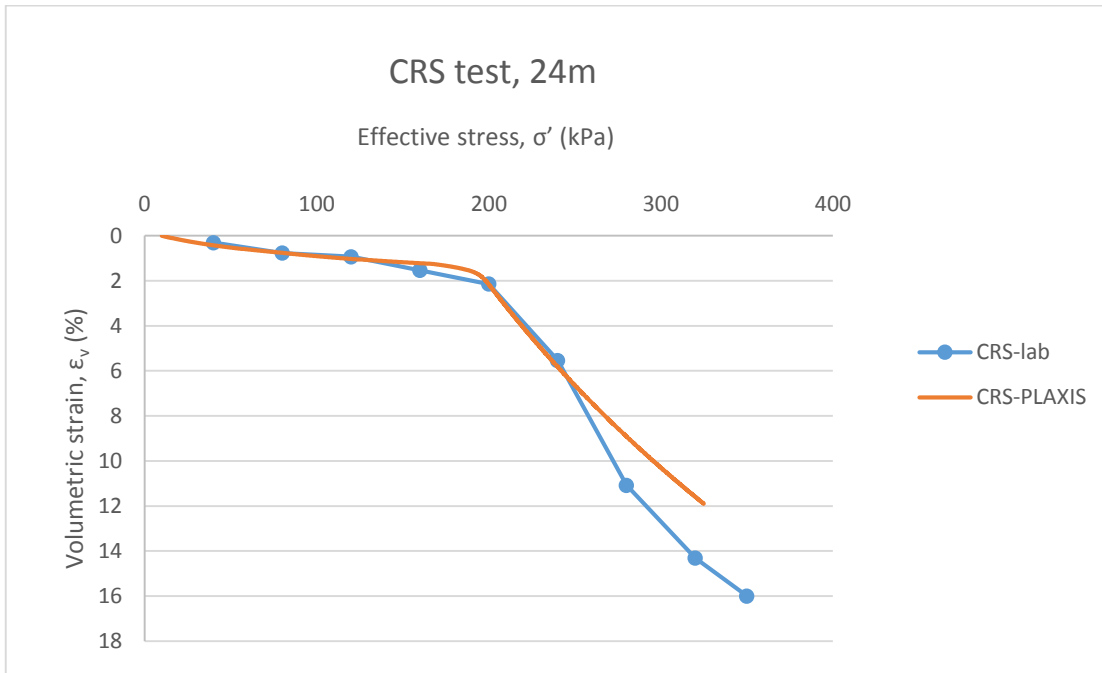


Figure 64: Comparison between the lab data and data evaluated from Soft Soil for the CRS test at 24 m.

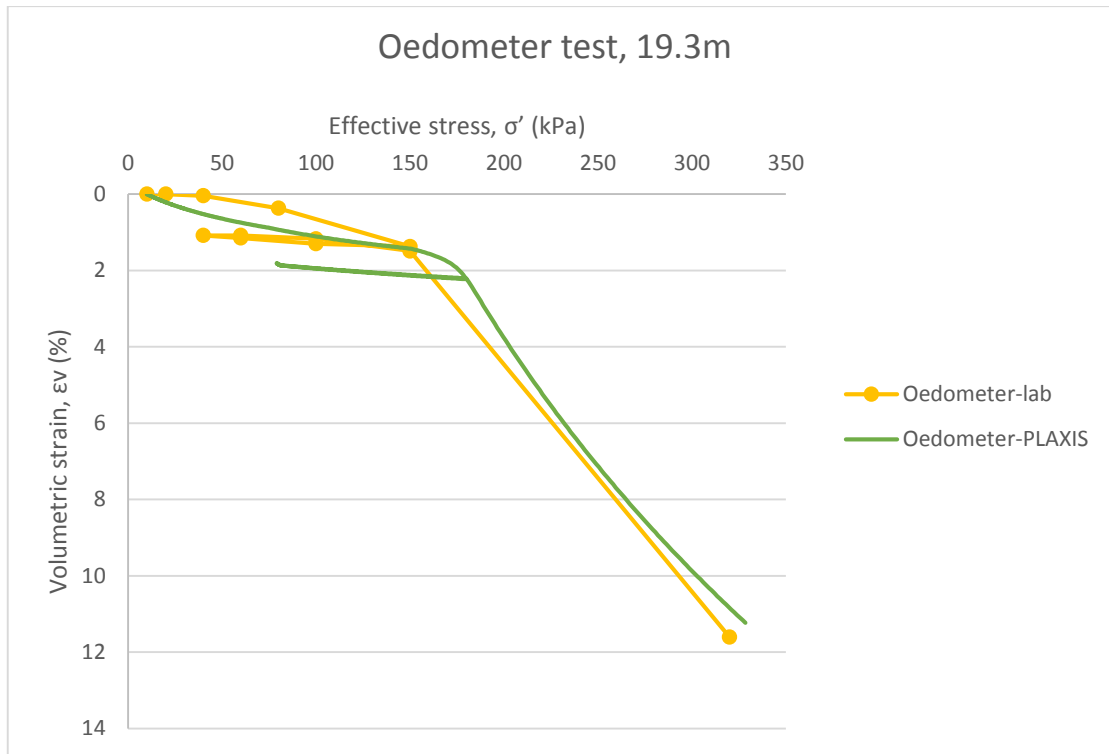


Figure 65: Comparison between the lab data and data evaluated from Soft Soil for the oedometer test at 19.3 m.

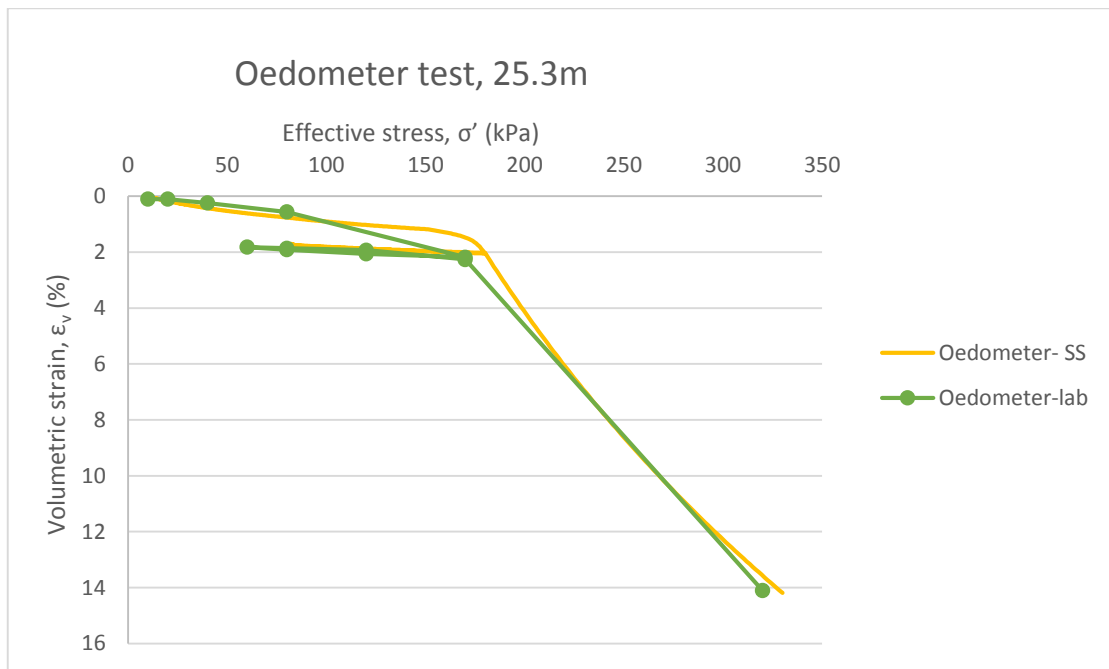


Figure 66: Comparison between the lab data and data evaluated from SoftSoil for the oedometer test at 25.3 m.

Table 46: Evaluated and calibrated parameters for the Soft Soil model.

Parameters	Evaluated parameters		Calibrated values		Units
	19.3 m	25.3 m	19.3 m	25.3 m	
Unsaturated unit weight, γ_{unsat}	16	16.5	16	16.5	kN/m ³
Saturated unit weight, γ_{sat}	16	16.5	16	16.5	kN/m ³
Modified compression index, λ^*	0.13	0.19	0.15	0.20	-
Modified swelling index, κ^*	0.0022	0.003	0.0082	0.007	-
Poisson's ratio for unloading/reloading, ν'_{ur}	0.15	0.15	0.15	0.15	-
Effective reference cohesion, c'_{ref}	3	3.7	3	3.7	kN/m ²
Coefficient of earth pressure at rest for normally consolidated clay, K_0^{nc}	0.6	0.6	0.6	0.6	-
Effective friction angle, φ'	30	30	30	30	°
Dilatancy angle, ψ	0	0	0	0	°
Vertical precon. pressure, p_c (oedometer= 90% of the CRS)	194	194	175	175	kPa

Appendix J- Calibration of the Hardening Soil model with small-strain stiffness parameters

In order to obtain the parameters for the HSs model, the drained triaxial and the CRS tests were simulated and calibrated in PLAXIS. For the former the strain increment was 0.06%/hour whereas for the latter it was 0.7%/hour. These rates were obtained from lab data. The input parameter for the calibration can be found in the Table 47.

Table 47: Initial and calibrated values for both the drained triaxial and the CRS tests at 19.3m (layer 1) and 27.7 m (layer 2).

Parameter	Evaluated values		Calibrated values		Unit
	Layer 1	Layer 2	Layer 1	Layer 2	
Unsaturated unit weight, γ_{unsat}	16	16.5	16	16.5	kN/m ³
Saturated unit weight, γ_{sat}	16	16.5	16	16.5	kN/m ³
Secant stiffness in standard drained triaxial test at reference pressure, E_{50}^{ref}	10 643	8105	5000	5000	kN/m ²
Tangent stiffness for primary oedometer loading at reference pressure, E_{oed}^{ref}	1465/20 14	1823	3051	3051	kN/m ²
Unload/reload stiffness at reference pressure, E_{ur}^{ref}	24 359	34 960	15 000	15 000	kN/m ²
Power, m	1	1	1	1	-
Effective Poisson's ratio for un/reloading, ν'_{ur}	0.15	0.15	0.15	0.15	-
Effective reference cohesion, c'_{ref}	3	3.7	3	3.7	kN/m ²
Effective friction angle, ϕ'	30	30	30	30	°
Dilatancy angle, ψ	0	0	0	0	°
Coefficient of earth pressure at rest for normally consolidated clay, K_0^{nc}	0.6	0.6	0.6	0.6	-
Reference stress, p_{ref}	100	100	100	100	kN/m ²
Shear strain level when $G=0.7G_0$, $\gamma_{0.7}$	0.0004	0.0004	0.0004	0.0004	kN/m ²
Undrained initial shear modulus at reference pressure, G_0^{ref}	21 600	21 600	21 600	21 600	kN/m ²
Scaling factor, R_f	0.9	0.9	0.9	0.9	-

Appendix K- Correlation between the Soft Soil and the Hardening Soil small-strain stiffness models parameters

CRS graphs- modified compression index

In Figure 67 and Figure 68 the difference between lab data, calibrated values and values according to the modified compression index can be seen for the CRS tests at both levels. Initially, the HSs parameters were calibrated according to the best fit and not the correlation to the SS model. Thereafter, the modified compression index used in the SS model was used to calculate the stiffness moduli and a new set of parameters were obtained.

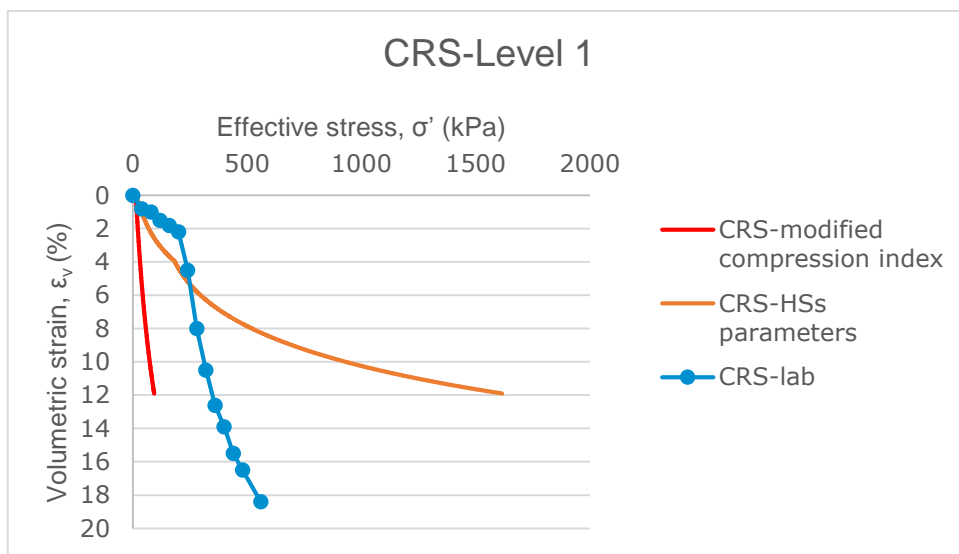


Figure 67: Comparison of the lab data and different ways to evaluate the stiffness parameters for the HSs model.

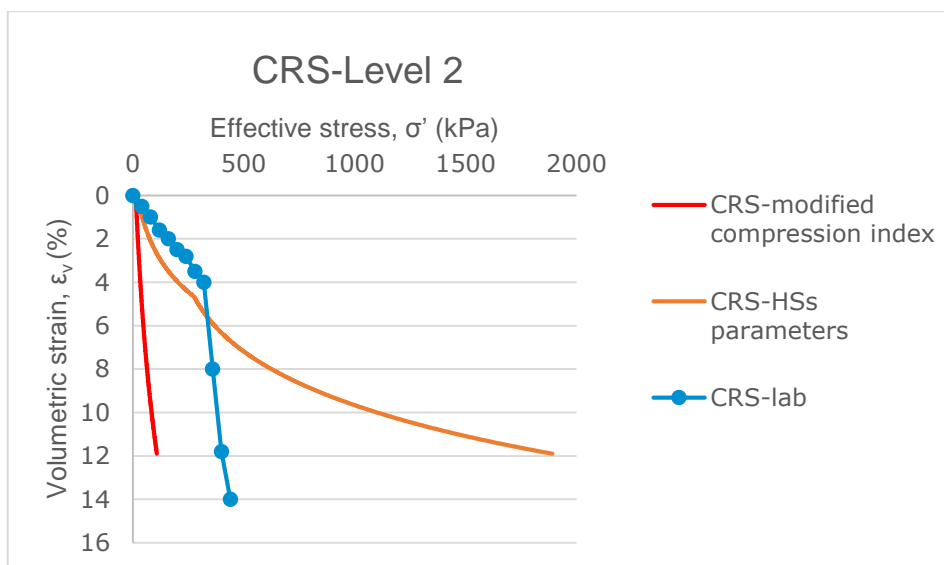


Figure 68: Comparison of the lab data and different ways to evaluate the stiffness parameters for the HSs model.

CRS graphs- modified swelling index

In Figure 69 and Figure 70 the difference between lab data, calibrated values and values according to the swelling index can be seen for the CRS tests at both levels. The manner in which the parameters were obtained is the same as above.

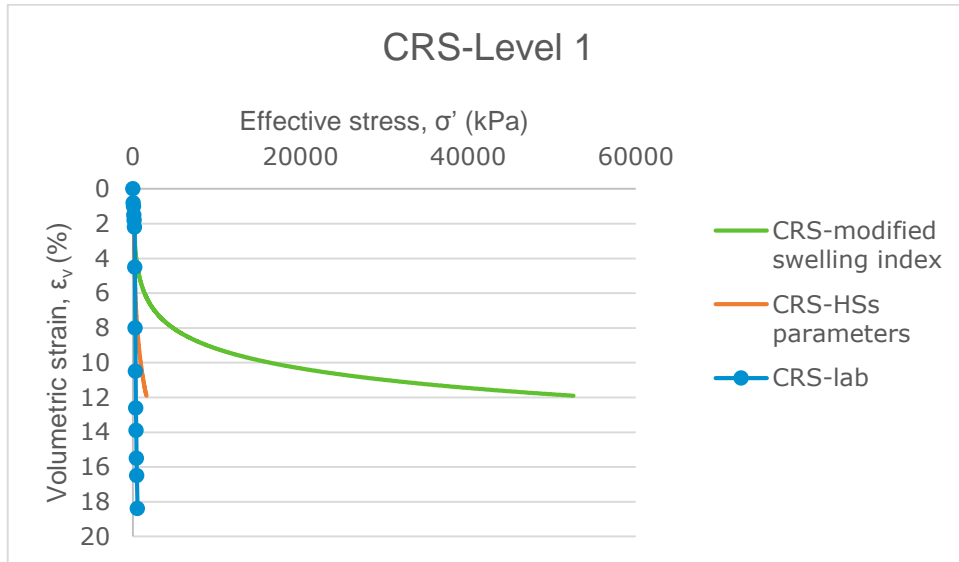


Figure 69: Comparison of the lab data and different ways in order to evaluate the stiffness parameters for the HSs model.

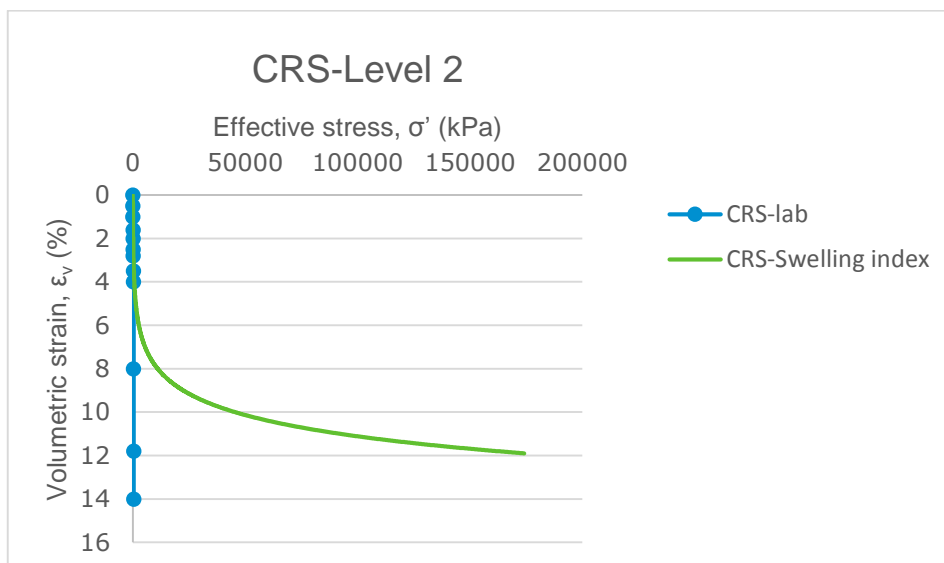


Figure 70: Comparison of the lab data and different ways in order to evaluate the stiffness parameters for the HSs model.

Drained triaxial graphs- modified swelling and compression indices

In Figure 71 and Figure 72 the drained triaxial graphs for both levels are presented. In these graphs the calibration according to both the compression and swelling indices are presented.

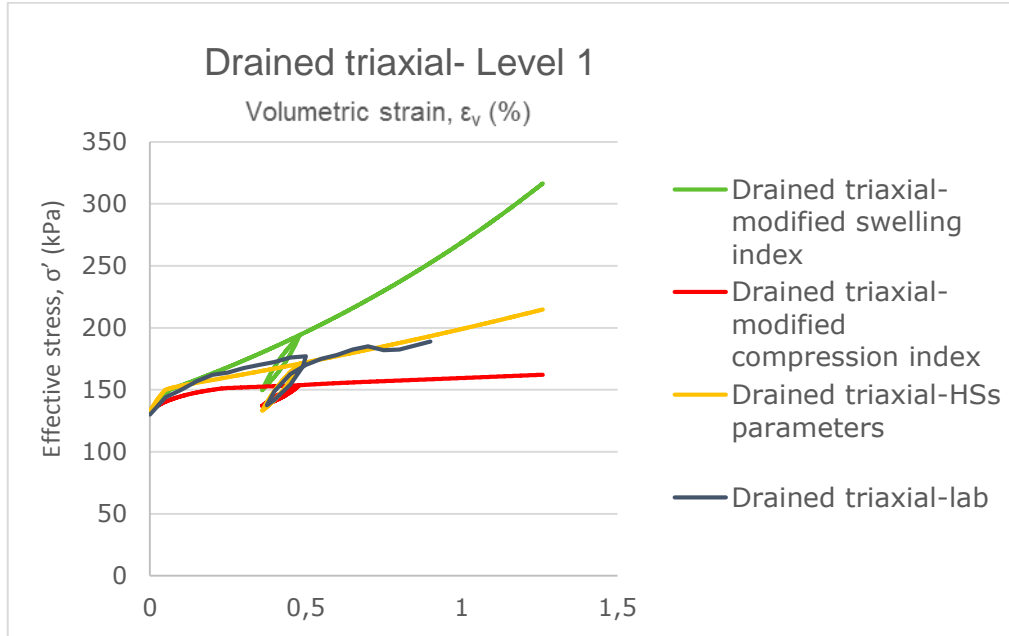


Figure 71: Comparison of the lab data and different ways in order to evaluate the stiffness parameters for the HSs model.

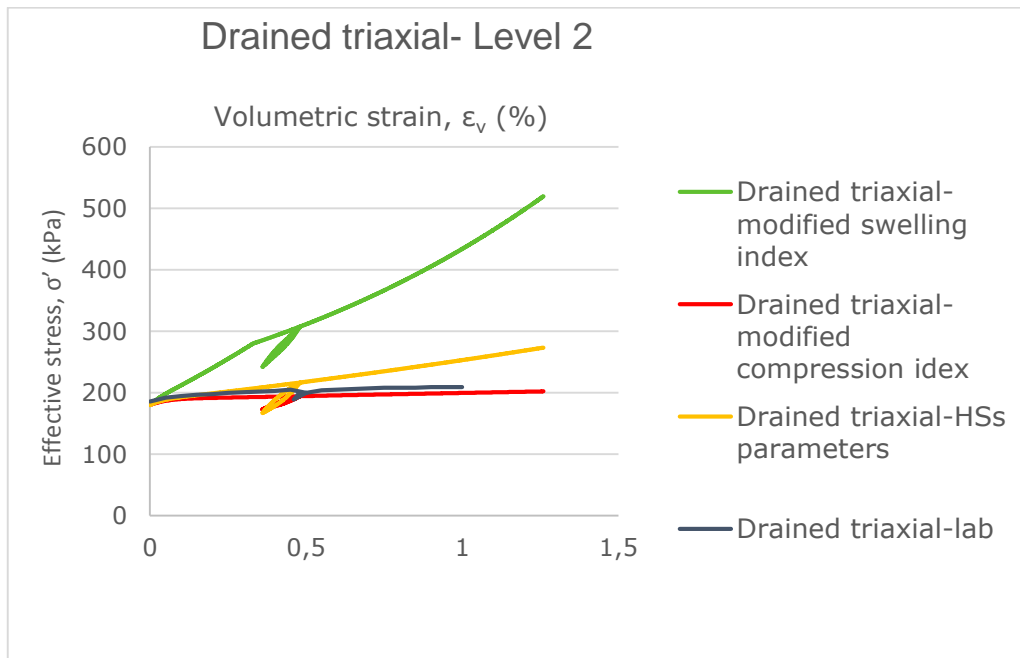


Figure 72: Comparison of the lab data and different ways in order to evaluate the stiffness parameters for the HSs model.

Appendix L- Analytical calculations

Calculations of basal heave for model 1-concrete slab, according to Terzaghi's method. Values can be found in Table 48 and the safety factor is calculated according to equation (42).

$$F_b = \frac{1}{H_e} \cdot \frac{5,7s_{u2}}{\gamma + \frac{q_s}{H_e} - \frac{s_{u1}}{0,7B}} \quad (42)$$

Table 48: Parameters for calculation of safety factor according to Terzaghi's method, concrete plate.

Parameters	Value	Units
Width of the excavation, B	40	m
Height of the excavation, H_e	14.8	m
Specific weight, γ	16	kN/m ³
Shear strength above the excavation, s_{u1}	15	kPa
Shear strength below the excavation, s_{u2}	52.2	kPa
Surcharge load, q_s	10	kN/m

Calculations of basal heave for model 1-concrete slab, according to Bjerrum and Eide's method. Values can be found in Table 49 and the safety factor is calculated according to equation (43).

$$F_b = \frac{N_c s_u}{\gamma H_e + q_s - q_c} \quad (43)$$

Table 49: Parameters for calculation of safety factor according to Bjerrum and Eide's method, concrete plate.

Parameters	Value	Units
Width of the excavation, B	40	m
Length of the excavation, L	120	m
Height of the excavation, H_e	14.8	m
Specific weight, γ	16	kN/m ³
Shear strength at the toe of the wall, s_u	52.2	kPa
Surcharge load, q_s	10	kN/m
Skempton's bearing capacity factor, N_c	6.3	-
Load from the concrete slab, q_c	45	kN/m

Calculations of basal heave for model 2-lime-cement columns, according to Bjerrum and Eide's method. Values can be found in Table 50 and the safety factor is calculated according to equation (44).

$$F_b = \frac{N_c s_u}{\gamma H_e + q_s - q_c} \quad (44)$$

Table 50: Parameters for calculation of safety factor according to Bjerrum and Eide's method, LCC.

Parameters	Value	Units
Width of the excavation, B	40	m
Length of the excavation, L	120	m
Height of the excavation, H_e	39	m
Specific weight, γ	16	kN/m ³
Shear strength at excavation toe, s_u	100	kPa
Surcharge load, q_s	10	kN/m
Skempton's bearing capacity factor	7.2	-
Load from concrete, q_c	23	kN/m

Appendix M- Loads, Mesh, failure surface and safety factor

In Figure 73 the location of the live load and the point load can be seen.

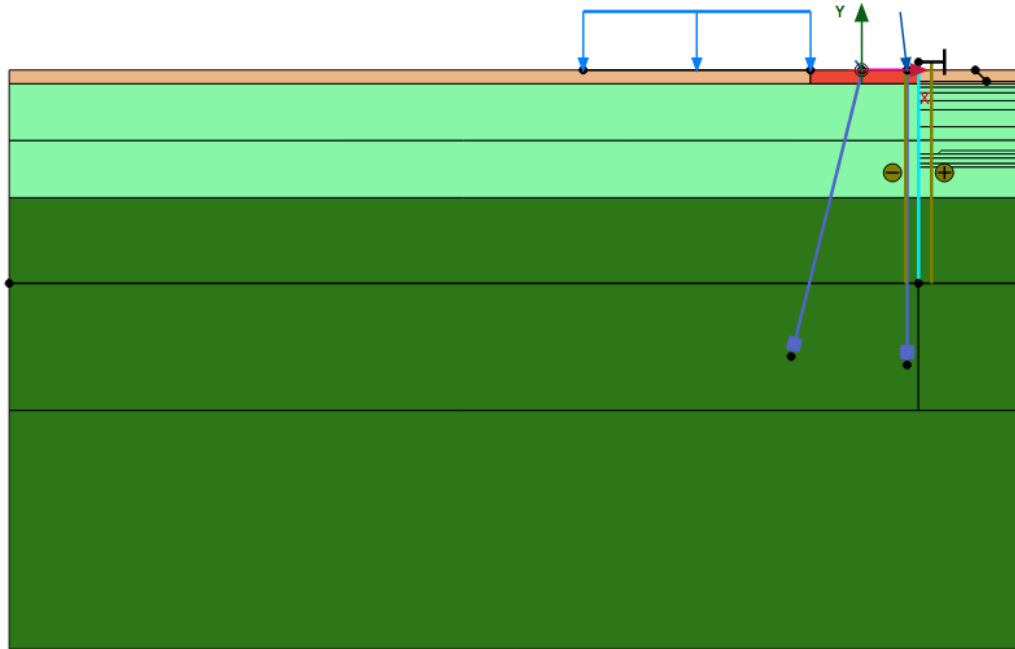


Figure 73 Live load and point load location, marked with blue arrows.

In Figure 74 and Figure 75 the mesh for the concrete slab for the Soft Soil and the Hardening Soil with small-strain stiffness models are presented.

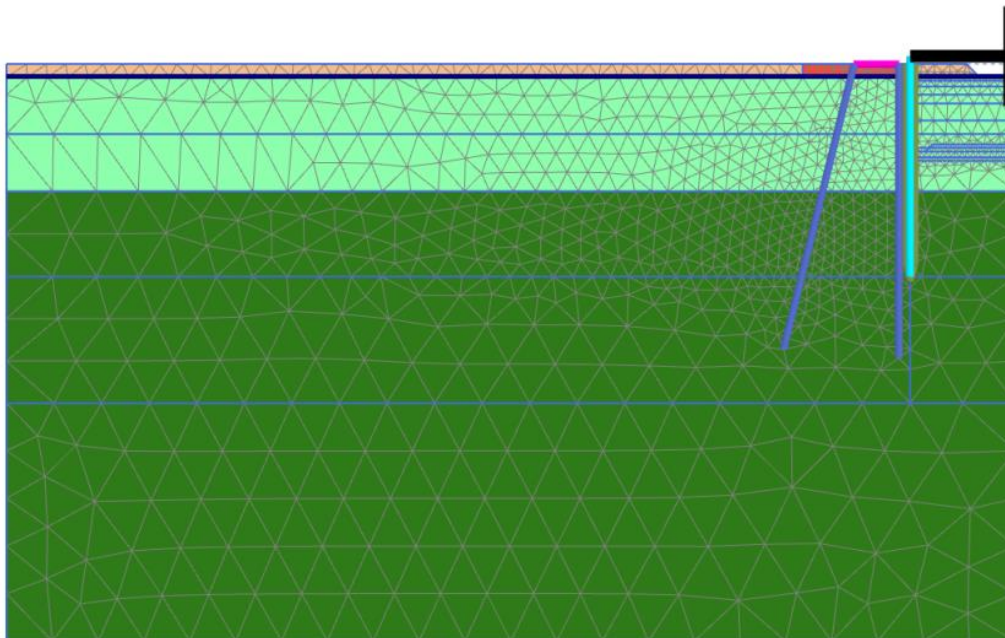


Figure 74: Mesh for the Soft Soil model, concrete slab.

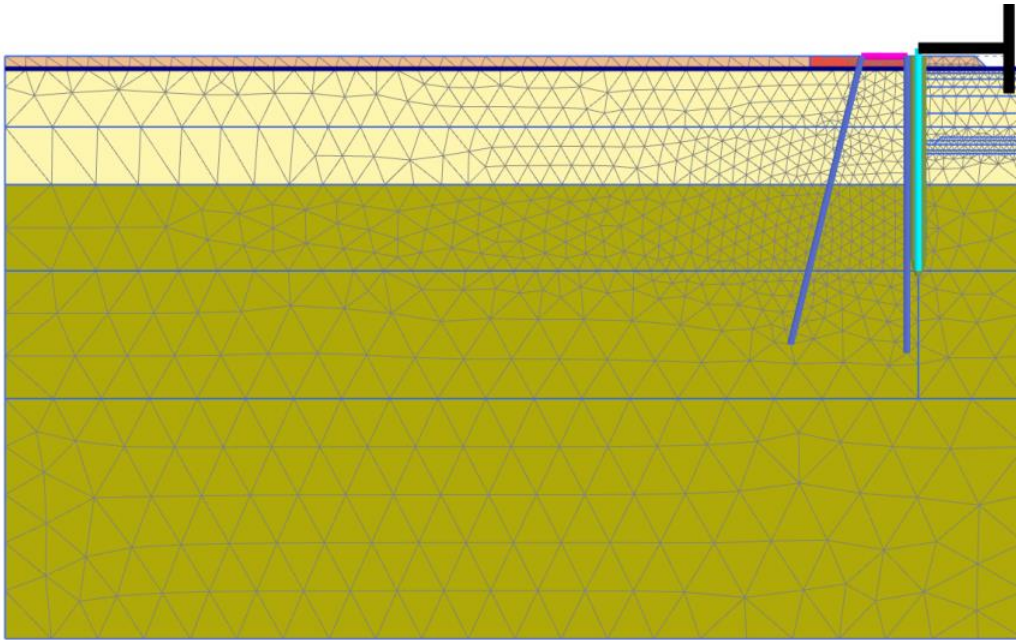


Figure 75: Mesh for the Hardening Soil with small-strain stiffness model, concrete slab.

In Figure 76 and Figure 77 the failure surface for the concrete slab for the Soft Soil and the Hardening Soil with small-strain stiffness models are presented. The failure surface is obtained from looking at the total displacement in the final factor of safety. The displacement values are not presented as they do not have any significance in the safety factor stage.

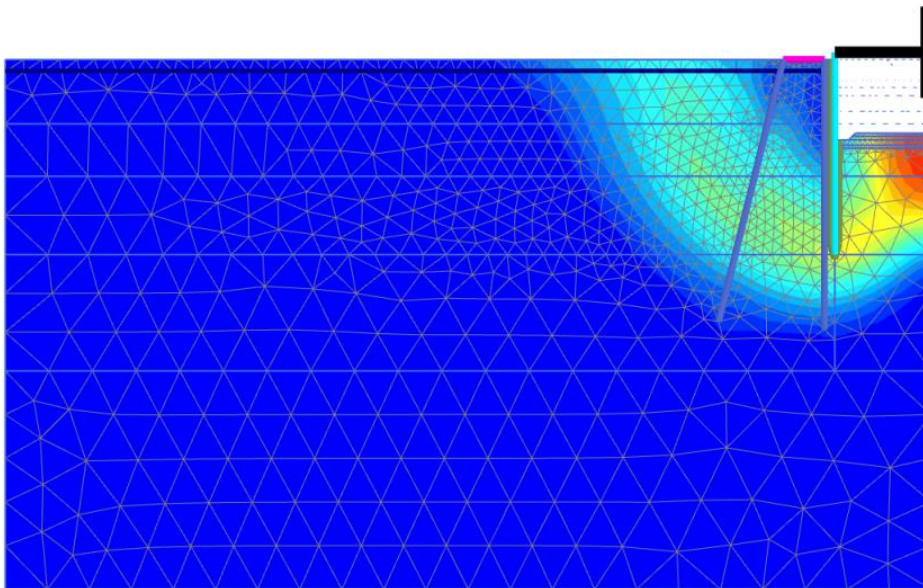


Figure 76: Failure surface for the concrete slab- Soft Soil model.

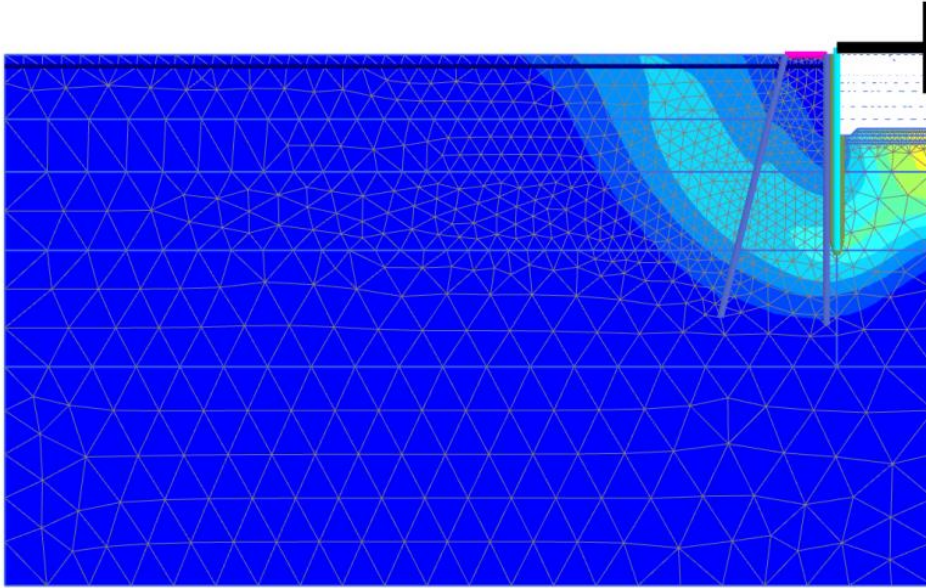


Figure 77: Failure surface for the concrete slab- Hardening Soil with small-strain stiffness model.

In Figure 78 and Figure 79 the safety factor for the concrete slab for the Soft Soil and the Hardening Soil with small-strain stiffness models are presented.

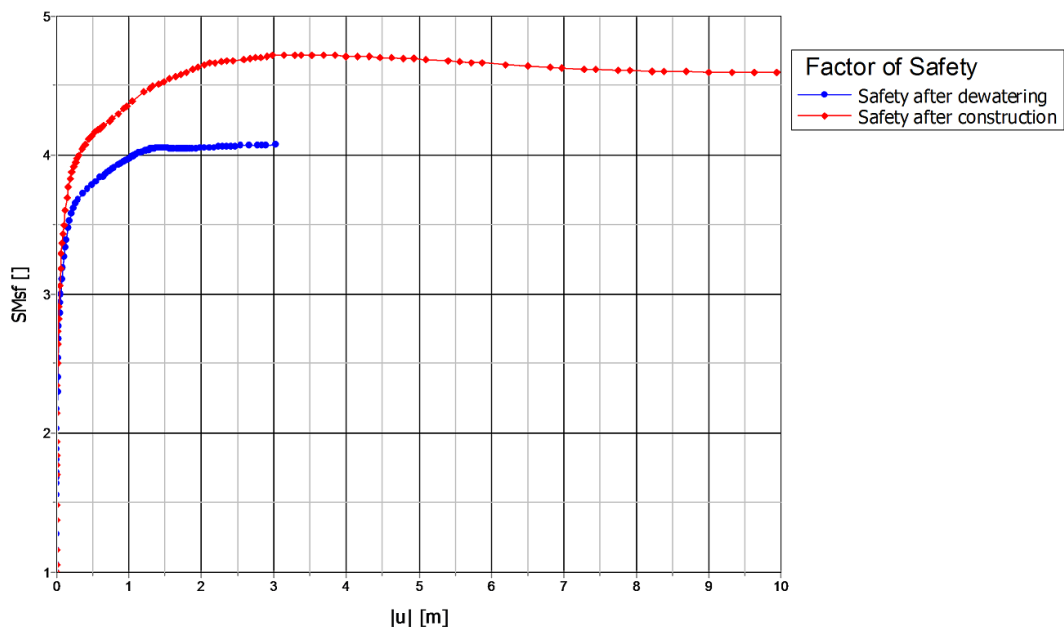


Figure 78: Safety factor for the concrete slab model- Soft Soil model.

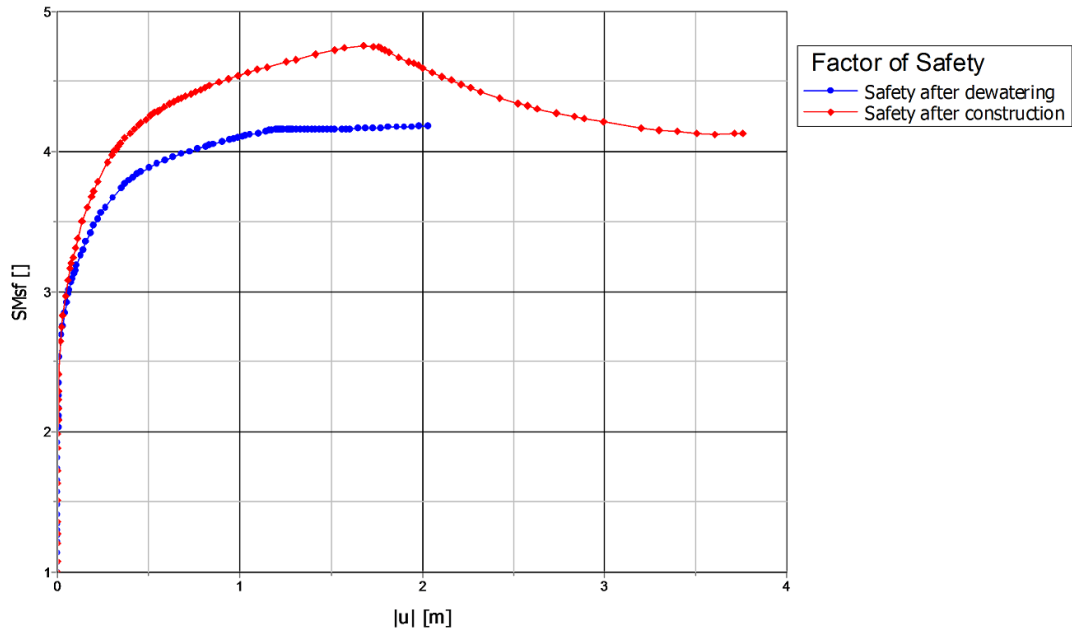


Figure 79: Safety factor for the concrete slab model- Hardening Soil with small-strain stiffness.

In Figure 80 and Figure 81 the mesh for the lime cement columns for the Soft Soil and the Hardening Soil with small-strain stiffness models are presented.

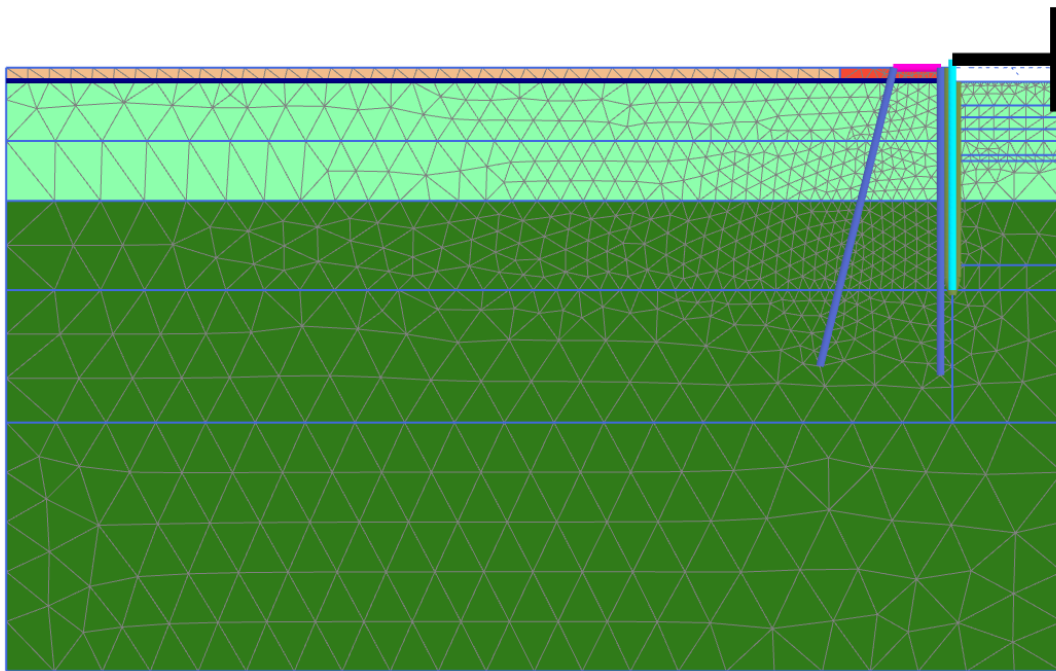


Figure 80: Mesh for the Soft Soil model, lime cement columns.

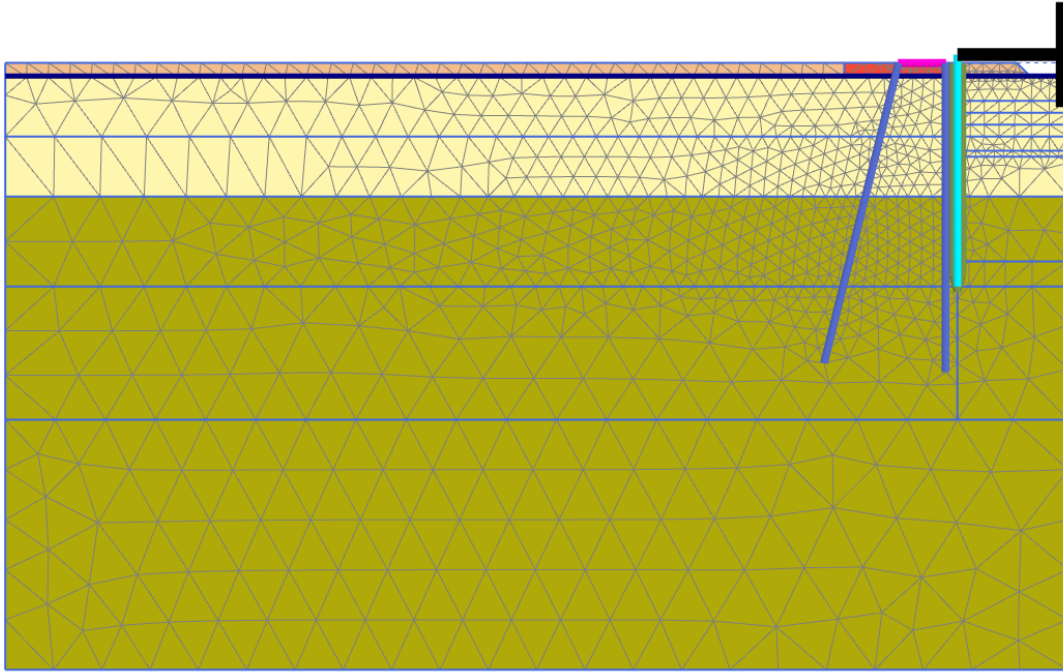


Figure 81: Mesh for the Hardening Soil with small-strain stiffness model, lime cement columns.

In Figure 82 and Figure 83 the failure surface for the lime cement columns for the Soft Soil and the Hardening Soil with small-strain stiffness models are presented. The failure surface is obtained from looking at the total displacement in the final factor of safety. The displacement values are not presented as they do not have any significance in the safety factor stage.

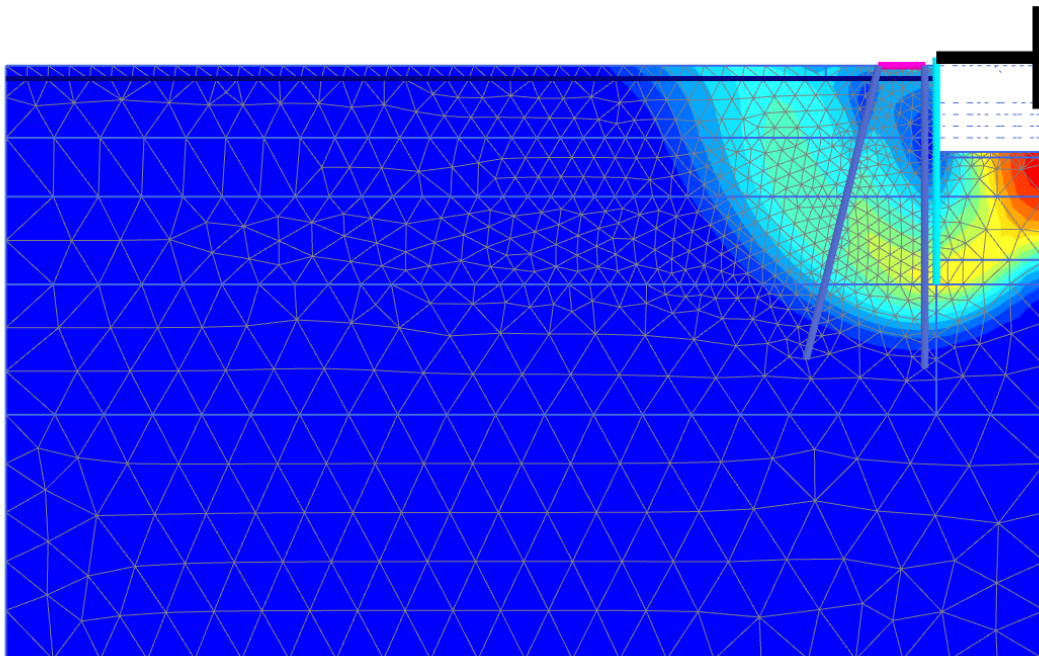


Figure 82: Failure surface for the lime cement columns- Soft Soil model.

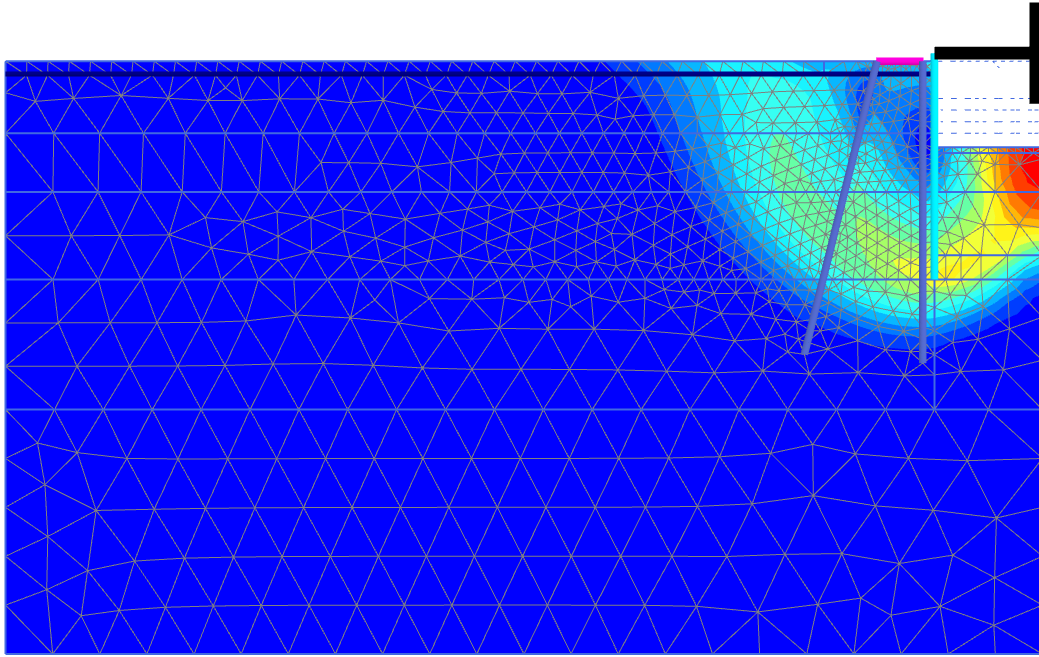


Figure 83: Failure surface for the lime cement columns- Hardening Soil with small-strain stiffness model.

In Figure 84 and Figure 85 the safety factor for the lime cement columns for the Soft Soil and the Hardening Soil with small-strain stiffness models are presented.

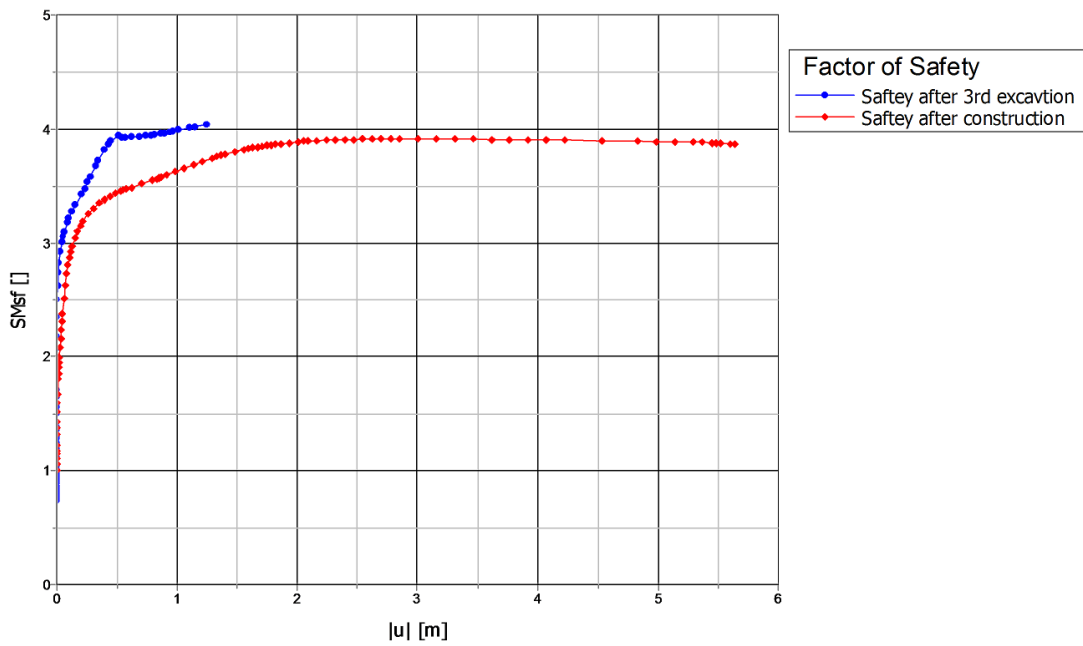


Figure 84: Safety factor for the lime-cement columns model- Soft Soil model.

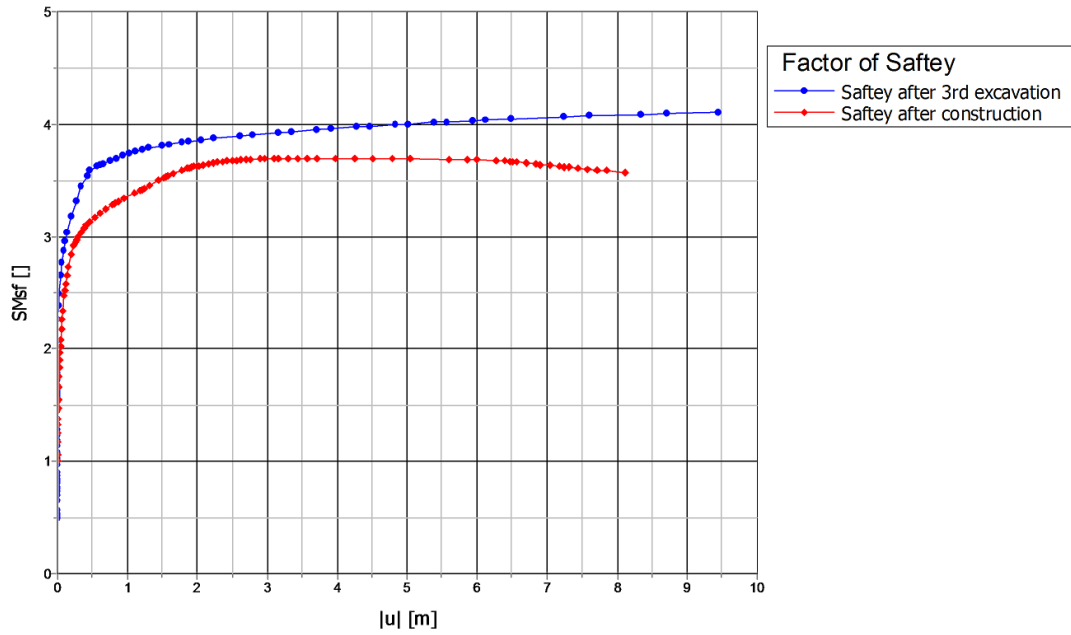


Figure 85: Safety factor for the lime-cement columns model- Hardening Soil with small-strain stiffness.

In Figure 86 a mesh close up of the lime-cement columns according to Ignat's method for the Soft Soil model is presented.

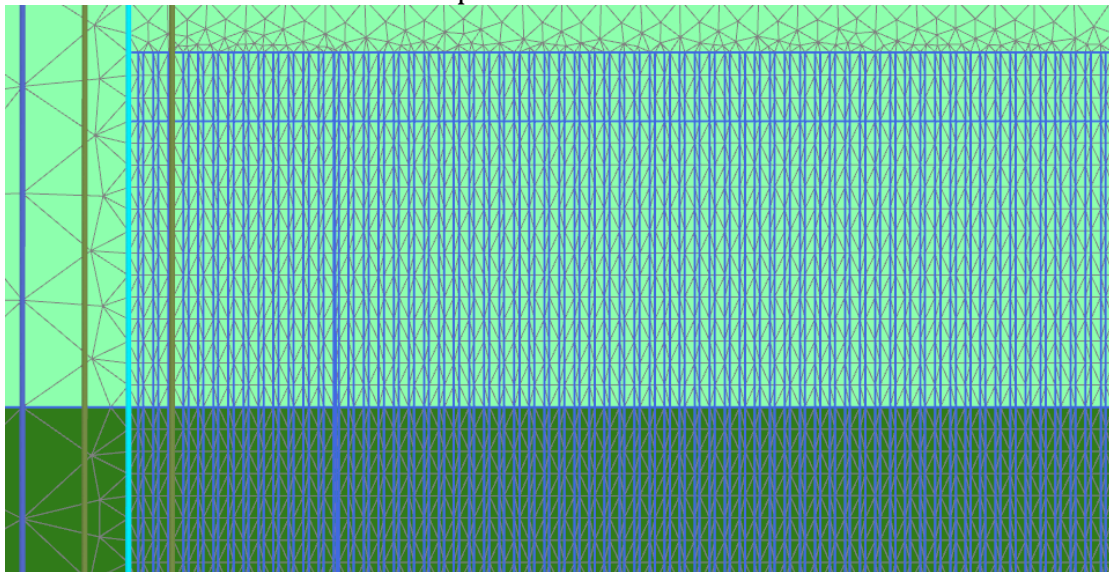


Figure 86: Mesh close up of the lime-cement columns according to Ignat's method.

In Figure 87 the safety factor for the Soft Soil model according to Ignat's method is presented.

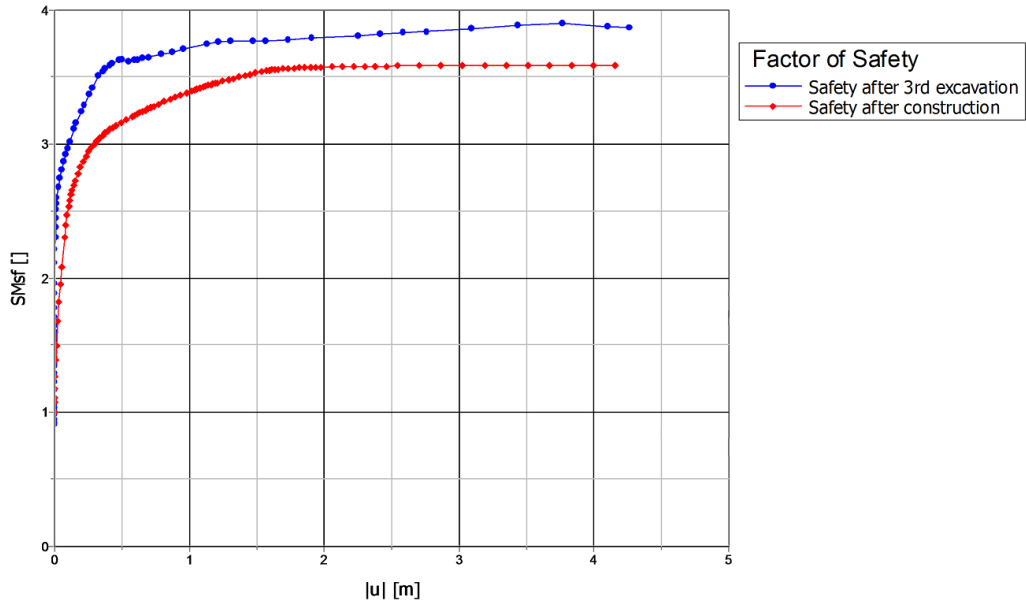


Figure 87: Safety factor for the lime-cement columns model according to Ignat's method- Soft Soil.

In Figure 88 and Figure 89 the safety factor for the lime-cement columns with an increased permeability and stiffness are presented.

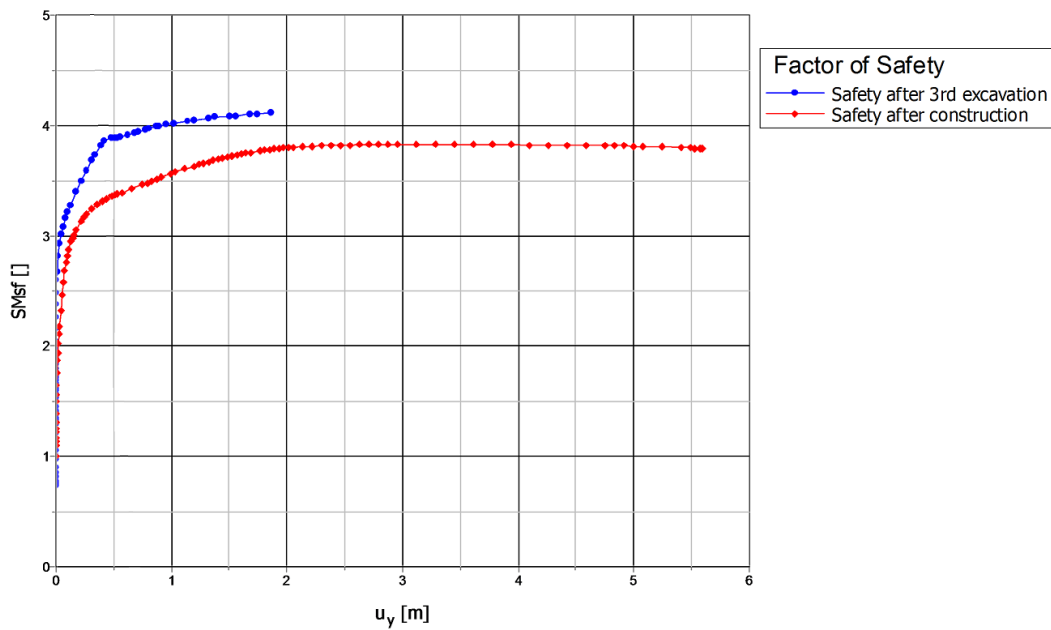


Figure 88: Safety factor for the lime-cement columns model with an increased permeability- Soft Soil.

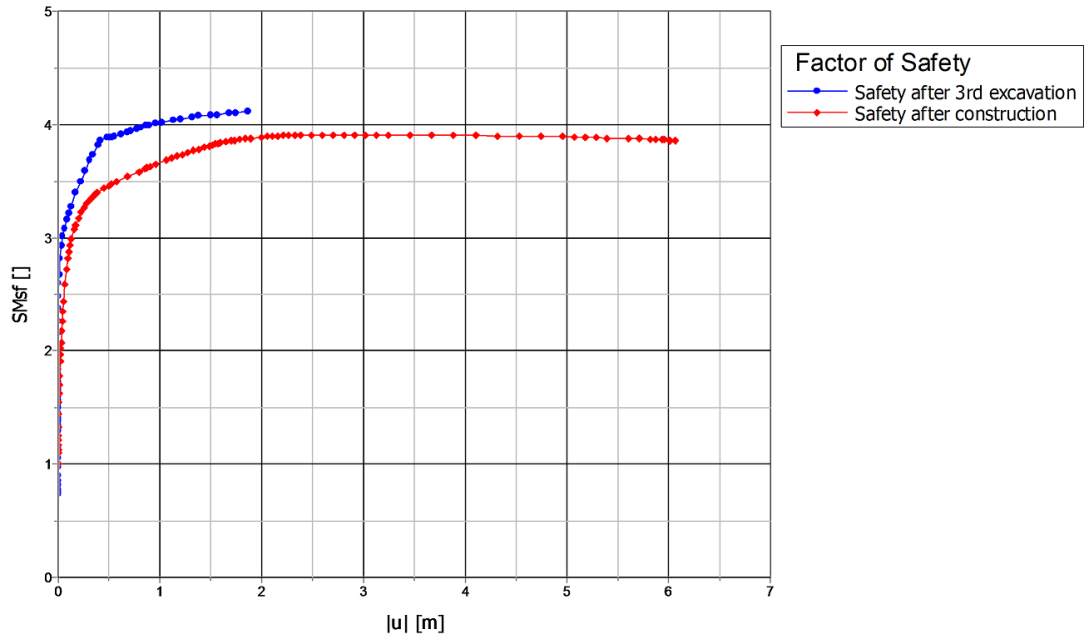


Figure 89: Safety factor for the lime-cement columns model with an increased stiffness- Soft Soil.:

Appendix N- Influence of loads- Model 1

Since the loads are only present until the retaining wall is installed, their effect on basal heave will be most significant up to that point. To be able to see the effect more clearly Figure 90 is only to 210 days, i.e. retaining wall installation. The live load added was 10 kN/m/m and the point loads are presented in Table 51.

Table 51: Point loads.

	Vertical component	Horizontal component	Units
Point load 1	106.2	12.54	kN/m
Point load 2	17.54	12.54	kN/m

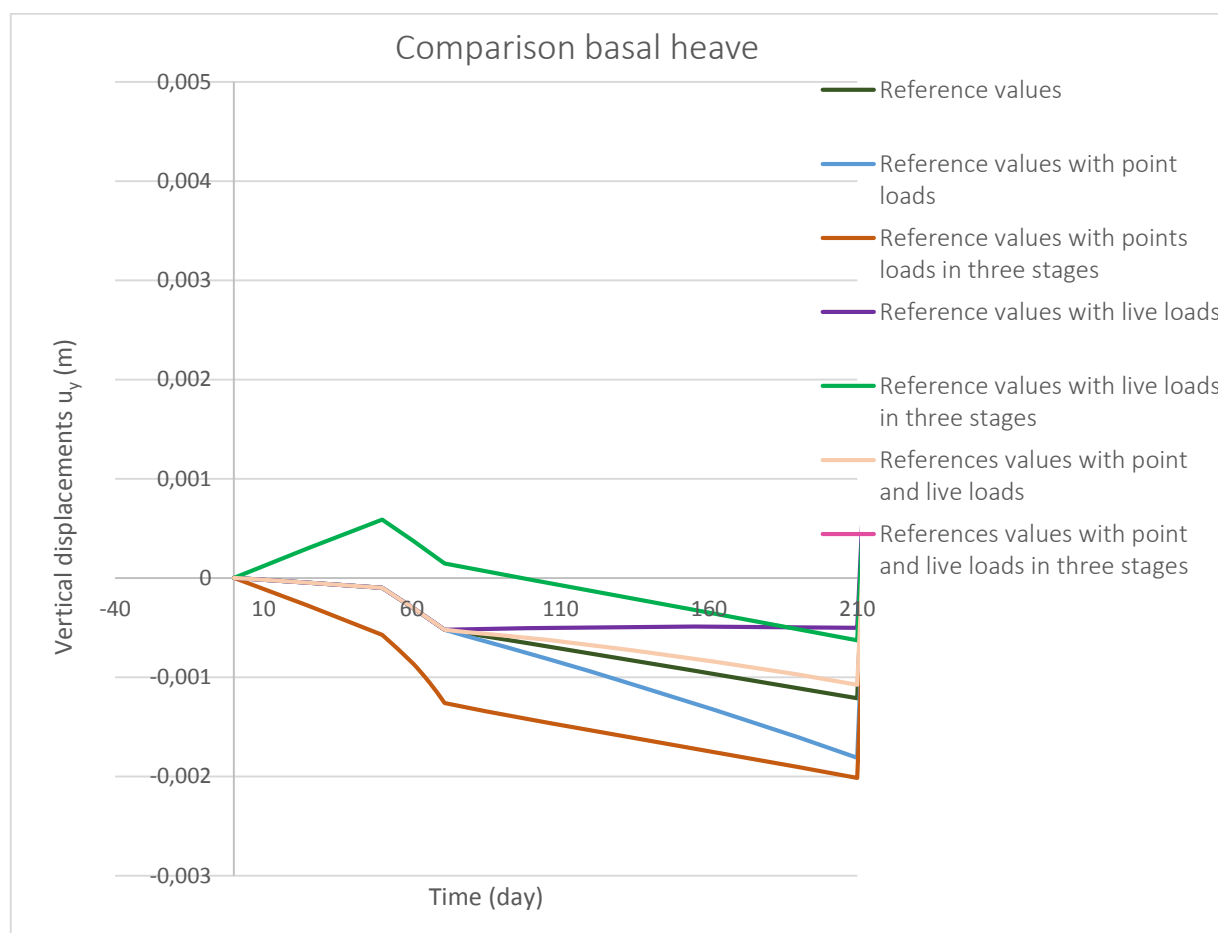


Figure 90: Comparison for basal heave due to the influence of loads.

Appendix O- Parametric studies- Model 1

Soft Soil model

In Figure 91 the lower and upper bound values for the parametric studies are compared with the reference values for the Soft Soil model. Some of the parameters do not have much influence on the excavation and are not visible in the graph since they are behind the reference line, these parameters are the following: minimum modified compression index, minimum effective cohesion and maximum effective cohesion. The values of the parameter variation are presented in Table 52 and Table 53.

Table 52: Parameter variation for the first clay layer.

Clay 1	Minimum	Reference	Maximum
Modified compression index, λ^*	0.13	0.15	0.15
Modified swelling index, κ^*	0.0022	0.0082	0.0082
Coefficient of earth pressure at rest for normally consolidated clay, K_0^{nc}	0.5	0.6	0.67
Effective Poisson's ratio for un/reloading, v'_{ur}	0.15	0.15	0.3
Effective cohesion, c'	0.7	0.8	1.3
Effective friction angle, φ'	29	30	31
Over Consolidation Ratio, OCR	1.1	1.15	1.25

Table 53: Parameter variation for the second clay layer.

Clay 2	Minimum	Reference	Maximum
Modified compression index, λ^*	0.19	0.20	0.20
Modified swelling index, κ^*	0.003	0.007	0.007
Coefficient of earth pressure at rest for normally consolidated clay, K_0^{nc}	0.5	0.6	0.67
Effective Poisson's ratio for un/reloading, v'_{ur}	0.15	0.15	0.3
Effective cohesion, c'	2.9	3.1	3.7
Effective friction angle, φ'	29	30	31
Over Consolidation Ratio, OCR	1.1	1.18	1.25

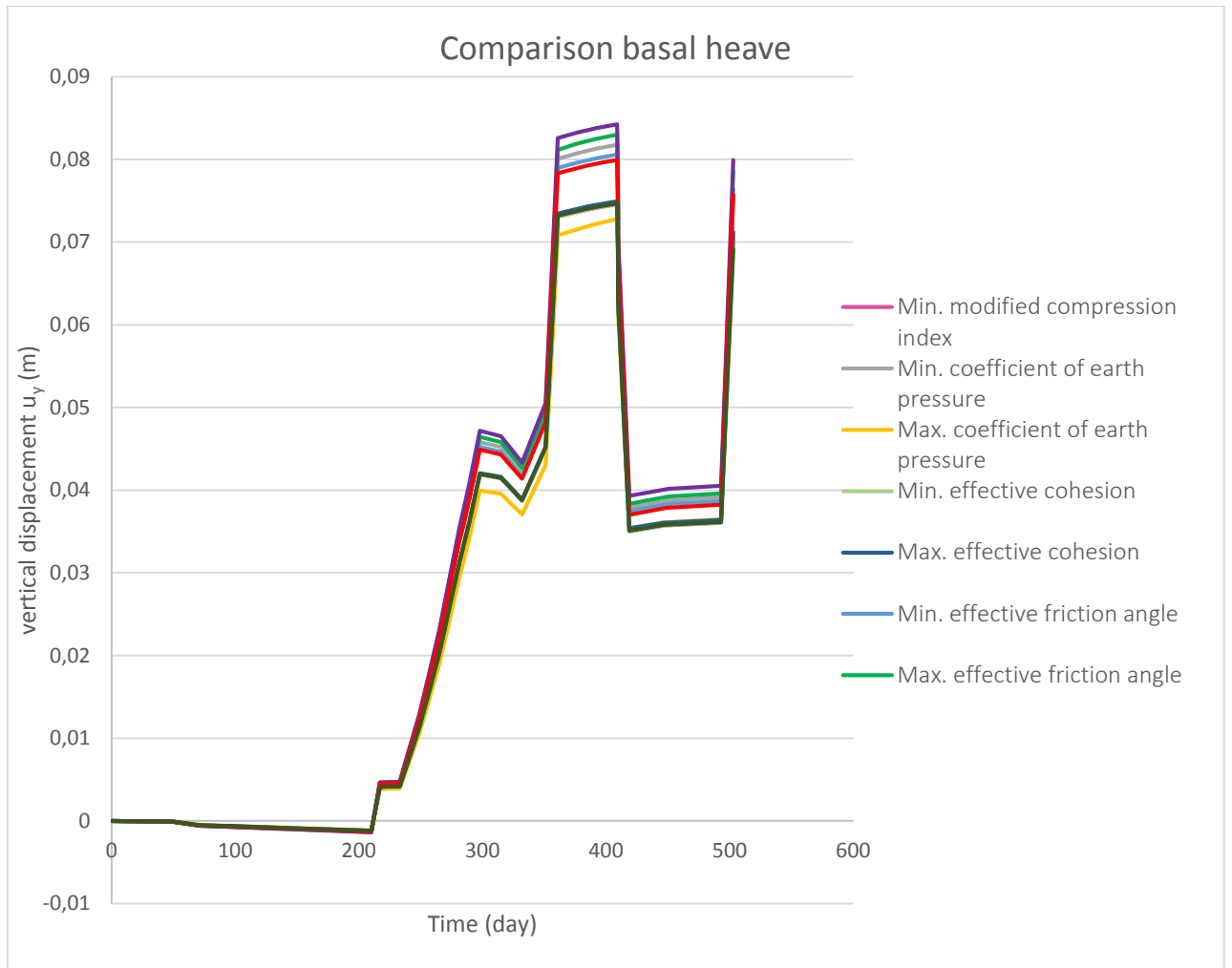


Figure 91: Comparison of basal heave for the parameter variation in the Soft Soil model.

Hardening Soil with small-strain stiffness model

In Figure 92 the lower and upper bound values for the parametric studies are compared with the reference values for the HSs model. The parameter with the least impact on the result is the minimum effective cohesion. The values of the parameter variation are presented in Table 54 and Table 55.

Table 54: Parameter variation for the first clay layer.

Clay 1	Minimum	Reference	Maximum
Secant stiffness in standard drained triaxial test at reference pressure, E_{50}^{ref}	833	5000	8130
Tangent stiffness for primary oedometer loading at reference pressure, E_{oed}^{ref}	667	3051	6504
Unload/reload stiffness at reference pressure, E_{ur}^{ref}	2500	15 000	24 390
Coefficient of earth pressure at rest for normally consolidated clay, K_0^{nc}	0.50	0.60	0.67
Effective Poisson's ratio for un/reloading, v'_{ur}	0.15	0.15	0.30
Effective cohesion, c'	0.70	0.80	1.3
Effective cohesion increase, c'_{inc}	0.091	0.114	0.138
Effective friction angle, φ'	29	30	31
Over Consolidation Ratio, OCR	1.1	1.15	1.25

Table 55: Parameter variation for the second clay layer.

Clay 2	Minimum	Reference	Maximum
Secant stiffness in standard drained triaxial test at reference pressure, E_{50}^{ref}	625	5000	9524
Tangent stiffness for primary oedometer loading at reference pressure, E_{oed}^{ref}	500	3051	7619
Unload/reload stiffness at reference pressure, E_{ur}^{ref}	1875	15 000	28 571
Coefficient of earth pressure at rest for normally consolidated clay, K_0^{nc}	0.50	0.60	0.67
Effective Poisson's ratio for un/reloading, v'_{ur}	0.15	0.15	0.30
Effective cohesion, c'	2.9	3.1	3.7
Effective cohesion increase, c'_{inc}	0.091	0.114	0.138
Effective friction angle, φ'	29	30	31
Over Consolidation Ratio, OCR	1.1	1.18	1.25

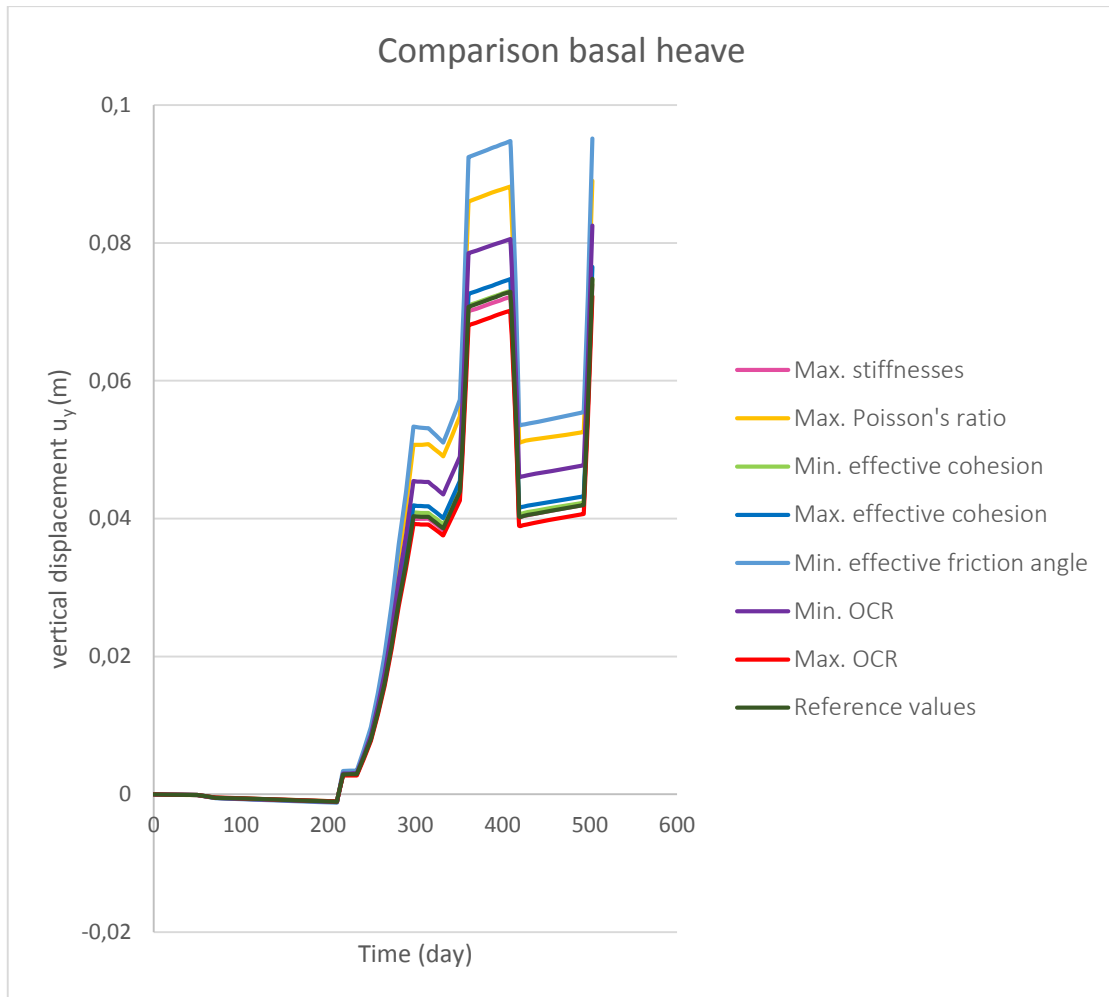


Figure 92: Comparison of basal heave for the parameter variation in the Hardening Soil with small-strain stiffness model.